Optimization of Mucoadhesive Polymer Micelles for Drug Delivery and Ophthalmic Formulations

by

Sukrit Rajpal

A thesis
presented to the University of Waterloo
in fulfillment of the
thesis requirement for the degree of
Master of Applied Science
in
Chemical Engineering (Nanotechnology)

Waterloo, Ontario, Canada, 2019

AUTHOR'S DECLARATION

This thesis consists of material all of which I authored or co-authored. Contributions are identified within the thesis in Chapter 4 where the co-authored material appears. This is a true copy of the thesis, including any required final revisions, as accepted by my examiners.

I understand that my thesis may be made electronically available to the public.

Abstract

Nanotechnology enabled medicine (nanomedicine) is expected to be the next advent of the health care market facilitating efficient, safe, and personalized therapies. Despite numerous publications demonstrating utility of nanoparticle platforms for drug delivery, analysis on commercial viability of these platforms indicates there are several challenges, often unique to the formulation, which still need to be addressed. Nanomedicine has thus far had limited penetration in the market. This thesis addresses some of these challenges and opportunities, with a focus on mucoadhesive polymer micelle nanoparticles for ocular drug delivery as a model system.

The eye is an exposed organ and several physiological and anatomical barriers have evolved to protect the organ from foreign particles. These barriers also restrict delivery of drug molecules to their intended targets. Topical administration is possible for the anterior segment and is the most popular route of ocular drug delivery. Only 5% of the administered dose is bioavailable for action at the target site, while the remaining 95% is removed via blinking, nasolacrimal drainage, degradation, or cleared with the tear film. Frequent administrations and concentrated doses are required to overcome these barriers to reach and maintain therapeutic concentration. In order to improve ocular drug delivery, nanotechnology enabled medicine aims to improve the retention time of the therapeutics on the ocular surface. One such strategy is the adhesion of molecules or particles to the mucus layer of the ocular tear film. This strategy (mucoadhesion) has been successfully demonstrated as a mechanism to bypass clearance by the tear film.

Mucus membranes exist throughout the body. Though the focus of the PLA-*b*-Dex-APBA polymer micelles developed by our group has thus far been limited to ocular drug delivery, we propose that the prolonged retention of therapeutics encapsulated within this platform will result in less frequent administration, local targeting of the tissue, a reduced administered dose and therefore reduced adverse side effects. By tuning properties of the block copolymer such as the conjugation of mucoadhesive ligand APBA, the other mucus membranes can be targeted, and the return on investment can be maximized. Studies on the major factors of the reaction mechanism were used to develop a model which can be utilized to target and fine tune the conjugation of mucoadhesive ligand. Through this work, the variance in the batch-to-batch synthesis can be reduced which is critical to commercialization.

Synthesis of nanotechnology enabled medicine is more complex than the conventional form, adding cost and requiring highly trained personnel. Herein, an alternate route for the conjugation of the mucoadhesive ligand to polymer is explored. The method is based on the principals of solid-state chemistry. Though conventional solid-state reaction conditions are impractical for carbohydrates, a semi solid-state reaction which reduces the synthesis time of our mucoadhesive polymer from 30 hours to only 10 minutes. The reaction is performed at 110°C (significantly lower than temperatures for conventional solid-state chemistry) and can thus be utilized to achieve efficient modification of carbohydrates.

Colloidal systems are far more unstable than conventional therapeutic forms; this has also limited market entry of nanotechnology enabled medicine. A short shelf-life dramatically increases the cost of production which may not be justified by the added benefit. Herein, flash freezing, and freeze-drying are explored, both viable options to improve shelf life of the PLA-*b*-Dex-APBA block polymer micelle suspension. Due to an inherent cryoprotective property, no modification needs to be made to the formulation while flash freezing. The stress imposed on the suspension during sublimation (drying stage of freeze-drying) destabilizes the particles, causing them to aggregate. Through this work, the addition of 2 wt% trehalose was determined to be optimal to improve the stability and recovery of nanoparticles post freeze-drying.

In order to commercialize the mucoadhesive platform, the formulation must be freeze-dried to increase the shelf-life. The current synthesis process requires the formation of an oil-in-water emulsion and subsequent preservation. Herein, a novel method of using freeze-drying to drive self-assembly of block copolymer micelles is demonstrated. The condensed product is a loose aggregate of particles which readily disperse upon rehydration. Synthesizing polymer micelles via this pathway was found to be optimal in a 2 wt% trehalose solution, resulting in particles which are acceptable under the guideless of the U.S. pharmacopoeia (USP) for ophthalmic preparations. The time prior to freeze-drying is reduced from 3 hours to 10 minutes.

Based on the conclusions of this work, it is recommended that the regression model be further validated and verified. The effect of different conjugation fractions should be investigated in vivo to determine the optimal adhesive strength for the various regions. Dextran functionalized with the mucoadhesive ligand was also studied as a simplified model and has the potential to improve upon current suspensions for dry eye. The solid-state method should be investigated for the synthesis of the entire block-copolymer to further reduce the synthesis complexity. The self-cryopreservation property

was identified for our nanoparticle formulation; it is recommended to try and extend this to other particle formulations. Lastly, the proof-of-concept study for the synthesis of polymer micelles under the stress of freeze-drying was explored. The next recommended step is to optimize the drug loading through this method.

Acknowledgements

Foremost, I would like to acknowledge the financial contribution of my thesis advisor Dr. Frank Gu.

I would like to express my deepest appreciation to Dr. Sandy Liu whose expertise, encouragement and generous guidance which made it possible for me to work on a project that was of great interest to me. His scholarly advice and scientific approach have helped me to a great extent in completing this work.

I am also fortunate to have worked with the members of this research group, namely Mr. David Wulff, Ms. Jenny (Chu Ning) Chan, Mr. Diogo de Oliveira Livera, Ms. Aaminah Ahmad, Mr. Mostafa Saquib, Ms. Michelle Si, and Ms. Lori Polit. I would also like to thank cooperative education students Ms. Jasmine Zhang, Mr. Zihan Li, and Ms. Katie Kobernyk for their contributions to the research.

In addition, I thank Mrs. Janet Venne, Nuclear Magnetic Resonance Technician, Department of Chemistry, Mr. Ralph Dickhout, Analytical Chemist and Manager of Laboratory Safety, Department of Chemical Engineering, and Mrs. Mishi Groh, Departmental Technician, Department of Biology, for their support and expertise with analytical instruments and assistance in developing the protocols for this work.

I further extend my personal gratitude to the experts at the members of the Nanotechnology Engineering Program at the University of Waterloo who have been instrumental in making this work possible. Dr. Jenn Coggan, Dr. Ahmad Ghavami, and Dr. Neil McManus have been more than generous with their lab space, equipment and expertise which was instrumental in completing this work. I am also grateful for the teaching assistantship opportunities they have provided me and enabling me to further develop my skills.

Lastly, I would like to express my gratitude to members of the Department of Chemical Engineering at the University of Waterloo namely Dr. Eric Croiset, Chair and Professor Dr. Nasser Mohieddin Abukhdeir, Associate Chair Graduate Studies & Associate Professor, and Mrs. Judy Caron, Manager Graduate Studies, for the numerous ways in which they have helped me complete this program.

Dedication

To my mother, Sanji Rajpal, and my father, Deepak Rajpal.

Table of Contents

List of Figures

List of Illustrations

List of Tables

List of Acronyms and Abbreviations

Chapter 1
Introduction

1.1 Overview

Topical administration is the most popular route of ocular drug delivery due to the accessibility of the anterior segment of the eye. However only 5% of the administered dose is bioavailable for action at the target site, while the remaining 95% is removed via blinking, nasolacrimal drainage, degradation, or cleared with the tear film. Frequent administrations of concentrated doses are required to overcome these barriers and to maintain therapeutic concentrations.

Adhesion to the mucus layer of the ocular tear film (mucoadhesion) has been successfully demonstrated as a mechanism to bypass clearance. Drug carriers capable of mucoadhesion exhibit improved retention on the ocular surface facilitating prolonged release of the encapsulated therapeutic closer to the target resulting in improved bioavailability. This strategy has been shown to result in a decrease in administration frequency, local targeting of the ocular tissue, a reduced dosage (concentration) as bioavailability improves and therefore reduced adverse side effects.

Previously published work by our group has demonstrated the utility of self-assembled block copolymer micelles consisting of hydrophobic poly(D,L-lactide) (PLA) in the core and hydrophilic dextran as the corona. The dextran chains are functionalized with 3-aminophenyl boronic acid (APBA) which forms covalent bonds with sialic acid residues on mucin, thereby anchoring the micelles onto the ocular surface. This unmodified block copolymer, APBA functionalized block copolymer, and the self-assembled micelles are herein referred to as PLA-*b*-Dex, PLA-*b*-Dex-APBA, and MNPs respectively.

In vivo studies on New Zealand White rabbits as animal models have demonstrated that APBA functionalized dextran (Dex-APBA) was retained on the ocular surface for up to 6 hours, whereas the unmodified dextran's presence was negligible. MNPs were loaded with a near infrared dye (indocyanine dye) demonstrated sustained release on the ocular surface, and the dye was observed beyond 24 hours. Whereas the control, free dye in solution, was cleared within 3 hours of administration.

This platform has been utilized to improve the administration of cyclosporine A (CsA) in vivo using female mice. Administration of MNPs loaded with 0.005 – 0.01 wt% CsA administered once a week resulted in elimination of inflammation and goblet cell recovery was observed. The control, Restasis® a 0.05 wt% CsA emulsion, was administered thrice daily and while inflammation was eliminated, recovery of the ocular surface was not observed.

Nanotechnology enabled medicine (such as the MNP platform) is expected to be the next advent of the health care market facilitating efficient, safe, and personalized therapies, but examples in the market are thus far limited. Despite numerous publications proving utility of nanoparticle platforms for drug delivery, analysis on commercial viability shows there are several challenges to be addressed. Challenges such as complex and costly synthesis mechanisms, and poor shelf-life compared to conventional formulations make these therapies much more expensive.

This thesis identifies barriers to entry for colloidal systems and proposes solutions in the context of a mucoadhesive polymer micelle platform designed for ocular drug delivery. These solutions are not limited to the mucoadhesive formulation studied for the purposes of this work and can be extended to other biomedical and pharmaceutical technologies currently under investigation to improve their commercial viability.

1.2 Research Objectives

The primary objective of this work is to identify challenges and key barriers to market penetration in the context of PLA-*b*-Dex-APBA polymer micelle formulations for ocular drug delivery. Solutions are explored and presented to improve on the existing drug delivery platform and to identify opportunities to improve commercial viability and portfolio diversification.

1. Control APBA conjugation on the PLA-*b*-Dex micelle corona via the reductive amination pathway.
    a) Perform a factorial study on the reductive amination reaction onto free dextran to determine the optimal reaction conditions for conjugation.
    b) Derive a regression model to predict and target the conjugation efficiency of APBA onto free dextran.
    c) Investigate the conjugation reaction onto PLA-*b*-Dex polymer micelle corona based on the findings on free dextran.

d) Derive a regression model to predict and target the conjugation efficiency of the mucoadhesive ligand onto the micelle corona by modifying the factors.

2. Investigate alternate reaction pathways for the conjugation of phenylboronic acid (PBA) onto dextran.

    a) Investigate the Williamson ether synthesis for the conjugation of PBA derivatives.

    b) Formulate a reaction scheme based on the principles of solid-state reaction for the modification of dextran with PBA derivative.

    c) Study the factors influencing the solid-state conjugation reaction and optimize the reaction mechanism.

3. Improve the shelf-life of the polymer micelle nanoparticle to improve commercial viability.

    a) Investigate the freeze-drying process for the preservation of the colloidal suspension.

    b) Optimize the protectant type and concentration per regulatory bodies.

    c) Examine the self-cryopreservation property and determine the cause as well as a potential for this preservation technique.

    d) Quantify the residual organic fraction remaining in the suspension via ^{1}H-NMR.

4. Explore alternate synthesis routes for the self-assembly of PLA-*b*-Dex-APBA block copolymer into polymer micelles.

    a) Demonstrate a direct synthesis method utilizing the stress from the freeze-drying process to drive self-assembly.

    b) Investigate the optimal formulation for the synthesis of statistically similar micelle nanoparticles.

1.3 Thesis Outline

This thesis is comprised of seven chapters: the introduction, literature review, four chapters detailing the experimental work, and a final chapter which summarizes the major conclusions and presents recommendations for future work.

Chapter 1 introduces the thesis objectives and the challenges to be addressed to improve the commercial viability of PLA-*b*-Dex-APBA block copolymer micelle nanoparticles.

Chapter 2 presents a review of the literature on the current state of ocular drug delivery with a focus on platforms designed to improve the residence time on the ocular surface. This section also presents an outlook the market for nanomedicine and the current challenges to commercialization of nanomedicine. The role of mucus membranes, differences physiological environments, and strategies to exploit them are explored. Lastly, this chapter focuses preservation strategies for pharmaceuticals and alternate synthesis routes for block copolymer self-assembly into micelles.

Chapter 3 explores the reductive amination pathway for the conjugation of the mucoadhesive ligand onto the backbone of dextran. Factors influencing the conjugation efficiency of the reductive amination pathway are investigated. The findings with dextran (as a model) are used to improve the design of the study on PLA-*b*-Dex block copolymer micelles. Regression models are derived to predict and target the conjugated ligand concentration onto free dextran and PLA-*b*-Dex polymer.

Chapter 4 explores an alternate synthesis route for the conjugation of the mucoadhesive ligand (PBA derivative) onto the backbone of dextran. The synthesis route is based on solid-state chemistry via the Williamson ether synthesis pathway to enable a time and cost effective alternative. This solvent free method of carbohydrate modification is optimized for dextran as a model and is intended to reduce the synthesis time and complexity for the preparation of phenylboronic acid modified PLA-*b*-Dex block copolymer.

Chapter 5 addresses the challenge of poor shelf-life and instability of many nanoparticle suspensions and investigates freeze-drying to isolate the polymer particles from the aqueous media. The freeze-drying process is studied, and the optimal protectant type and concentration are determined per regulatory guidelines. A self-cryopreservation property was identified, and the components of the formulation are studied to identify the underlying cause.

Chapter 6 investigates an alternate synthesis route for the PLA-*b*-Dex-APBA block copolymer micelles. The findings from Chapter 5 are used to adapt a method of employing stresses created during the process of freeze-drying to drive self-assembly of the micelles.

Chapter 7 summarizes the major conclusions from the experimental work, Chapter 3 through Chapter 6, and proposes future work to further improve this block copolymer micelle platform as well as opportunities to further strengthen the portfolio of possible therapies.

Chapter 2
Literature Review

2.1 Overview of the Ocular Anatomy

The human eye can be broadly divided into the posterior and anterior segment. The posterior segment consists of the retina, vitreous humour, choroid, and back of the stroma, while the anterior segment consists of the cornea, iris, lens and aqueous humour[1]. The posterior segment constitutes the bulk of the ocular structure and is not visible (internal). This region is vascularized in contrast to the anterior segment which relies on the tear film to supply nutrients. The lack of vascularization in the anterior segment is a consequence of the cornea's transparency. This also means that there is a lack of a systemic immune response pathway on the surface of the eye. However, both segments of the eye are well adapted to removing foreign antigens and maintaining its integrity through a variety of biological barriers.

The cornea is a transparent dome, 0.5 mm thick structure covering the iris, responsible for focusing light rays[2]. The cornea itself is composed of five layers known as the epithelium, Bowman's layers, stroma, Descemet's membrane and the endothelium[2]. The organization of these layers forms barriers to transport of macromolecules and hydrophilic molecules into the anterior chamber; small lipophilic molecules may undergo passive diffusion but the transport is nevertheless hindered[2]. The epithelial multilayer (35 – 50 µm thick)[2] forms tight junctions which prevents the penetration of foreign molecules greater than 500 Daltons, including drugs, into the eye particularly hydrophilic molecules.

The Bowman's layer and stroma are composed of collagen composed of hydrophilic collagen fibrils, with the latter having a high water content. In combination with tight junctions, these layers act as barriers to hydrophobic molecules[2], while hydrophilic molecules and nutrients pass through the "leaky" endothelium to enter the anterior chamber[3]. The corneal endothelium is a monolayer of highly metabolically active hexagonal cells responsible for synthesis, transport, and secretion of the Descemet's membrane[2,3].

Furthermore, the tear film is a physiological barrier which aids in removal of foreign substances which might otherwise damage the sensitive organ[2]. The film is composed of three primary layers: the outer lipid layer, aqueous layer, and innermost mucus layer[2]. The lipid layer prevents evaporation of the tears and hinders passage of hydrophilic compounds. The aqueous layer lubricates the surface of

the eye and hinders hydrophobic compounds from reaching the tissue[2]. The mucus layer facilitates adhesion of the tears, and filters particles via size and charge exclusion due to the presence of negatively charged glycosylated proteins known as mucins which adopt a mesh-like conformation. The tear film is discussed further in Section 2.4.

The aqueous humour is found acts as a blood surrogate for the avascular cornea, providing nutrients and removing metabolites, as well as maintaining intraocular pressure (IOP). It is found in two chambers: i) between the cornea and the iris, and ii) between the iris and the lens[4]. The vitreous humour is a connective tissue with a gel like structure composed of 99.9% water, hyaluronic acid, and collagen[2]. It constitutes the bulk of the posterior segment i.e. the space between the lens and retina, and as such is clear and avascular.

The sclera is a dense irregular arrangement of collagen fibrils and mucopolysaccharides which create the opaque and white structure[5,6]. The structure is porous and poorly vascular, and continuous with the cornea extends to the back of the eye and is poorly vascular but porous[5]. The conjunctiva, a transparent membrane, covers the anterior scleral surface and lines the inside of eyelids[5]. Though the conjunctiva is more porous than the sclera and cornea offering a noncorneal route for molecules to enter the eye, it prevents the entrance of microbes[5].

The iris is a circular muscle which controls the size of the pupil to adjust the amount of light to permit into the eye which is then focused by the lens. The ciliary bodies are responsible for intercommunication between the anterior and posterior chambers as well for secretion of aqueous humour[5]. The retina is a light sensitive film responsible for converting the focused light focused by the lens into neural signals sent to the brain via the optic nerve. The choroid is a vascular layer which sits between the sclera and retina and provides nourishment to the outer retinal layers[2]. The blood retinal barrier is composed of retinal pigmented epithelial (RPE) and retinal capillary endothelial cells (RCE)[5]. The RPE cells are selectively permeable to nutrients from the choroid[5]. RCE cells form tight junctions[5] which limit permeability of molecules circulating in blood as well as proteins and hydrophilic compounds[7,8].

2.2 Conventional Ocular Drug Delivery

The eye consists of three layers: i) outer coat (sclera and cornea), ii) uveal coat (iris, ciliary body, and choroid), and iii) inner coat (retina)[2,9]. Delivery to the posterior segment (treatment of vitreous body and retina) is typically achieved through invasive treatments including intravitreal and periocular injections, or via systemic administration[1,10]. Treatment regimens generally require frequent injections over the course of the patients' lifetimes. Frequent administration via this invasive route can increase the chances retinal detachment, uveitis, and intraocular hemorrhages among other visually impairing conditions[1]. This, as well as the high risk of severe adverse effects which contribute to low patient tolerance[10].

Periocular injections are administered via the choroid or sclera and are a less invasive route to reach the posterior segment of the eye. After penetrating the sclera, the drugs may enter the posterior chamber. The major drawback is the short drug retention time[1,11,12]. Intravitreal injections administer the drug directly into the vitreous, typically near the retina. They are the only viable option at present for treatment of posterior segment diseases such as age-related macular degeneration (AMD) and diabetic retinopathy[5]. The vitreous impedes the movement of drug molecules due to the viscosity and high water content which hinders diffusion of hydrophobic molecules. Drugs administered via this route may also diffuse into the anterior segment[5].

Systemically administered drugs experience two major intraocular barriers, namely the blood-retinal barrier (BRB) in the posterior chamber and blood-aqueous barrier (BAB) in the anterior chamber[5]. Together, tight junction between retinal pigment epithelium, and tight junctions od the retinal vascular endothelium for the BRB. Drug molecules must overcome the hepatic second pass, and these barriers inhibit penetration of systemically administered drug into the intraocular chamber[1]. Only 1 – 2% of the administered drug can reach the retina and vitreous body. The low efficacy is paired with high risks for systemic side effects and frequent administrations[1].

Patients prefer non-invasive administration routes because they are painless and do not require professional intervention[13]. Topical administration is the preferred route for ocular therapeutics targeting the anterior segment of the eye[14] because of the simplicity and patient adoption[9]. Unlike eye drops, the distribution of the drug molecules administered via intravitreal injections may be heterogenous[1], and movement is diffusion dependent[15]. The conjunctiva is the layer of epithelium

lining the eyelids and sides of the sclera. Topically administered drugs may be absorbed through the conjunctiva, and then penetrate the poorly vascularized sclera.

The eye has what is known as immune privilege; this means that the detection of foreign substances is less likely to trigger inflammation due to the low expression of MHC class Ia molecules, increased complement inhibiting surface molecules, and local production of immunosuppressive cytokines such as TGF-beta, neuropeptides, and expression of Fas ligand as well as structures which limit lymphatic drainage[16]. This ultimately means that administered drugs are less likely to cause inflammation or damage to the ocular tissues.

Dosing forms include solutions, suspensions, and ointments with eyedrops accounting for 90% of formulations available in the market[10,11]. A small percentage of the topically administered drug dissolved in the aqueous humour may reach the posterior chamber. However, when topical administration is used for delivery to the anterior segment, only 5% of the administered dose is bioavailable for action at the target site. The remaining 95% is removed via several anatomical and physiological barriers.

2.3 Challenges to Topical Ocular Drug Delivery

The importance of vision to our evolutionary survival and quality of life cannot be understated. The eye is one of the few accessible organs for direct drug delivery. Nevertheless, eye has evolved various anatomical, physiological, and physiological barriers to protect itself against foreign agents.

The biggest challenges to effective treatment are the same precorneal physiological barriers which have evolved to protect the underlying tissue[9,14]. These include: tear film and tear turnover, nasolacrimal drainage, and blinking[1,14] to name a few. The cul-de-sac can only accommodate 30 µl of the administered dose resulting in the resulting volume being removed by nasolacrimal or gravity-induced drainage as well as via blinking[1]. The administered drug must also traverse through the dynamic mucus-aqueous tear film, discussed further in Section 2.4[9,13]. This results in only 5% of the administered dose is bioavailable for action at the target site[9,10,13]. Frequent administrations of concentrated solutions are required to overcome these barriers maintain therapeutic concentrations[9].

Glaucoma, for example, is a group of disorders characterized by progressive degeneration of the optic nerve (optic neuropathy) as a result of higher than normal IOP[17]. Atrophy of the optic nerve and loss of retinal ganglion cells produce visual field defects and subsequent loss of vision[17]. The disease has

a significant impact on one's quality of life and is the leading cause of irreversible blindness worldwide[18–20]. Dorairaj and Vianello report risks of falling and motor vehicle accidents increase by three and six times respectively for patients with glaucoma[21]. It is predicted that 111.8 million individuals will be affected in 2040 and 13% will suffer from acute bilateral blindness as a result[18,21].

Despite the availability of therapeutics in the market, the prevalence of glaucoma is a result of several factors. Firstly, the condition goes undiagnosed until it has begun to severely impair vision[21]. Secondly, patient compliance is key to effective treatment which requires maintenance of the therapeutic dose in the target tissue. This necessitates administration at regular intervals two or even three times daily[22]. Voluntary and involuntary noncompliance has been shown to result in higher IOP thus resulting in the progression of the disease[23].

Figure 2.1 illustrates the accumulation of drug over multiple dosage regimens if the concentration and dosing interval remain equal. The therapeutic window is defined as the drug level where the active pharmaceutical ingredient (API) has the desired therapeutic effect. In the figure, the therapeutic window is illustrated between the toxicity threshold and the minimally effective concentration. A single dose of drug is eliminated exponentially from the body and is generally insufficient to reach the therapeutic window. Several doses are required to maintain to build up and maintain the drug concentration within the therapeutic window.

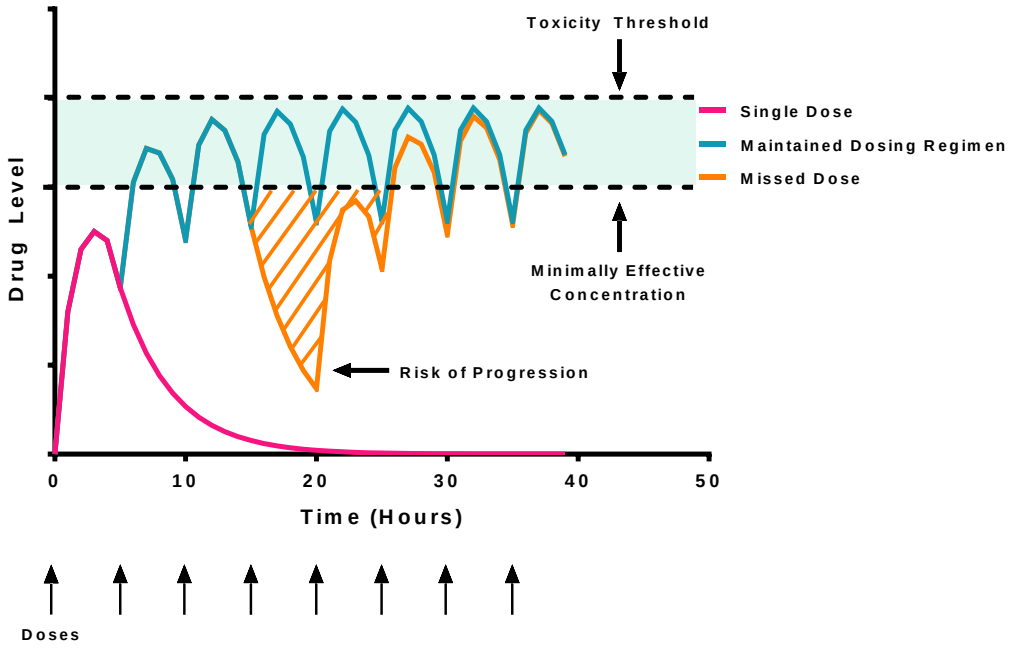

Figure 2.1: Multiple dosage regimen illustrating the loading period for a drug to reach therapeutic concentrations and the effect of a missed dose on the accumulated drug levels.

Non-compliance with a prescribed therapy or a missed dose as shown in Figure 2.1 results in a significant drop in the drug levels. Several consecutive doses are required to build up the drug concentration again. This problem is exacerbated when drug loading takes weeks or when several consecutive doses are missed. Diseases like glaucoma have a high risk of progression during this period as the current therapies act only to slow or inhibit the progression by eliminating the cause of high IOP. Similarly, patient non-compliance and non-adherence to prescribed therapies is an additional factor resulting in poor treatment efficacy.

Approximately 1.3 billion people globally are affected by vision impairment, 80% of which is considered avoidable in a report by the World Health Organization (WHO) in 2018[24]. Chronic conditions such as glaucoma can be controlled through strict adherence or compliance to a dosing regime of appropriate therapeutics, and proper administration techniques[25]. A 2005 study found an alarming 30% of their sample were subject to involuntary non-compliance specifically incorrect regimes[25]. A common phenomenon noted be Reardon et al. is the mistaken cessation of treatment by patients[26]. Non-compliance has been linked to progression of preventable diseases, and the lack of

response to treatment results in a cascade towards more toxic medication and complex regimes as described Buller et al[25].

The primary interest is to improve the bioavailability of drugs in ocular tissue to improve the efficacy of the treatment. Improving the efficiency of the delivered dose would result in a reduced administration frequency and a reduction in the dose concentration (reduction in adverse side effects). Developing a therapy which reduce the frequency of administration and improve the bioavailability of the therapeutic will improve the quality of life for the patient.

Common debilitating diseases have a high chance of resulting in severely impaired vision or blindness. Fortunately, ophthalmic pharmaceutical industry continues to develop novel therapeutic agents and strategies to improve the residence time and patient compliance to treat these ailments[9]. The global ophthalmic pharmaceutical market was valued at [27]USD 30.3 billion in 2018[27] and is expected to exceed USD 34 billion by 2026[28] with some projections as high as USD 42.6 billion[27–29].

2.4 Ocular Tear Film

The ocular tear film has a thickness of 3 – 10 µm with a volume of 10 µl and is composed of three distinct regions[9] as shown in Figure 2.2. The superficial lipid layer is the outermost layer with a thickness of 100 nm and is secreted by meibomian glands embedded on the eyelids[9,13]. The lipids act as a barrier to evaporation and help maintain the osmolality[9].

Tears are produced by the lachrymal gland in order to maintain the physiological processes, but may increase as a result of reflex and emotions[9]. The aqueous layer contains inorganic salts, carbohydrates, proteins, immunoglobulins, and glycoproteins[9]. The pH is maintained around 7.2 – 7.5[2], and the administered formulations must be buffered around physiological so as to mitigate irritation. The total turnover of tear volume ranges between 2 – 3 minutes at a rate of 15 – 30% per minute[5]. Majority of the topically administered dose is cleared within the first 15 – 30 seconds results in poor bioavailability (typically less than 5% of the administered dose)[5].

The mucus layer is secreted by goblet cells to facilitate adhesion of the tears, and to protect the underlying epithelia from damage by trapping foreign bodies and antigens[9,13]. The penetration of positively charged nanoparticles through the tear film overall is better than negative particles[13] which can be attributed to the negatively charged mucin. The volume of mucus secreted by the goblet cells is

2 – 3 µL, and the turnover rate is 15 – 20 h[9,13]. By targeting the mucus layer primarily, the retention of the drug on the ocular surface can therefore improve the efficacy of the therapy.

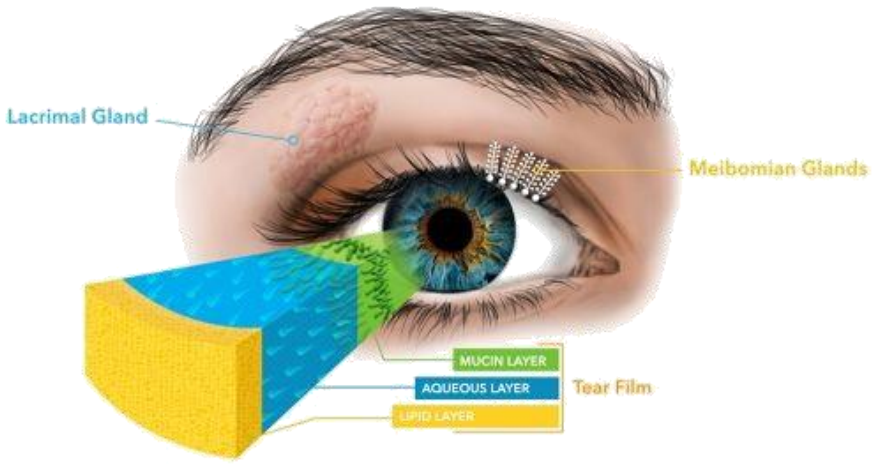

Figure 2.2: The normal ocular tear film and its three distinct layers: lipid, aqueous, and mucin. Lacrimal glands secrete aqueous layer, and meibomian glands secrete the lipid layer[30].

2.5 Mucus

The mucus membrane(s) or mucosa(e) separates internal and external environments and exist in various parts of the body. Mucosae play a major role in protecting the underlying epithelium by trapping and removing particles, bacteria and virus[13]. Under high shear stress, the mucus layer deform and behaves like a liquid, and an elastic solid under low shear[13]. Very few particles can permeate through the mucus layer without hinderance. Generally, only small uncharged molecules are able to pass, avoiding the size exclusion of the mucin mesh and electrostatic interactions with the negatively charged fibers[13].

On the ocular surface mucus allows the aqueous layer to spread over the ocular surface and facilitates adhesion of the tear film to the eye[13]. Mucus on the ocular surface is secreted by goblet cells located inside the bulbar conjunctiva[13]. Goblet cells are found in single layered epithelia such as those in the stomach, intestines, and lungs and mucus is secreted directly onto the epithelial surface[31]. Regions with stratified epithelia typically have adjacent tissue and glands which secrete the mucus such as salivary glands in the oral cavity[31].

The composition and properties of mucus as well as the production and clearance rates vary according to the requirement of the physiological regions[13]. Viscoelasticity can also be affected by the pH of the physiological region; pH of the ocular mucin is around 7.8[13]. The thickness of the mucus layer also varies by region; the ocular mucin layer is only 0.2 – 1 μm thick[13]. The mesh-like structure functions as a hydrogel to prevent water loss, lubricates surfaces and is part of the innate immune system[13]. Only 3% of the mucus membrane by weight is composed of solids (proteins, salts, lipids, and cellular debris)[13].

The most important class of proteins are mucins (large O-glycosylated proteins) which constitute 30% of all solids[9,13]. Tandem repeats of the proline, serine, and threonine (PTS) domains are linked by cysteine-rich domains which facilitate cross-linking into the mesh-like structure[13]. The diameter of individual fibers ranges between 3 – 10 nm with 20 – 30 carbohydrates per 100 amino acids in the PTS domain (approximate 25% of amino acids are glycosylated)[9,13,32].

The link is formed between the N-acetylgalactosamine of the sugar and hydroxyl groups on the serine and threonine residues[9]. The carbohydrates (comprising 80% of the dry mucin weight) are often terminated with fucose or sialic acid (N-acetylneuraminic acid)[13] shown in Figure 2.3. The high concentration of sialic acid residues and sulfates imparts a negative charge at physiological pH[9] which results in rigidity of the fiber via electrostatic repulsion[13]. Mucin oligomers are stabilized by a combination of entanglement and hydrogen bond formation between adjacent carbohydrate residues[9]. The tertiary structure is a result of hydrophobic interactions, entanglement, and disulfide bridges[9].

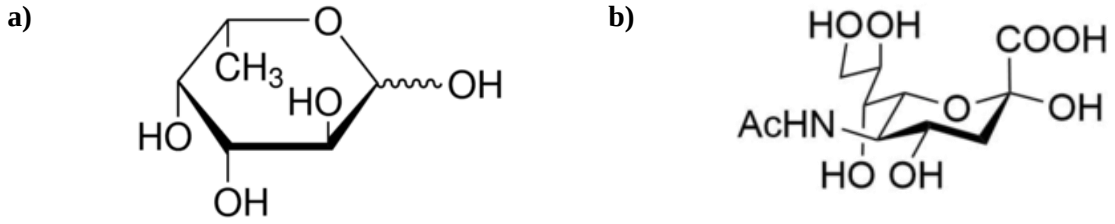

Figure 2.3: Structure of a) L-fucose and b) sialic acid, common components of N- and O-linked glycans such as those found as residues on mucin.

The mucosa may be bound to the epithelial surface existing as a gel layer (ten identified) or suspended (seven identified)[13,31]. Of the 17 known human mucins, five are expressed on the ocular surface with MUC5AC being responsible for the gel-formation and cationic shielding[9]. Alteration of mucin composition or distribution has been observed certain ocular diseases[9].

Generally, permeability through the mucin membrane is greater for particles of smaller size[13]. Positively charged molecules are trapped via electrostatic interactions with the negatively charged mucin fibers[13]. However, large molecules such as antibodies (30 – 60 nm) and antigens such as the polio and hepatitis virus are able to readily diffuse through mucus membranes[13]. By studying these macromolecules and their behaviour on the ocular surface nanoparticles can be engineered to avoid adhesion and circumvent the size exclusion by controlling the size[13] or to exploit the properties of mucin. Natural and synthetic polymers can form a variety of structures applicable in different dosage forms and encapsulated drug can be released at the site of action[13].

2.6 Mucosal Drug Delivery

Mucus membranes are found in various regions of the body including the mouth, nose and respiratory tract, the eye, and the gastrointestinal tract. Mucosal drug delivery is a strategy to exploit the physiochemical and physiological properties of mucosae to improve the bioavailability of a therapeutic in the target tissue or organ. There are three primary mucosal drug delivery strategies: i) mucoadhesion, ii) mucopenetration, and iii) mucolytics. Mucoadhesion aims refers to the adhesion of molecules or particles to the mucosae to increase the residence time above the underlying epithelium. Mucopenetration refers to the penetration of particles deeper into the mucosae resulting in a more uniform distribution closer to the epithelium. Mucolytic strategies disrupt the structure of the membrane to allow particles and drug molecules to reach the epithelium.

2.6.1 Mucoadhesion

Mucoadhesion has been successful for buccal and oral applications, and continues to be investigated for ocular formulations[9,33]. By adhering to the mucin, the nanoparticles are able to bypass clearance by the tear film[13]. For this reason, mucoadhesion is correlated with improved bioavailability[13].

Mucoadhesive nanoparticles have prolonged retention and facilitate sustained release of poorly absorbable drugs at the target site[13]. For mucoadhesion to occur, the particles must first overcome the repulsive forces and interact with the mucin via weak van der Waals attraction or hydrogen bonding. Due to their size, the nanoparticle-mucus interaction is more significant because the particles are much larger than the drug molecules[13]. It is proposed that mucoadhesion may result in less frequent administration, local targeting of the ocular tissue, a reduced administered dose and therefore reduced adverse side effects[33].

There are five primary models for mucoadhesion, though more are being proposed and explored[9,34,35]. The first theory is adhesion through wetting of surface irregularities by low-viscosity bioadhesives which then hardens anchoring to the surface[36]. The affinity between the surface and liquid must be sufficient to facilitate spreading and can be measured through contact angle measurements as higher affinity results in lower contact angle[36]. The spreadability is effectively a consequence of the surface and interfacial energy which may be controlled with composition to facilitate mucoadhesion[36].

The second approach of electrostatic attractions exploits the negative charge on mucin fibers [33,34]. Cationic polymers (e.g. chitosan), anionic polymers (e.g. carbomers, carboxymethylcellulose, and alginate), and non-ionic polymers (e.g. hydroxypropylmethylcellulose, hydroxymethylcellulose and methylcellulose)[33,34] have been utilized. Physiological conditions such as pH and ionic strength influence these electrostatic interactions[13]. Chitosan is able to interact with mucin only in neutral or alkaline conditions when its amine groups are deprotonated[13]. Some non-ionic polymers are bio-inert and can avoid entrapment until they have penetrated the mucosae, thereby increasing residence time. Alternatively, non-ionic polymers may be functionalized with ligands (such as amino acids) which are positively charged in physiological conditions.

Mucoadhesion is a combination of attractive and repulsive intermolecular forces. Anionic particles are generally repelled by the negative mucosa. However, the anionic polymer poly(acrylic acid) (PAA) has been very successful for mucoadhesion due to abundance of hydroxyl groups which form hydrogen bonds with mucin, best described by the adsorption theory[37].

The adsorption theory of mucoadhesion maintains that the adhesion is a consequence of chemisorption or chemical bond formation[36]. Secondary interactions such as hydrogen bonding, hydrophobic interactions and weak van der Waal's interactions are proposed to dominate this mechanism[36]. The carbohydrate groups are available for hydrogen bonding, and in fact help to stabilize the mucin oligomers and create a rigid structure[9]. The polymer may carry functional groups such as hydroxyl, carboxyl, amide, and sulfate on the backbone or can be functionalized with ligands capable of interacting with the mucin. Thiolated polymers adhere via disulfide bonds with the cysteine rich domains of the mucin[13]. Hydrophobic interactions between polymer and hydrophobic domains of mucin can result in interaction and subsequent entanglement as described by the diffusion theory. Lectins are proteins and glycoproteins which form specific reversible noncovalent bonds with the

carbohydrate residues on mucin[37]. They have been widely explored for application in drug delivery and particular for formulations designed for subsequent uptake into the epithelial cells[36].

The diffusion theory of mucoadhesion is based on the physical entanglement of the polymer chains with the mesh-like mucin structure[36]. Long chains have better bioadhesion because shorter chain particles are more rigid and thus has better diffusion[13]. The concentration of the mucoadhesive polymer can influence the strength of attraction and diffusion rates[13]. High molecular weight PAA has been widely used in literature for this application[33,34]. Generally no gain in adhesive strength is observed above a molecular weight of 100 kDa[36]. Some exceptions include dextran which exists in a helical conformation which shields adhesive groups as compared to linear polymer chains[36]. The degree of optimal entanglement varies between formulations, but the degree of cross-linking in the polymer has been shown to decrease the degree of diffusion[36]. As the degree of cross-linking increases, the particle becomes more rigid and is unable to hydrate and swell in order to anchor itself[36]. Furthermore, cross-linking can affect the encapsulation and release of drug molecules and hence must be optimized in combination with the mucoadhesive strength[31,36].

The fracture theory of adhesion assumes that the forces of adhesion and fracture are equal[36]. This theory has given rise to a method of determining the bio adhesive strength with tensile apparatus[36]. Films, patches and rigid or semi-rigid bioadhesives are well represented by this theory because this theory does not account for interpenetration and diffusion which is more common for flexible and polymeric bioadhesives[31,36]. Mucoadhesive platforms have been developed in various dosage forms to suit the target sites[36]. Oral strips were developed for oral delivery[36]. Films are promising alternatives for buccal delivery as an alternative to gels and pills. Nanoparticles and powders have been explored for nasal and ocular drug delivery[36]. They have proven utility for drug delivery because of the improved residence time of the dosage form resulting in higher bioavailability and sustained action[37]. In the cases of local delivery, the onset of action is rapid and bypasses the physiological clearance mechanisms and reduces systemic side effects[37]. The encapsulated therapeutic also benefits as it is protected from the harsh exterior such as acidic conditions in the gut[37]. Nevertheless, there are some drawbacks to mucoadhesive platforms resulting from the prolonged contact of the drug or drug containing surface a localized part of the body[37]. In some cases, ulcers have formed at the site of contact and, in the case of buccal mucoadhesive platforms, the formulation leaves a lingering taste or

eating, and drinking may be prohibited for a duration of time[37]. This can ultimately lead to low patient compliance for some of these formulations[37].

2.6.2 Mucopenetration

The mucoadhesive platforms suffer from poor penetration into the adherent mucus layer which has a slower clearance rate than the mucosal surface or luminal mucus layer where the mucoadhesive particles generally localize[33,38]. Mucopenetration is a strategy utilized to overcome this shortcoming by forming muco-inert particles which are able to resist entrapment until reaching deeper into the mucosa[38]. The improved diffusion in the mucosa also results in a more uniform distribution[33].

This technique has been particularly attractive for gastrointestinal drug delivery, specially targeting the intestinal mucosa[33,38]. However, the muco-inert property poses its own unique challenges resulting in elimination prior to penetrating the target[33]. The most popular approach in literate is to use a coating of poly(ethylene glycol) PEG which is a biologically inert, hydrophilic and uncharged polymer[33]. The molecular weight and the density of the coating are critical factors because a low density coating and high molecular weight PEG demonstrate adhesive properties[33,38]. The core nanoparticle size has also been shown to be a factor with larger particles (which can support denser surface coatings) exhibiting faster transport through the mucosa[33].

2.6.3 Mucolytic

Mucolytic refers to the disruption of the mucus membrane to facilitate diffusion and permeation through the mesh-like structure[38]. This technique is more sensitive to physiological factors which cannot be controlled such as the mucosa thickness, uniformity, and distribution[38] which vary between populations and disease states[9]. Disrupting the mucosa to enhance permeation of drug molecules or carriers will increase the risk of antigen permeation as well. However, this technique can be utilized for drug delivery for the treatment of some diseases where the mucus layer is abnormally viscoelastic such as cystic fibrosis and chronic obstructive pulmonary diseases (COPD)[39]. One of the progressive respiratory diseases encompassed under COPD, chronic bronchitis, and cystic fibrosis have an increased production of mucus. Using mucolytic agents such as Pulmozyme® has been shown to reduce the degree of cross-linking between mucin fibers resulting in decreased viscoelasticity and improved permeation for particles[38,40,41].

2.6.4 Buccal Mucosa

The buccal mucosa lines the inner regions of the cheeks and has been explored for the treatment of local and systemic conditions[36]. The buccal mucosa ranges between 0.1 – 0.7 nm in thickness and is a component of the saliva secreted by the salivary glands[36]. The underlying buccal epithelium ranges between 500 – 800 nm and is refreshed every 5 – 6 days[36]. Drug absorption may take place in the buccal mucosa as well as the soft palate, side of the tongue, and the mouth floor. This route has been successful for both hydrophilic drugs via paracellular transport and hydrophobic drugs via transcellular transport[36].

Due to the ease of access buccal and sublingual route of administration is the most common route of administration for mucoadhesive platforms[36]. The most popular dosage forms are gels and ointments due their ease of application but mucoadhesive tablets are the most common[36]. Dosage forms such as patches & films are also being explored but patient comfort and compliance are challenges[36]. Oral administration can also be easily terminated as compared to the other drug delivery platforms by removing the dosage form from the oral cavity[36]. Drug delivered via this method for systemic conditions may still suffer from hepatic first-pass clearance[36].

Boyapally et al. have developed theophylline (TPL) tablets composed of a blend of six mucoadhesive polymers (Carbopol®, polycarbophil, polyox, alginic acid, sodium alginate, and hydroxypropyl methylcellulose) for adhesion to the buccal mucosa[42]. The grade and ratio of polymer did not show significant effect on the adhesion and release pattern but did impact the release profile of TPL. The drug is water-soluble typically used for the treatment of chronic respiratory diseases such as asthma, emphysema, or obstructive pulmonary disease[42]. Through commercial administration routes the drug is highly metabolized resulting in low bioavailability, and in many cases insufficient for a therapeutic response[42]. Polyox tablets exhibited the highest adhesive strength attributed to the linear chains and high molecular weight facilitating interpenetration into the mucus and subsequent hydrogen bonding[42]. It was also concluded that the tablets prepared with polymers which facilitate fast swelling in water exhibited higher adhesion strength attributed to the rapid increase in surface area[42]. At slightly acidic pH the carboxylic groups on some of the polymers were ionized and thus unable to form hydrogen bonds but facilitate swelling[42]. The work demonstrated that the prolonged release of TPL and the patterns of release may be modified by changing the composition of polymer in the mixture[42].

Petelin et al. studied the in vivo effects of three bioadhesives in benzyl nicotinate (BN) ointments administered buccally in adult female Wistar rats[43]. The formulation with polymethyl methacrylate (PMM) had the lowest lag time, and highest increase in ΔpO_{2max} as compared to Carbopol and Orabase formulations[43]. The control ointment (absent of mucoadhesive polymer) had a lag time of only 10 min but the action was only sustained for 15 min whereas the ointment containing PMM sustained action for 40 minutes[43]. Despite the varying mucoadhesive strengths, an in vitro washing study showed that similar concentrations of the ointments remained on the oral mucosa surface[43]. The improved action was therefore attributed to the contact of PMM and the oral mucosa being more intimate which facilitates better permeation of BN[43].

Oral ointments tend to have a burst release followed by diminishing transient release[44]. Patches containing ionic mucoadhesive polymers were studied by Nafee et al. for the delivery of miconazole nitrate (MN), an antifungal agent used for the treatment of candidiasis. MN has previously been encapsulated within chewing gums and tablets, but patches tend to have higher patient compliance than these dosage forms[44]. The addition of MN (a hydrophilic molecule) into the polymer matrix resulted in greater swelling as compared to the plain patches but also increased the erosion rate[44], thus making the drug loading a limiting trade-off. The swelling creates pathways for MN to diffuse out; over time however, the diffusional pathway increases[44]. Patches with hydrophilic polymers had higher dissolution rate and drug release rate. Therefore, drug release in buccal patches can be controlled by controlling the swelling and dissolution rate. This has been demonstrated through the use of viscoelastic polymers such as poly(vinyl propylene) (PVP) and slightly more hydrophobic polymer such as hydroxyethyl cellulose[44]. The optimal formulations was determined to be 10% w/v poly(vinyl alcohol) PVA and 5% w/v PVP because they exhibited moderated swelling and adequate drug release owing to the slow dissolution[44]. The buccal patches sustained drug release 4.6 times longer at an elevated concentration despite being at a lower loading of MN (10 mg) as compared to the commercial ointment (25 mg)[44].

2.6.5 Nasal Mucosa

The intranasal cavity has a relatively large surface area of approximately 160 cm^2 and volume of 20 ml and is highly vascularized making it an ideal target for drug delivery[36]. The nasal mucosa is comprised of three cell types, basal cells, goblet cells, and columnar cells which facilitate the mucociliary movement responsible for clearance of the mucosa and trapped foreign particulates[36]. The goblet cells

and submucosal glands secrete the mucus layer which ranges between 5 – 20 μm in thickness and has a turnover of about 10 – 15 minutes[36]. The mucosa is strongly influenced by the presence of enzymes, irritation of the nasal cavity, increased mucocilliary action, and pathological conditions[36]. These factors can have a significant impact on the overall efficacy of the formulation[36]. Conventional formulations may experience reduced bioavailability, where as a mucoadhesive formulation may overcome these physiological barriers.

Systemic delivery through this route facilitates bypass of the first-pass clearance because the blood from the nose directly enters systemic circulation. The most common therapeutic delivered via the nasal route are vasoconstrictors for relief from nasal congestion. Systemic delivery of these drugs has been shown to cause cardiac episodes in patients with high blood pressure. This risk can be alleviated through targeted nasal delivery. Several formulations included microparticles have been successfully demonstrated for nasal delivery.

Jain et al. explored cross-linked mucoadhesive starch nanoparticles for insulin delivery via the trans-nasal pathway taking advantage of the highly vascularized surface area and large surface area[45]. The size of the nanoparticle was shown to influence the diffusion rate with larger particles having a relatively higher diffusional pathlength and therefore slower release[45]. With the addition of permeation enhancers, insulin loaded nanoparticles were able to sustain action for 6 h in streptozotocin induced diabetic rats[45]. The rapid release has been in part attributed to the correlation between the large surface area and concentration gradient[45].

Nasal inserts composed of chitosan have been studied for the delivery of chlorpromazine hydrocholirde (an antipsychotic drug) via the trans-nasal route[46]. The introduction of pectin resulted in a more porous structure during sublimation which improved the swelling capacity and therefore the mucoadhesion[46]. Under slightly acidic conditions the mucus and pectin both carry a negative charge but appeared to have stronger mucoadhesive properties as compared to the negative mucin and positive chitosan due to the differences in water uptake[46]. This suggests hydration and swelling which influence the polymer chain diffusion and ability to interact and entangle with the mucin have a stronger influence on the resulting net mucoadhesive force than electrostatic interactions[46].

2.6.6 Colorectal Mucosa

Oral administration is the most common and economic form of drug delivery overall, this method has several drawbacks including hepatic first-pass clearance, and degradation of the drug in the acidic environment[36]. The colorectal mucosa's primary function is to protect the tissue from friction occurring from its function and maintains pH near neutral[47]. The local environment has low enzymatic activity which is beneficial for drug delivery and access to the portal system and inferior vena cava enable bypass of the first hepatic pass[47]. A major challenge is the redistribution of administered drugs during bowel movements[47].

2.6.7 Ocular Mucosa

Various dosage forms have been successful or ocular drug delivery including ointments, inserts, gels, and liquid drops of drug solutions or suspensions[48]. The ocular mucosal environment has low viscosity and several physiological and anatomical barriers to foreign molecules which greatly limits the ocular retention of drugs[36]. As ophthalmic drug delivery is a primary focus for the particles discussed in this thesis examples of mucoadhesive dosage forms and platforms developed to increase the retention on the ocular surface are detailed in Section 2.7.

Thiolated poly(acrylic acid) ocular inserts achieved controlled release and were shown to maintain fluorescein (model drug) concentrations as opposed to unmodified poly(acrylic acid) inserts in human eyes[49]. The unmodified PAA inserts dissolved completely within 15 minutes of incubation in simulated lacrimal fluid at 32°C whereas modified inserts remained stable for 24 hours[49]. The cysteine modified inserts also demonstrated controlled release due to the matrix formation via disulfide bridging between the insert and mucosa in contrast for burst release observed for unmodified inserts[49]. Fluorescein administered via eye drops were completely removed from the ocular surface after 2 hours and a similar profile was observed for unmodified inserts due to the dissolution[49].

Eye drops generally experience rapid elimination from the ocular surface and alternate dosage forms are being studied for their improved retention. For example, Grześkowiak reports ocular ointments may remain on the surface for up to 8 hours[50]. Qi et al. addressed this issue with a thermosensitive *in situ* gelling system based on Carbopol, poloxamer and its analogs which attaches to the ocular mucosa and was shown to maintain in vitro release for a period of 8 hours[51]. Lux et al. developed a lyophilisate which are soft tablets which dissolve, typically intended for sublingual administration[52]. The

lyophilisate loaded with fluorescein was applied to the eye and resulted in corneal bioavailability 11 times higher, and anterior chamber bioavailability 8.7 times higher as compared to conventional fluorescein eye drops[52].

2.7 Nanosystems for Topical Ocular Drug Delivery

There are several challenges to conventional drug formulations and dosing forms resulting in poor bioavailability of the drug at the target site[14]. Majority of the administered dose is distributed systemically resulting in the metabolization and excretion of the therapeutic[10,14]. Hydrophobic drugs constitute approximately 60% of drug molecules[5,53]; hydrophobicity is correlated with poor bioavailability[14]. Consequently, the drug concentration cannot be maintained at therapeutic levels over extended periods of time necessitating frequent administrations and higher concentrations in the administered dose[11]. This is often the cause of adverse side effects and toxicity in non target organs[2].

Several nanosystems have been explored in literature to improve the bioavailability of the administered dose, and a few have already been commercialized. Some strategies include: improvement of retention time on the ocular surface, penetration enhances to access deeper tissue, and sustained release platforms to reduce the frequency of administration[11,48]. Furthermore, this method is non-invasive, portable, and is suited for self-application. However, the major challenge remains the low bioavailability of administered drugs. Researchers have been investigating various nanosystems to address this challenge.

Nanotechnology enabled therapeutics are regarded as the next generation of pharmaceuticals due to their ability to encapsulate and protect the drugs from physiological environments and targeting ability via a plethora of surface modifications. The term nanoparticle encompasses as variety of structures, composed of various molecules. One important consideration when developing nanotechnology for biological application is biocompatibility. Several reports published in literature are not practical due to the toxic nature of some of the structures.

Biocompatible polymers have already been approved by the United States Food and Drug Administration (FDA) and other regulatory bodies around the world. These polymers due to not illicit an immune response and are generally well tolerated, degrading within in the body without harmful degradation products. There are many factors which must be addressed during the process of drug formulation for it to be commercially successful. A variety of strategies are used to overcome the low

bioavailability in order to reach the therapeutic concentration. Furthermore, the formulation must be tolerable on the ocular surface and have a stable shelf life. The drug approval process is lengthy but may be reduced with a strong understanding of the regulatory bodies and their requirements. The polymer and it's degradation products should be non-toxic and nonabsorbable, as well as non-irritant to the mucus membrane[34].

2.7.1 Nanoparticles

Nanoparticles are by far the most investigated form of nanotechnology for use in ophthalmic therapeutics. Evaluation of nanoparticles for topical delivery started as early as 1986. Polybutylcyanoacrylate nanoparticles were the first to be researched in vivo to deliver progesterone [54], pilocarpine[55] and to evaluate the transport pathway of these nanoparticles[56]. Using radioactive progesterone, researchers found a 4-5 fold increase of tissue drug concentrations compared to a control solution containing the same amount of drug[54]. This increase in bioavailability was confirmed when the nanoparticle solution resulted in an increase in the area under the curve of a concentration time graph by 23% for pilocarpine as compared to the aqueous control solution[55]. There was an increase of elimination half life as well as a prolonged effect of drug[55]. As for the transport pathway, Zimmer *et al*. observed penetration of their particles transcellularly into the cornea and within conjunctival cells[56]. De Campos et al. in 2004 also investigated the in vivo fate of fluorescent chitosan nanoparticles and found 2-fold increase in concentration when compared to free chitosan-fluorescein solution and 4-fold increase compared to free fluorescein in the cornea and conjunctiva[57]. By tagging chitosan nanoparticles with fluorescein isothiocyanate-bovine serum albumin de Salamanca further showed in vivo uptake of nanoparticles by the conjunctiva and corneal epithelia; the bulbar conjunctival epithelium (apical membrane), palpebral conjunctival (throughout cells) and goblet cells indicated fluorescence[58]. Other studies also showed the uptake of nanoparticles into the conjunctiva and cornea [59–61].

Many groups have evaluated nanoparticle delivery of cyclosporine A, a drug used to treat inflammation. De Campos et al. in 2001 were the first, and used chitosan nanoparticles to achieve 2-6 fold higher therapeutic concentrations of drug in ocular tissues (cornea and conjunctiva) as compared to the chitosan aqueous solution with no significant differences in retention time[62] suggesting an increase in penetration of drug with the nanoparticle formulation. Yenice et al. in 2008 used hyaluronic acid coated poly-ε-caprolactone/benzalkonium chloride nanoparticles and found a close to 100-fold

increase in cyclosporine A concentration in ocular tissues compared to a castor oil solution of cyclosporine A[63]. Solid lipid nanoparticles increased retention 4-fold in rabbits[64] and demonstrated prolonged delivery of cyclosporine A for at least 48 hours to both the aqueous and vitreous humor in sheep[65].

In 2014, a topical formulation of chitosan nanoparticles was reported to deliver drugs to the aqueous humor and vitreous humor for 72 hours[66]. The researchers attribute this to the enhanced residence time at the corneal and conjunctival surfaces[66]. Eudragit® RL100 delivered cloricromene, an anti-inflammatory used to treat uveitis, increased the bioavailability compared to an aqueous solution of cloricromene[67]. Another nanoparticle formulation based on Eudragit® RL100 loaded with the anti-inflammatory agent aceclofenac showed a 2-fold higher penetration through the cornea, improved lid closure scores, and more effective immune cell inhibition compared to an aqueous solution with equivalent drug content[68]. Eudragit® RS100 was also evaluated for the delivery of piroxicam in vivo on rabbits with endotoxin-induced uveitis[69]. The nanosuspension treated eyes showed no clinical signs of uveitis compared to the control (drug only)[69]. Flurbiprofen, another anti-inflammatory ocular drug, was delivered using poly(lactic/glycolic) acid nanoparticles to rabbit eyes[70]. A commercial formulation of OcuFlur® was used as a control against a drug loaded nanocarrier prior to sodium arachidonate-induced inflammation; the nanoparticle formulation showed better prevention of inflammation than OcuFlur®[70].

Chitosan based nanoparticles and nanoemulsions containing indomethacin were evaluated and showed increased healing of corneal chemical ulcer as well as moderate effective inhibition of immune cell infiltration[71]. Zirconia beads delivered indomethacin also reduces post-operative inflammation and increases corneal penetration 4-fold compared to commercial eye drops[72]. Triamcinolone acetonide was evaluated by Sabzevari et al. in 2013 which showed that their poly β-amino ester biodegradable nanoparticles had a similar effect in inhibiting inflammation as a subconjunctival injection of the same drug[73]. Other anti-inflammatory agents such as flurbiprofen, oleanolic acid or ursolic acid and diclofenac sodium have showed prevention of sodium arachidonate induced inflammation[74] and higher retention in corneal tissues after administration in nanoparticle formulations[75,76].

As glaucoma is one of the leading causes of blindness, many IOP lowering therapeutics have been investigated using nanoparticle delivery. In 2002 Chu et al. delivered a pressure lowering compound

(7-hydroxy-2-dipropyl-aminoteralin) to rabbit eyes using calcium phosphate nanoparticles[77]. In this study the hypotensive effect of drug delivered using the nanoparticles was more pronounced than the free drug solution, they also found that the IOP decrease was sustained for at least 7 hours compared to 2 hours for the free drug[77]. Epinephrine was also evaluated as a glaucoma drug using poly-N-isopropylacrylamide nanoparticles which showed an IOP response which lasted 6 times longer than the control[78]. Timolol and dorzolamide are two other more commonly used drugs to treat glaucoma, Wadhwa et al. investigated their delivery in hyaluronic acid modified chitosan nanoparticles and showed significant reduction in IOP levels using nanoparticles in comparison to free drug solution[79]. As timolol is a beta-blocker, systemic absorption may induce undesirable cardiovascular side effects, in this study the researchers showed a higher decrease of IOP in the contralateral eye with the marketed formulation compared to the nanoparticle solution, showing that their formulation decreased systemic absorption of drug[79]. Dorzolamide bioavailability was also increased using 6-O-carboxymethyl chitosan nanoparticles[80], poly(lactic-co-glycolic acid)/vitamin E TPGS nanoparticles[81], γ-cyclodextrin nanoparticles[82,83], hybrid dendrimer hydrogel/poly(lactic-co-glycolic-acid) nanoparticles[84] and chitosan nanoparticles[85].

Carteolol is another beta-blocker and has been delivered using chitosan nanoparticles which prolonged precorneal retention as well as efficacy of the drug compared to cateolol aqueous solution[86]. In the same study, the researchers saw significant radioactivity (radiolabelled carteolol) in other body organs when delivered using nanoparticles, but radioactivity was seen in the systemic circulation as well as other organs after 6 hours with the aqueous solution of carteolol[86]. Dexamethasone was also evaluated by Gan et al. using monoolein liquid crystalline nanoparticles, and by Fabiano et al. using ammonium-chitosan conjugate nanoparticles showing similar results of prolonged effect and increased tissue levels of drug[87,88].

Methazolamide is another glaucoma treating drug which decreases the amount of fluid production within the eye by inhibiting the enzyme carbonic anhydrase. Chen et al. used calcium phosphate nanoparticles to deliver it into rabbit eyes which showed a drop in IOP for 18 hours, which is significantly prolonged compared to commercial eye drops AZOPT® (briminodine) with a 6 hours effect of lowering IOP[89]. Solid lipid nanoparticle delivered methazolamide also showed higher therapeutic efficacy and a prolonged effect compared to AZOPT®[90]. Cationic nanostructured heterolipid matrices[91] and solid lipid nanoparticles modified with low molecular weight chitosan[92]

lowered IOP for a longer duration than free methazolamide solution and AZOPT® respectively. Another carbonic anhydrase inhibitor, acetazolamide, shows a longer and stronger effect of lowering IOP compared to 0.5% acetazolamide when delivered using Eudragit® RL100 nanoparticles with an equivalent drug dose; IOP lowering was also prolonged with the nanoparticle solution[93,94].

IOP lowering effects of nanoparticle delivered brimonidine showed significant improvement of drug effects compared to commercial eyedrops Iobrim®[95] and Alphagan®P[96]. Yang et al. also investigated brimonidine and was able to lower IOP in normotensive rabbits by 18% for 4 days[97]. Brinzolamide is also used to lower IOP; liquid crystalline nanoparticle delivered brinzolamide was contrasted with AZOPT® and was superior in drug concentration in tissues, permeability and efficacy[98]. Melatonin's hypotensive effect has been investigated and when delivered in nanoparticles the compound was more efficacious than when delivered in aqueous solution[99,100]. Lastly, disulfiram's ability to reduce IOP was evaluated with delivery using nanoparticles. The nanoparticle delivered drug remained on the ocular surface 1.45-fold longer, and the IOP decreased more with the nanoparticle solution than the free drug solution in rabbits[101].

Antibiotics are another class of drugs commonly used topically for ocular infections. Cavalli et al. in 2002 delivered tobramycin using solid lipid nanoparticles and showed a 50% maximum aqueous humor concentration increase when compared to Tobral®, the commercial formulation[102]. Another group researched poly(D,L-lactide-*co*-glycolide) nanoparticle delivered sparfloxacin to show longer pre-corneal retention; using gamma scintigraphy and radiolabelling of sparfloxacin the researchers also showed that after commercial formulation administration significant radioactivity was recorded in the kidney and bladder after 6 hours, but this radioactivity was not seen after nanoparticle formulation administration of drug[103]. Chitosan delivered moxifloxacin, another antibacterial agent, increased bioavailability fourfold in the aqueous humor after a single topical instillation[104]. Levofloxacin delivered using nanoparticles showed similar results with radioactivity seen throughout the rabbit body tissues after commercial product administration but not after nanoparticle delivery of the same dose[105]. Gatifloxacin is another antimicrobial drug and Kalam and colleagues delivered it using solid lipid nanoparticles to find a 3.37-fold increase in relative bioavailability compared to the commercial product[106]. The last antibiotic agent that has been delivered using nanoparticles is sparfloxacin. With poly(lactic-co-glycolic acid) nanoparticle laden in situ gel and radiolabelled sparfloxacin, an increased retention of drug was found compared to the commercial formulation and while radioactivity was seen

in the kidney and bladder after administration of the marketed formulation, none was seen with the nanoparticle in situ gel formulation[107].

Antiviral agents such as acyclovir have been evaluated for topical delivery using nanoparticles as well. Giannavola et al. delivered acyclovir using nanospheres which increased aqueous humor levels of drug by 12.6-fold[108]. Furthermore, as the ocular surface may be affected by the herpes simplex virus type I (HSV-1), researchers have investigated ocular vaccination. Hu et al. looked into iron oxide nanoparticles coated with glutamic acid for herpes stromal keratitis prevention with a HSV-1 vaccine[109]. Higher levels of neutralizing antibodies in tears and enhanced cytotoxicity of natural killer cells were seen after administering nanoparticles containing the deoxyribonucleic acid (DNA) vaccine compared to the control. Keratopathy scoring furthermore showed a lesser degree of herpes stromal keratitis when compared to the mice receiving the vaccine alone (without nanoparticle vehicle)[109].

Exonazole, an antifungal agent, was delivered using chitosan/sulfobutylether-β-cyclodextrin nanoparticles and tested in vitro as well as in vivo[110]. Although there was no difference in inhibition of C. albicans in vitro between commercial product and nanoparticle solution, there was a significant improvement of antifungal activity in vivo when delivered using nanoparticles[110]. Natamycin delivered using mucoadhesive lecithin/chitosan nanoparticles showed a 7.4-fold improvement compared to the commercially available suspension[111]. Amphotericin B is commonly used for treating fungal infections and when delivered via poly(lactic acid)-grafted chitosan copolymer nanoparticles, residence time of the drug on the ocular surface is prolonged and permeation is markedly increased[112]. Lecithin/chitosan nanoparticles were also used to deliver amphotericin B for the treatment of fungal keratitis in a rabbit study which showed a significant increase in bioavailability as well as precorneal residence time compared to Fungizone®[113].

Gene therapy has also been investigated by multiple research groups. de la Fuente et al. in 2008 evaluated hyaluronan-chitosan nanoparticles for gene delivery across the ocular mucosa. They showed that the nanoparticles became assimilated by corneal and conjunctival epithelial cells and efficient delivery of fluorescent plasmid DNA using nanoparticles resulting in reaching significant transfection levels; fluorescence was maintained for more than 7 days[114]. Zorzi et al. reported successful gene delivery of MUC5AC messenger ribonucleic acid (mRNA) into conjunctival cells using cationized gelatin nanoparticles[115] as did Contreras-Ruiz et al. in 2013[116]. Cationic core-shell lipo-nanoparticles to deliver genes have also been studied using fluorescent protein as a reporter gene; compared to regular

chitosan nanoparticles there was a 2.52-fold increase in fluorescent protein expression[117]. DNA delivery using plasmids has also been investigated using non-viral gemini surfactant-phospholipid nanoparticles which showed localization of nanoparticles to anterior chamber tissues[118]. Gene therapy for X-linked juvenile retinoschisis using dextran and protamine-based solid lipid nanoparticles showed transfection into corneal cells after topical application[119]. In 2013, Tandon et al. successfully transferred the BMP7 gene into rabbit keratocytes which decreased corneal haze scored with the Fantes grading scale[120]. Gene silencing using biopolymer based nanoparticles showed internalization of nanoparticles into the corneal and conjunctival tissues which provided a significant synthetic RNA (siRNA) gene silencing effect[121].

Other substances investigated for nanoparticle delivery include 5-fluorouracil[122–124], baicalin[125], pirfenidone to treat alkali burn[126] and mitogenic protein lacritin[127] which all showed either an increase in bioavailability or an increase in efficacy of corneal healing and wound regeneration. Nanoparticles coated with anti-TLR4 antibodies were shown to anchor ketoconazole loaded gelatin nanoparticles and also resulted in a down-regulation of inflammatory cytokine levels in eyes with keratitis[128]. Chi et al. investigated the efficacy of nanosheets compared to nanoparticles, concluding nanoparticles demonstrated superior permeability in isolated corneas and prolonged precorneal retention time in vivo[129]. Dexamethasone delivered via lipid nanoparticles was observed in rabbit aqueous humour for up to 24 hours, compared to 8 hours for the aqueous suspension[130]. In 2016, Liu et al. published work on a mucoadhesive polymeric nanoparticle with a residence time exceeding 24 hours. Restasis, a suspension of cyclosporin A, is typically administered twice daily (b.i.d) or thrice daily (t.i.d), but the drug loaded nanoparticles demonstrated elimination of inflammation and recovery of ocular surface goblet cells in mice. This formulation improves the residence time and bioavailability of the drug and aims to improve patent compliance through a reduction in overall dosage[131].

2.7.2 Liposomes

Liposomes are some of the earliest nanostructures investigated for their potential in drug delivery due to their biodegradable and biocompatible nature. The inner aqueous core is protected by a phospholipid bilayer. Liposomes are spherical vesicles that have an aqueous core and an outer phospholipid bilayer, liposomes are inherently biodegradable and nontoxic. Hydrophilic drugs may be encapsulated within the core, while hydrophobic drugs can be trapped with the lipid layer.

Research of liposomes for ophthalmic purposes began as early as 1982, when Stratford et al. evaluated L-α-phosphatidylcholine and cholesterol liposomes for the delivery of epinephrine and inulin[132]. These liposomes increased inulin pre-corneal residence time and delivery to ocular tissues but, actually decreased epinephrine delivery[132]. In 1987 acetylcholinesterase, a prophylactic drug, was evaluated in its ability to counteract the toxicity of diisopropylfluorophosphate (DFP) which causes a decrease in pupillary size, the researchers found that the positively charged liposomes provided the best prophylactic effect (80% pupil size) while free acetylcholinesterase showed no protection against the DFP challenge (50% pupil size)[133]. Enhanced pre-corneal retention of drugs and increased bioavailability was also shown in delivery of tropicamide[134,135]. Pre-corneal retention was measured using gamma scintigraphy and bioavailability measured using the mydriatic activity (pupil dilation) of tropicamide which showed significantly increased effects when delivered using liposomes compared to an aqueous solution[134]. The same group evaluated pilocarpine delivery using mucoadhesive liposomes and demonstrated that mucoadhesive polymer (Carbopol® 1342) coated liposomes delivered drugs for a prolonged duration[136]. The next year the delivery of FK506 in olive oil as a vehicle or liposomes was compared; concentrations of drug in the aqueous humor was substantially higher for the liposome (5-28ng/g) compared to the olive oil (0.1 – 2 ng/g) formulated drug[137].

Topical delivery of plasmid DNA to intraocular tissues was evaluated using liposomes and the researchers found that topical delivered liposomes are capable of transfecting retinal ganglion cells[138] and delivering fluorescent molecules to the retina[139]. Researchers also showed that liposome gels are capable of delivering oligonucleotides to rabbit ocular tissues in higher concentrations than liposomes alone[140]. Topical drug delivery to the posterior segment was also achieved by Lajunen et al. using liposomes with a diameter of less than 80nm which penetrated to the posterior layer of the retina; they found that liposomes larger than 100nm ended up in the choroidal endothelium[141].

In 1998 Srinivasan et al. incorporated penetration enhancer polyoxyethylene-9-lauryl ether with liposomes to deliver insulin[142]. They demonstrated prolonged drug action when delivered topically using liposomes (more than 5 hours) compared to administration subcutaneously and intravenously (2 hours)[142]. Insulin delivery was also investigated by Jain et al. in 2007 using liposomes coated with chitosan and Carbopol®; they found increased bioavailability as their liposome formulation showed a 30% reduction of blood glucose levels up to 24 hours whereas control formulations show no effect after approximately 10 hours[143]. Chitosan-coated liposomes were used to deliver coenzyme Q10, the

liposomes prolonged the retention time by 4.8-fold compared to control[144], to deliver ciprofloxacin which showed 1.737-fold permeability compared to free drug solution[145] and a 2.76-fold increase in drug residence time compared to the commercially available drug[146]. Chitosan-coated liposomes were further used to deliver vitamin A palmitate where the bioavailability increased by 16.6-fold compared to Oculotect® gels[147]. Other mucoadhesive polymers (sodium hyaluronate and carboxymethylcellulose) have been incorporated into liposomes to increase efficacy[148].

Acyclovir delivery using liposomes was investigated by three different groups which found liposome encapsulated acyclovir to significantly increase drug levels in the aqueous humor (88.95 μg/mL) compared to free drug solution (2 – 3 μg/mL)[149], increased pre-corneal residence time[150] and increased bioavailability[151]. Cortesi et al. delivered anti-herpetic peptides in rabbits and found that when vaccinated using their liposomal formulation before the herpes-simplex virus (HSV) infection rabbits were protected from this lethal infection[152]. For the treatment of acyclovir resistant HSV, distamycin A is used; liposome delivered distamycin A reached IC50 values without any transcorneal penetration, decreasing cytotoxicity as well as doubling precorneal retention compared to free drug solution[153].

Hathout et al. demonstrated that positive multilamellar acetazolamide liposomes increased bioavailability by measuring reduction in IOP for a prolonged duration in rabbits[154]. Diltiazem hydrochloride is also used to decrease IOP and liposome delivered drug had a significantly prolonged period of activity (24 hours) compared to free drug solution (5 hours)[155]. In ganciclovir delivery, Shen et al. found that there was no difference in pre-corneal elimination rate between the liposome formulation and free drug solution[156]. But, the ocular distribution of drug via liposomes was 2 – 10 fold higher in the sclera, cornea, iris, lens and vitreous humor when compared to free drug administration[156], suggesting that uncoated liposomes increase corneal penetration rather than pre-corneal retention. Interestingly, a group evaluated the use of a liposome topical spray in increasing the lipid layer thickness and were successful in improving the lipid layer significantly at 30 and 60mins post treatment[157].

Another class of drugs delivered using liposomes are the antifungals, Habib et al. evaluated fluconazole delivery in rabbits and found that 86.4% of rabbits showed complete recovery with the liposomal formulation compared to only 50% of rabbits delivered free drug solution[158]. Voriconazole, another antifungal drug, was successfully delivered in porcine cornea to a concentration higher than the

minimal inhibitory concentration of several fungi species which cause clinical cases of corneal keratitis[159]. Liposome delivered substances can furthermore prevent light induced retinal damage[160]. As shown by Shimazaki et al. in 2011 where edaravone delivered in liposomes prevented increase of cells with DNA marked by fragmentation signals in mice[160]. Shafaa et al. showed a noteworthy increase in bioavailability of timolol maleate when they tested efficacy in glaucomatous rabbits; liposome delivered drug decrease intraocular pressure for 160 hours whereas the free drug showed no activity after 5 hours[161]. Hyaluronan modified liposomes delivering doxorubicin exhibited more than 4-fold increased retention time as well as a 1.7-fold increased area under the curve for aqueous humor concentration[162].

Liposomes have high precorneal clearance rates due low viscosity. Yu et al. employed the interaction between gellan gum and the cations in tears for in situ gelling. Higher retention times on the ocular surface, and a decrease in IOP for a longer duration than the bare solution was reported. Release profiles can be tuned by controlling the extent of gelation[163]. A formulation of liposomes encapsulated with montomorillonite intercalated with betaxolol hydrochloride was used by Huang et al. and which maintained the drug concentrated on the ocular surface and resulted in prolonged reduction in IOP[164]. Nasir and colleagues concluded that liposomes are more effective for delivery for lipophilic substances. Compared to topical suspensions of hydrophilic molecules, liposomes resulted in a lower precorneal concentration[165].

2.7.3 Nanoemulsions

Oil/water nanoemulsions are capable of solubilizing hydrophobic drugs and may act as penetration enhancers for corneal drug delivery. They are capable of distributing more uniformly on the corneal epithelium but suffer from extensive precorneal loss. To overcome this challenge, Morsi *et* al. have demonstrated sustained drug release using a mucoadhesive gellan/xanthum gum capable of ion induced in situ gelling by incorporating a nanoemulsion[166]. The dispersed peanut oil was stabilized with a surfactant and cosurfactant mixture of Tween® 80, Cremophor EL®, and Transcutol® P was used to encapsulate acetazolamide. The mucoadhesion prevents rapid drainage and extends the precorneal residence time[166].

2.7.4 Dendrimers

Dendrimers are nanosized, highly branched, star shaped polymeric systems. The branched structure of dendrimers allows both hydrophobic and hydrophilic drugs to be incorporated into the structure. Furthermore, the highly branched structures provide many terminal end functional groups which can be utilized to conjugate targeting moieties[167].

Vandamme et al. investigated drug delivery using poly(amidoamine) (PAMAM) dendrimers to deliver plocarpine nitrate and tropicamide[168]. Pre-corneal residence time was evaluated using 2 w/v% fluorescein and an increase from 30 minutes to 4 – 5 hours was observed with incorporation of dendrimers. Furthermore, the miotic and mydriatic activity of pilocarpine nitrate and tropicamide were increased and prolonged when combined with dendrimers[168]. In 2010 Durairaj et al. reported a dendrimeric polyguanidilyated translocator system for the delivery of gatifloxacin[169]. The dendrimeric gatifloxacin system increased the areas under the curve for concentration by ~13-fold in the conjunctiva and ~2-fold in the cornea when compared with free gatifloxacin after a single instillation in vivo. Furthermore, a single dose of the drug-dendrimer system made drugs detectable in the cornea for up to 6 hours in the cornea whereas the control showed drug in the cornea for up to 2 hours[169]. Also in 2010, researchers developed puerarin and PAMAM dendrimers which prolonged the residence time compared to puerarin eye drops. The dendrimer solution half life was approximately 1.8 hours compared to the control eye drops 0.8 hours[170]. The delivery of acetazolamide using poly(propyleneimine) dendrimers was evaluated and ocular residence time was found to increase by more than 10-fold compared to the free drug solution; a reduction in intra ocular pressure with the dendrimer solution persisted for twice as long as the free drug solution[171]. Romanowski et al. utilized polyanionic dendrimers to inhibit adenovirus related ocular infections. The charged dendrimer was shown to adhere to the virus and inhibit penetration into potential host cells in New Zealand White rabbits[172].

Bravo-Osuna et al. developed acetazolamide eyedrop formulations utilizing anionic and cationic carbosilane dendrimers. Formulations containing a small fraction of cationic carbosilane dendrimer led to a rapid and extended hypotensive effect. Anionic dendrimers exhibited non-permanent adhesion, likely due to electrostatic repulsion with the negatively charged mucin[173]. Work by the same group on surface plasmon resonance to investigate interactions between mucin and dendrimers reveals that dendritic structures such as PAMAM display strong permanent interactions with transmembrane ocular

mucins[174]. Liu et al. explored PAMAM dendrimer formulations containing a penetratin and red fluorescent protein plasmid for intraocular gene delivery to the posterior segment of the eye via a non-corneal pathway as a substitute for intravitreal injections. The formulations were instilled in the conjunctival sac of rats, and evaluations revealed expression of the fluorescent protein in the posterior segment of the eye[175].

2.7.5 Nanomicelles

Nanomicelles are composed of fatty acid molecules which arrange themselves into a spherical form in aqueous solutions, with the hydrophilic heads of the lipids facing outward and hydrophobic chains in the inside of the structure. The beginnings of nanomicelle in vivo testing for bioavailability began with Gupta *et al*. in 2000 who evaluated nanomicelles made of copolymer *N*-isopropylacrylamide, vinyl pyrrolidone, and acrylic acid for ketorolac delivery[176]. Albino rabbits with induced inflammation were used as the animal model. The free drug solution did not show any inhibition of lid closure or polymorphonuclear (PMN) migration but, the nanomicelle formulation inhibited lid closure for 3 hours and PMN migration for 5 hours[176].

In 2001, Liaw and colleagues used nanomicelles to deliver genes[177]. Plasmids with the lacZ gene were administered topically three times a day for two days onto rabbit eyes and showed expression around the iris, sclera, conjunctiva, and lateral rectus muscles for 48 hours (detected using X-gal staining). This is significant because no expression was detected in the ocular tissues of eyes in which naked DNA plasmids were delivered, the negative control group[177]. Tong et al. also investigated gene delivery with nanomicelles; they specifically looked at gene delivery with cornea-specific promoters[178]. The enzymatic activity of the gene delivered significantly increased in both mouse and rabbit corneas[178]. The same authors investigated delivery of anti-apoptotic genes in rabbits with model epithelial injury induced by epithelial debridement. The mRNA of the anti-apoptotic gene was significantly increased (2.2-fold) at 48 hours after administration compared to non-treated rabbits[179].

In 2010 two groups studied dexamethasone delivery using nanomicelles[180,181]. Pepic et al. found a prolonged decrease in intraocular pressure as well as a 2.4-fold increase in area under the curve for the concentration of drug delivered with chitosan nanomicelles compared with a standard dexamethasone suspension[180]. Rafie et al. applied the nanomicelle formulation to rabbits with endotoxin-induced uveitis and measured inflammation using Hogan's classification. Both the nanomicelle formulation and free dexamethasone solution reduced symptoms of uveitis for 48 hours after endotoxin injection, but

there was a significant difference between the two formulations after 24 hours[181]. Nanomicelles used to deliver diclofenac showed a 2-fold increase in area under the curve for 24 hours compared to the drug in phosphate buffered saline solution[182]. Chitosan is often incorporated into ocular drug formulations as it is mucoadhesive. For example, pluronic-chitosan micelles were shown to be superior to commercial eyedrops delivering metipranolol [183]. Permeation is also increased with nanomicelles as shown by Salama et al. who used tri-tetra-block co-polymeric nanomicelles to deliver lornoxicam [184]. Beack et al. contrasted a topical suspension of Flt1 peptide- hyaluronate conjugate micelles with a subconjunctival injection in a murine model. The topically administered micelles demonstrated an increased residence time on the corneal epithelia. Furthermore, the topical suspension administered BID for two weeks resulted in a comparable therapeutic effect subconjunctival injection administered once for 2 weeks [185].

In 2015, Li et al. demonstrated deep corneal penetration of fluorescein dye loaded micelles composed of poly(ethylene glycol)-poly(e-caprolactone)-g-polyethyleneimine triblock copolymer. Within 30 minutes of administration, a fluorescent signal corresponding to the fluorescein was observed in the stromal layers of the cornea[186]. Shi et al. formulated a nanosuspension of Nile red encapsulated within chitosan grafted chitosan grafted methoxy poly(ethylene glycol)-*b*-poly(e-caprolactone) micelles. Compared to the aqueous solution of the dye, the micellar formulation demonstrated enhanced pre-corneal retention and penetration. The same system used for the delivery of encapsulated diclofenac resulted in the 2.3 times higher aqueous humour concentration compared to commercial eye drops[187].

Liu et al. investigated Cyclosporine A encapsulated micellar nanoparticles for the treatment of dry eye. The suspension, administered once or twice a week, resulted in a slight increase of tear production 7 days after induction of dry eye in rabbit models. Furthermore, clearance of inflammatory infiltrates and complete restoration of the ocular surface was observed. In contrast, Restasis, a commercial formulation of Cyclosporine A, was topically administered t.i.d and did not show improvement in tear production 7 days after induction of dry eye[188].

2.7.6 Niosomes

Niosomes are vesicles made of non-ionic surfactants and are biodegradable. Studies have shown that niosomes are more stable than liposomes[189], offering greater chemical stability at a lower cost as compared to liposomes[190]. They can entrap both hydrophobic and hydrophilic drugs. Some non-ionic surfactants commonly used for ocular delivery are Solulan™, chitosan, Carbopol® and dicetylphosphate. Researchers have also shown that minimal side effects occur and no irritation was seen when niosomes are administered topically[191].

Timolol maleate delivery using niosomes coated with chitosan or carbopol showed an effect for up to 8hrs compared to the control solution's effect of 2 hours[192]. The same group showed a decrease in drug entering the systemic circulation as the intraocular pressure of the contralateral eye (untreated) decreased by 20 – 40% (of treated eye) with niosomal formulations and 100% with the marketed gel formulation[192]. Acetazolamide delivery using niosomes was investigated by two groups who found an increase in efficacy as well as duration of effect[193] and a comparable efficacy to Dorzox® with a 4-fold lower concentration in the niosomal formulation[194]. Flurbiprofen (FBP) is a nonsteroidal anti-inflammatory drug prescribed for ocular inflammatory diseases and following procedures such as cataract surgeries. Span® 60 niosomes in a gel formulation loaded maintained FBP concentrations in the aqueous humour for almost 12 hours, thereby contributing to higher useful absorption[190].

Carbopol® is a bio-adhesive commonly use in topical preparations to improve residence time. A carbopol hydrogel containing Span® 60 niosomes encapsulated with atenolol resulted in greater reduction in IOP as compared to the hydrogel or noisome alone[195]. Zubairu et al. also prepared bio-adhesive Span® 60 niosomes (surfactant:cholesterol = 50:50) with chitosan. The formulation was retained on the ocular surface for more than 12 hours[196]. Lomefloxacin is an antibacterial requiring frequent administration (up to 8 times a day). This motivated Khalil et al. to develop a niosomal formulation which demonstrated a biphasic release behaviour[197]. Two key factors to consider niosomal vehicles are the properties of the surfactant, and surfactant:cholesterol ratio[197].

2.7.7 Nanocapsule

Nanocapsules are made of a thin polymer membrane which encapsulates an oily or aqueous core. Researchers have investigated the use of nanocapsules for delivering metipranolol, a beta-blocker. Using a colloidal suspension of poly-ε-caprolactone nanocapsules with an oil core, Losa et al. showed comparable efficacy to commercial eye drops Betamann® and a reduction of cardiovascular side effects measured directly and indirectly with their nanocapsule formulation of metipranolol[198]. Compared to the commercial product, the duration of bradycardia was greatly reduced when metipranolol was delivered using nanocapsules[198]. The same group further evaluated metipranolol delivery using the same nanocapsules incorporating polyisobutylcyanoacrylate by measuring the ability of a beta-adrenergic agonist (isoprenaline) to increase heart rate, an indirect measure of systemic levels of metipranolol. Again, systemic effects were drastically lowered while the pharmacologic response was unaffected[199]. Another beta-blocker carteolol was delivered using poly-ε-caprolactone nanocapsules and compared to Carteol eye drops; the researchers found a decline of cardiovascular side effects, measured indirectly using isoprenaline, in comparison with the aqueous eye drops which suggests reduced undesirable non-corneal absorption[200].

Calvo et al. investigated indomethacin delivery using poly-ε-caprolactone[201] and chitosan-coated and poly-L-lysine-coated poly-ε-caprolactone[202] nanocapsules. These nanocapsule formulations increased drug concentrations in the cornea, aqueous humor, iris-ciliary body more than 3-fold compared to the commercial solution as well as increased ocular penetration[201,202]. The same group evaluated polyester nanocapsules with an oily core of Migliol 840 for cyclosporine A delivery[203]; drug levels in the cornea increased up to 5-fold with the encapsulated cyclosporine A compared to an oily solution of the same drug[203]. Reimondez-Troitino et al. synthesized arginine-rich polyarginine and protamine nanocapsules for the delivery of cyclosprin-A and vitamin A. The positive domains contribute to the interaction and adhesion of the nanocapsules to corneal epithelial cells[204].

In 2000, Desai et al. used a Pluronic® F127-based gel system with polyisobutylcyanoacrylate nanocapsules to deliver pilocarpine, they found that the nanocapsule and gel together increase contact time of pilocarpine with the surface of the eye and therefore increased ocular bioavailability[205]. Lastly, De Campos investigated the interaction of chitosan coated and PEG coated nanocapsules with the eye's surface[206]. They found that chitosan coated systems especially enhanced penetration of the

encapsulated dye through the cornea, furthermore, the coating of the nanocapsules affects bio-distribution which can be used as a targeting strategy[206].

Carbone et al. developed dioctadecylammonium bromide (DDAB) coated, positive nanocapsules for ocular delivery of hydrophilic compounds without significant energy input making them eco-friendly[207]. An aqueous phase containing a combination of Brij® 98 with Span® 60 or Span® 80 was introduced into the oily phase containing PLA or capric triglyceride (CTC)[207]. To modulate surface properties and to impart a positive charge, the nanocapsule was coated with DDAB. The positive charge is capable of adhereing to the negatively charged ocular surface, and complexing with negatively charged cargo, for example DNA or ribonucleic acid (RNA) for gene therapy.

2.8 Block Copolymers

Block copolymers are polymers consisting of two or more monomer units in an arrangement such that distinct chains (blocks) for each monomer are grafted together as shown in Figure 2.4. They may be synthesized through a variety of polymerization techniques such as anionic polymerization, ring-opening polymerization, or radical polymerization[208]. In these techniques the reactive terminus is "living" meaning it may still react in the presence of a monomer. Once the monomers for the first block have been consumed, the monomeric units for the second block can be introduced in the system[208]. Alternatively, two blocks may be synthesized separately and combined create the final block copolymer[208]. This can occur by combining two polymers with unterminated chains from the polymer synthesis itself, or modification and combination of two pre-synthesized blocks[208]. The selected application is based on the latter[208].

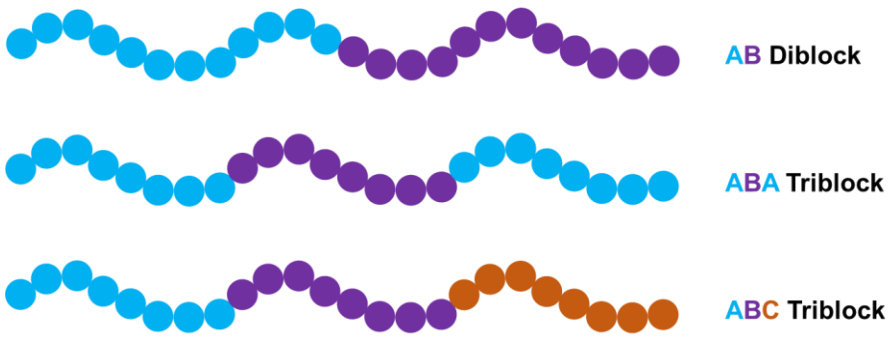

Figure 2.4: Arrangements of common linear block copolymers. A, B, and C represent different monomer units which constitute the chains of the block copolymer.

2.8.1 Polymer Micelle Self-Assembly

Each block exhibits the physical and chemical properties of the monomer subunits. In the case of amphiphilic block copolymers in an aqueous solution, hydrophobic interactions between the apolar/lipophilic polymer chains result in the spontaneous formation of micelles[208]. The self-assembly of block copolymers into micelles and other structures is driven by intermolecular forces[208]. These include electrostatic interactions, metal complexation, and hydrophobic forces; the latter are responsible for self-assembly of PLA-*b*-Dex and PLA-*b*-Dex-APBA polymer micelles utilized in the experimental work for this thesis. The withdrawal of the hydrophobic block from the aqueous environment results in a net entropy gain making this process spontaneous.

Drug loading and self-assembly of polymer micelles can occur simultaneously or as independent steps as described by Gaucher et al.[208]. The simplest technique involves block copolymer composed of two hydrophilic chains where one has slightly greater hydrophobicity, which drives the self assembly. The drug molecules introduced following the synthesis of the particles and diffuse into the particles[208]. This is suitable only for "moderately hydrophobic"[208] species such as poloxamers otherwise the polymer will precipitate without the presence of an organic phase in the initial phase.

Another technique is to dialyze a solution of block copolymer and drug dissolved in an organic solvent such as acetone, acetonitrile or dimethyl sulfoxide (DMSO)[208]. The dialysis media is aqueous and, and the organic phase is slowly exchanged. The hydrophobic blocks and drug molecules withdraw from the aqueous phase, associating with the remaining organic phase and other hydrophobic blocks[208]. Third, an oil-in-water emulsion technique can be utilized where droplets of the polymer and drug solution in an organic solvent are added to an excess of aqueous media[208]. Generally, the organic phase is immiscible in water and requires high energy input[208]. Agitation may be required to create small droplets of the organic phase with which the hydrophobic blocks can associate. These techniques are best performed with copolymers with blocks that are insoluble in water such as poly(lactic acid) [208]. The mucoadhesive platform investigated in this thesis is synthesis using the oil-in-water emulsion approach with DMSO as the organic phase. DMSO is polar and miscible in water resulting in smaller droplets and therefore nanoparticles instead of microparticles. Fourth, the evaporation of the organic phase from the solution results in a condensed polymer film which produces drug-loaded micelles upon rehydration[208]. This method does not require the introduction of an organic phase. Instead the removal of solvent drives association of the blocks.

The freeze-drying process generates stress at various stages which can destabilize colloidal suspensions. Typically, this process is utilized for extraction of solutes from aqueous media for preservation. Gaucher et al. report a method of utilizing freeze-drying to synthesize micelles. The synthesis technique utilizes the stresses to synthesize particles from a mixture of water, polymer, drug, and an organic phase. The result is a dried porous "cake" which is an aggregate of particles which disperse upon rehydration[208]. This is a novel method and has much to be explored, especially the behaviour co-solvent and interactions with water during lyophilization[208]. The freeze-drying process and the stresses are further described in Section 2.9.

2.9 Freeze-Drying

Colloidal systems have demonstrated utility as carriers for drugs, especially water-insoluble, sensitive, or toxic molecules. Brownian motion opposes gravitational forces allowing the molecules to remain suspended in solution[209]. However, these systems are physically unstable resulting in aggregation and precipitation over time, and chemically unstable especially in the case of biodegradable carriers[209]. The addition of excipients such as polymers in ophthalmic preparations may induce bridging and subsequent aggregation (flocculation)[209]. Upon storage of aqueous nanoparticle suspensions for prolonged periods, drug leaching and particle breakdown has been observed. Water is believed to be the primary cause of particle instability.

Particle breakdown and drug leaching returns the formulation back to the conventional state of preparation today (free drug suspended in an aqueous solution). Drug leaching over time may result in inconsistent doses with a potential for reduced efficacy or adverse side effects. In some instances, nanocarriers are utilized to encapsulated drug molecules susceptible to degradation in aqueous environment[209]. Furthermore, aggregates may cause irritation and foreign body experience on the resulting in elimination of the formulation via nasolacrimal drainage on the ocular surface for example. Poor shelf-life of these colloidal systems has been recognized as a barrier to the commercialization of nanosystems for drug delivery.

A shorter shelf-life drives the cost up for both manufacturers and payers as the shelf-life is reduced. Pharmacies will be incapable of storing the suspensions for prolonged periods of time. Formulation would be produced in smaller batches or upon request to minimize waste. The utility time would be further reduced by the lag time before the patient receives the formulation. Therefore, for nanoparticle

formulations to be commercially viable, the issue of nanoparticle instability must be addressed in the context of increasing shelf-life.

A common technique to remove water from pharmaceuticals is freeze-drying, also known as lyophilization. Aqueous samples are frozen, and the dehydration occurs via sublimation of ice under low pressure. The performance of the dried formulation must be identical or indistinguishable over time upon reconstitution (rehydration of the dried nanoparticle system). Despite being effective for small molecules, the processes of freezing and drying creates stresses which can destabilize nanoparticulate systems. To alleviate these stresses, protectants (most commonly carbohydrate monomer or oligomer units containing diols) are utilized.

The three keys to the success of this process are the constituents of the formulation, the freeze-drying process, and storage of the dried formulation. The constituents of the formulation determine the physio-chemical properties of the suspensions. These protectants however are used in significant quantities in literature, sometimes upwards of 20 wt%[209]. In some instances, even higher concentrations have been unsuccessful in stabilizing the formulation[209]. Examples in literature suggests that the protectant, mechanism of action, and concentration have to be optimized for each individual formulation. Formulations for topical ocular drug delivery for example, have stringent guidelines on the osmolality and concentrations of excipients to prevent irritation and damage to the eye[210] . Hence, the ideal protectant candidate would result in stable dried formulation which can be reconstituted to generate statistically

Excipients used in the pharmaceutical industry fall into five broad categories. During the freezing process and formation of the pH of the cryo-condensed suspension relative to the starting solution. The salts also result in a buffered solution upon reconstitution[209]. Bulking agents are when freeze-drying low concentration solutions to yield an “elegant cake” effectively adding bulk to the dried formulation[209,211]. Tonicity adjusters are used to control the final concentration to yield isotonic formulations if required for optimal administration[209,211], and help control osmotic pressure[209]. Tonicity adjusters may be added to diluent instead of the freeze-dried cake.

The collapse or eutectic temperature of a formulation establishes the maximum temperature at which the primary sublimation can occur without melting or collapsing[212]. A viscous cryo-condensed state inhibits further ice crystal formation and finally freezes[209]. The resulting frozen product has a crystalline (well defined collapse temperature) as well as amorphous and semi-crystalline phases (have

a glass transition temperature)[212]. The collapse temperature tends to be 1 – 3°C higher than the glass transition temperature[213]. The second phase of drying removes water from the amorphous component[213] and takes longer[209,212,213] hence should always be performed at a temperature lower than the glass transition temperature[209]. Collapse temperature modifiers are added to formulations to increase the maximum allowable drying temperature[209]. This addition is critical when the desired result is a porous cake as the collapse temperature can alter the size of the pore and resulting properties[214].

The final type of protectants are stabilizers which protect the drug molecules or colloidal particles from freezing stress (cryoprotectant) and drying stress (lyoprotectant)[209]. As the water freezes the remaining liquid becomes increasingly concentrated with the dissolved or suspended molecules and is referred to as cryo-concentrated solution. The cryo-condensed state destabilizes colloids via induced aggregation as a result of the concentration and viscosity increase, and due to the mechanical stress generated during ice crystallization. The drying process occurs in two stages. The first removes ice through sublimation yielding a porous cake or brittle film. The second phase involves the removal of adsorbed or bound water which does not freeze and remains in the liquid state and hence does not sublime[209]. Examples of common protectants include sucrose, trehalose, mannitol, polyethylene glycol and dextran[209].

2.10 Commercialization of Nanotechnology Enabled Medicine

Nanotechnology is a multidisciplinary field expected to have a substantial effect in the field of medicine, improving the conventional therapies or replacing them altogether. Due to the poor efficacy conventional drug delivery techniques, the bioavailability of the drug in the target tissue is limited. Furthermore, the risk of adverse side effects and non-target organ toxicity are increased. The applications of nanotechnology in medicine can be divided into three categories: i) diagnostics, ii) regenerative medicine/tissue engineering, and iii) pharmaceuticals/drug delivery[215,216]. At present, the most relevant application of nanotechnology is pharmaceuticals[215,216] with over 200 companies[216], over 1,500 filed patents[217], and approximately 100 applications of nanomedicine have been approved by the FDA[218]. Some examples include Doxil® (doxorubicin encapsulated in liposomes)[217,218], Estrasorb® (estradiol encapsulated within a micellar emulsion)[218], and Zilrettea® (triamcinolone acetonide embedded in PLGA hydrogel)[218]. However, it is also necessary to recognize that the field of nanomedicine has fallen prey to “the current trend of overclaiming in science,” as described by Boisseau et al.[216].

To address the challenges of conventional formulations, various nanostructures as vehicles for drug delivery are being explored as discussed in Section 2.6 and Section 2.7. Figure 2.5 illustrates the increase in publications exploring various nanocarriers every year. Unfortunately, the commercial viability for the vast majority of the reported nanocarriers has thus far been limited[219]. The data was collected from Web of Science maintained by Clarivate Analytics. These works have demonstrated several advantages compared to conventional therapies.

Compared to the number of publications, there are few nanocarriers currently undergoing clinical trials. Data was collected from the clinicaltrials.gov database provided by the U.S. National Library of Medicine. Liposomes have an overwhelming majority of clinical trials with 223 active trials, 73 of which are in phase III, and 388 studies currently recruiting. This iss not surprising as they are also the oldest, most well understood, and biocompatible system. The next largest segment was nanoparticles with 38 active trials, five of which are in phase III, and 74 recruiting. Only nanoparticles, liposomes, and hydrogels (not shown in the figure) were found to have reached this stage while the other structures have thus far not reached this milestone. The total of global clinical trials for these structures was 3,156 with approximately 100 approved for marketing[218]. This illustrates the high-risk investment in pharmaceuticals and the importance of pharmacoecono mics for biotechnology and pharmaceutical industries.

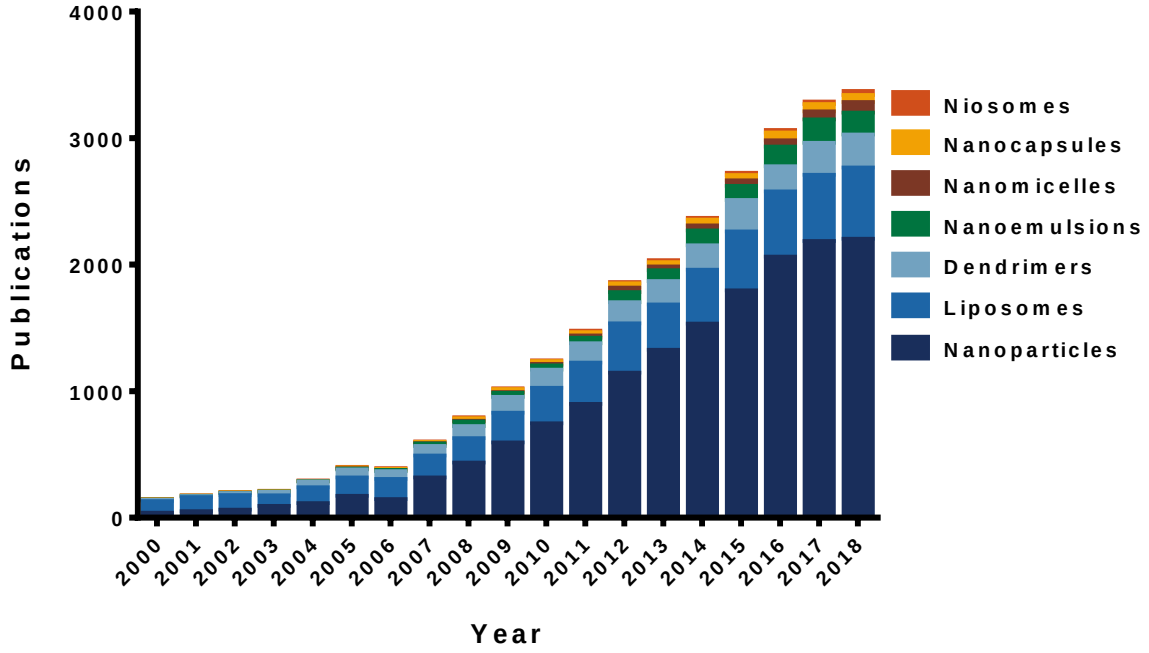

Figure 2.5: Number of publications per year for various nanocarriers illustrating the increase in the research interest in nanomedicine.

Clinical translation is an expensive and time-consuming process but is also compounded with greater complexity and uncertainty when nanomedicine is concerned. The behaviour of materials at the nanoscale is different than bulk due to the greater surface area to volume ratio and high energy of the particles. Furthermore, due to their size nanostructures have the ability to enter cells, bioaccumulate in organs, or cross physiological barriers conventional drug molecules cannot. Furthermore, the varied nature of the particles requires unique validation methods. These factors increase the risk associated with regulatory approval. The large-scale manufacturing of nanomaterials is also more complex and generally more expensive than conventional forms. Therefore, the overall cost-effectiveness must be greater than conventional therapies in direct competition for there to be a return on investment (ROI). These concepts are further explored in Section 0 and Section 2.10.2.

2.10.1 Regulatory Approval of Nanomaterials

Materials and devices behave differently at the nanoscale compared to bulk, and their properties as well as interactions with biological systems change with size and shape. Nanotoxicology is a major concern with the advancements in the field. In the context of medicine, the pharmacokinetics of these novel materials and drug carriers must be well characterized. Due to the small size, these particles are often able to cross cell membranes and have been shown in literature to bioaccumulate. With novel nanomaterials still being developed, regulatory bodies have found it challenging to create a uniform portfolio of evaluations with which to characterize the safety and efficacy of nanomaterials and devices. Consequently, more stringent and thorough analyses need to be performed on these candidates on a case-by-case basis.

Preclinical testing involves four key steps: i) in vitro and in vivo primary pharmacological studies, ii) pharmacological studies on major organ systems, iii) pharmacokinetic studies, and iv) toxicological testing[220]. The two primary goals are to i) to validate therapeutic effect, and ii) demonstrate satisfactory pharmacokinetics and clearance (toxicological) effects[221]. Due to the significant cost of these and subsequent studies, the results are periodically evaluated to determine the likelihood of success[220]. The cost of toxicological studies has been increasing over the years, and the practice of animal testing is a serious ethical issue.

Similarly, clinical trials take place in four stages, each with their own goals[221]. Phase I evaluates the toxicological effects of the drug candidate on healthy humans as well as pharamocokinetics and pharmacodynamics[221]. Phase II establishes the dose-response relationship and efficacy of the drug at treating the disease[221]. This is also the stage at which most drug candidates fail. The most expensive stage is phase III which is carried out at a larger scale to establish validity of the effects. Upon completion of phase III and FDA approval, the drug can be marketed and may even be prescribed or available over the counter. Typically, clinical outcome data used for pharmacoeconomic analysis is collected during phase III. However, significant resources have typically by invested by this stage, and the goal is to validate safety and efficacy of the candidate. Phase IV validate the long-term safety and efficacy of the drug. During this time the company may also start to expand the application to alternate diseases or formulations.

The value of a drug candidate increases as it progresses through the stages of development[221]. As an invention progresses through these stages, the value and the cost of failures increases. On average

the drug development process can take 12 -16 years with an average cost of USD 802 million[221] (including the cost of failures)[221]. Approximately one of 5,000 – 10,000 candidates proceed to preclinical trial, only one third of new molecules are evaluated in clinical trials, and half of the clinical trials fail in phase II[220]. Furthermore, Miller reports that a significant proportion of drugs are unable to pass through phase III clinical trials due to economic reasons. Mehta reports that only 1% of the compounds which enter preclinical trials become successful in the market[221]. Majority of failures occur as a result of poor efficacy and toxicity (animal and/or human)[220].

The FDA categorizes nanomedicine into three broad categories: drugs, devices, and in vitro diagnostics. The compatibility and toxicity are assessed under the same regulations as conventional forms. Each category has its unique requirements however, standard protocols for the assessment of toxic potential of the nanomedicine is a limitation for researchers[217]. The FDA has established a commission to regulate nanomaterials, but this is has still proven to be a challenge due to the varying properties and biological behavior of nanomaterials. The FDA's review period after phase III clinical trials can take up to two years, but due to the nature of the industry and variance in the interventions especially nanotechnology, each has to be assessed case-by-case. In 2006, the FDA formed the FDA Nanotechnology Task Force to develop regulatory approaches for nanotechnology by identifying and proposing recommendations for knowledge or policy gaps. Patra et al. recommend cooperation between regulatory agencies in order to achieve a simplified process and shorter time for approval[217].

As reported by Boisseau et al. in 2011, the European Medicines Agency recognizes the need for greater understanding of nanomedicine and additional methods to complement the existing regulatory guidelines[216]. Nanotechnology enabled pharmaceuticals were evaluated with the same benefit/risk management and environmental protection framework as conventional pharmaceuticals[216]. Agence française de sécurité sanitaire et des produits de santé also used the existing guidelines for evaluation of toxicology, however some methods have been identified as inadequate for evaluation of nanomedicine[216].

Intellectual property rights can influence the development plan and access to segments of the highly regulated healthcare market[221]. Patients are generally not the primary payers or decision makers[221]. Physicians make the decision on the best intervention, while the government or insurance companies reimburse the cost to the patient and are the true payers[221]. For this reason, manufacturers must

quantify and demonstrate value to the payers and prescribers[221]. Monitoring legislators is crucial as policy changes may alter product development processes[221].

With an aging population and increasing prices, there is a pressure to reduce prices or introduce generics in markets such as the US[222]. Despite patent protection, several drugs offer the same benefits, thus strong competition exists in the market[222]. The high prices of drugs are a consequence of the financial investment and high risk required to bring the product to the market[222]. Pricing is challenging as it must be low enough for adequate reimbursement and provide patients with the care they need, while also ensuring the company has a ROI[222].

The negotiation power of payers can significantly impact the price a manufacturer is able to charge[221]. More recently, there has been a demand for lower-cost generics in economics with public-aided health care, but also the US[221]. With rising development costs, pharmaceutical companies must compare the probability of ROI before moving forward with a candidate[221].

The drug discovery and development process are costly and risky. Changes in legislation during later phases could be detrimental or result in additional financial burden. Patents for blockbuster patents are about to expire, and generics will soon take over the market[221]. The global biotech market continues to increase at an exponential rate despite the high costs[221]. Consequently, manufacturers continue to develop the portfolio of their approved products to maximize the ROI on their invention. In literature, nanotechnology has demonstrated improvements in effectiveness of existing products and thus have generated significant interest.

2.10.2 Pharmacoeconomics

Pharmacoeconomics is a multidisciplinary field combing clinical, economic and humanistic outcomes[223]. The analysis combines the cost of treatment in its entirety (therapeutics, services, and other products) with the outcomes[223]. Clinicians are concerned with the care a new therapeutic can provide, but payers must manage the cost of care[223]. The analysis can be applied on a higher level or patient-to-patient basis when evaluating the best treatment option[223].

Pharmacoeconomics in drug discovery influences decision making and the development of projects[224]. Drug discovery is an expensive endeavor financially and in terms of time. An estimate from 2000 suggests that the average cost of developing a new drug is USD 802 million including the cost of failures[221]. The cost increases as a drug candidate moves through the development phases,

making early pharmacoeconomic evaluations extremely valuable as they may help to eliminate unattractive projects early and to maximize the return on investment (ROI).

Novel interventions do not always provide a significant improvement over the incumbent, and in some cases are less effective, but at a higher cost[223]. At the external level pharmacoeconomic analyses are utilized to communicate the benefits of an intervention to payers, clinicians (prescribers) and to decision makers. The studies are key to achieving regulatory approval, reimbursement from the payer (i.e. insurance or social health care in Canada)[223]. At the internal level, PE influences decisions on research and development (R&D) resource allocation during drug discovery, development, and clinical pathways to market. Hence, PE is critical throughout the drug delivery cycle, and contributes to commercial success

The simplest analysis is cost-minimization analysis (CMA) which assumes equivalent outcomes and only considers the cost of intervention[223]. This technique is only used for comparison of two equivalent outcomes i.e. if two therapeutics are determined to be equivalent by the FDA, the only difference which remains is cost[223]. When comparing two therapeutics with varying efficacy based on cost would be incorrect[223].

Cost-effectiveness analysis (CEA) relates the costs to easily quantified clinical outcomes collected in clinical trials and general practice[223]. Comparisons can only be made when the clinical outcomes being monitored are the same[223]. Differences such as adverse effects and their magnitude may not be correctly represented in this analysis[223]. CEA measures the cost for additional years of life gained as a result of the intervention[223]. Cost-utility analysis (CUA) is considered a subset of CEA as it measures the utility or quality of the additional years gained (measured in CEA)[223]. However, the measure of utility is not standard and is only a rough estimate[223]. In cost-benefit analysis (CBA) costs and benefits are measured monetarily[223]. This allows for the comparison of interventions with similar and unrelated outcomes[223]. The values associated with the costs and benefits are estimates which can be drawn from narrow or broad population distributions[223]. Furthermore, putting a monetary value on life and health outcomes can be difficult[223]. Different measurement of utilities has been proposed, and CBA can change depending on the method used[223].

Economic studies are limited to the country in which they are performed[223]. It is important to consider demographics of the market as some populations have a higher prevalence of diseases, or the pathophysiology may differ rendering some therapies ineffective[221]. An example is glaucoma which

has a higher prevalence in East-Asian countries but is a result of narrowing of the trabecular meshwork which restricts aqueous humour drainage. Interest and investment in biotechnology continues to grow, and areas such as nanotechnology are even receiving government funding[221]. Interventions for specific diseases and outbreaks are prioritized and streamlined through the approval process[221].

Expanding the market for a therapeutic is met with several challenges such as differences in diseases and incidence rates, availability and laws around generics, and policies[223]. In countries with government funded health care have, the government has leverage during price negotiations and reimbursement decisions[223]. A pharmacoeconomic portfolio must be presented demonstrating the added and return for the value a manufacturer wants to charge[223]. However, not all interventions are equally compensated, and in some cases the generic is favored over the branded equivalent[223]. Filing and maintaining a patent is also an expense which a company may have to bear in domestic and international markets[221]. As patents expire, lower-cost generics are able to penetrate the market, significantly affecting revenues of the inventors[221]. Furthermore, generics have entered the market prior to patent expiration legally in some cases[221].

Despite the potential benefits of many inventions, achieving commercial success is not possible without market research and economic analysis. Market research develops an understanding of the current state of the market, the demand, competition, and opportunities for new products. Determining the scope and size of the market, and the potential for profit stream is imperative before investing time and money into developing an invention.

Negotiations with health-care payers are highly dependent on the pharmacoeconomic portfolio[224]. The FDA only considers efficacy since countries such USA give manufacturers to charge what the market is willing to pay[224]. This has resulted in therapeutics for rare diseases costing hundreds of thousands of dollars[224]. In countries with a public health care system such as Canada, a strong pharmacoeconomic evaluation is even more important as the manufacturer must justify the efficacy and cost for reimbursement[224]. Pharmacoeconomics is starting to become part of manufacturers' due diligence as it encourages better understanding of the clinical pathways for drug use (often resulting in discovery of alternate applications) and a good market research tool[224]. The higher cost of the therapeutic may be offset by decreasing hospital admissions, cost of services such as paramedics[223], and therefore would result in an overall cost savings to the payer. Expenditure on health in the United States alone was $2.7 trillion in 2010 with only 12% accounting for medications[223].

Furthermore, each country and every province/state in that country may have its own policy on coverage and recommendations for manufacturers[223]. The United States lacks standardization of pharmacoeconomic evaluation as it is both privately and publicly funded[223]. The citizens may be the primary payers and thus it is important for them to be able to evaluate the intervention options[223]. Thus, a complete pharmacoeconomic analysis is critical for the success of therapeutics[223]. The evaluation is dynamic and evolves over time with the development life cycle, market, and policies[223]. The approval processes for new drugs is strenuous and extremely expensive, and pharmacoeconomic analyses are important in determining which drugs to invest in[223]. Researchers and larger pharmaceutical agglomerates alike must understand the competition and market environment for successful development[223].

2.11 Mucoadhesive Nanoparticles for Treatment of Chronic Dry Eye

2.11.1 Dry Eye

Dry eye syndrome (DES) is a consequence of tear film instability or abnormal composition resulting in symptoms including discomfort, visual discomfort, and in some cases eye damage[131,225]. Alterations may occur as a result of dysfunction or pre-existing disease. The stress in the ocular environment triggers an inflammatory response which may become chronic if left untreated.

2.11.2 Cyclosprine A

Cyclosporine A (CsA) is an immunosuppressant approved by the FDA in 2003 for use as an ophthalmic emulsion for the treatment of DES. Restasis® is a 0.05% ophthalmic emulsion of CsA administered twice daily at high doses as previously described increasing the prevalence of side effects[131]. Inflammation in DES is a response associated with the proliferation of the CD4 T cells[226,227] which are central to autoimmune response initiated upon detection of foreign antibodies[228]. Calcineurin phosphatase is involved in the transcription of the pro-inflammatory cytokine IL-2 which signals activation of T-cells[226,229]. Upon entering the cell, CsA binds to cyclophilins which inhibit calcineurin phosphatase, thus inhibiting the inflammatory response[226]. However, this pathway for T-cell activation exists in several cell types and may result in serious side effects especially in the kidneys and liver[226].

Approximately 25% of the phase III clinical trial subjects reported adverse side effects and ocular discomfort[131,225]. Due to the hydrophobicity, the therapeutically active fraction of the dose, or bioavailability, on the eye is reduced. Incorporating a small volume of organic solvent may improve dispersibility and concentration, but this results in ocular discomfort[226]. Treatment of DES requires long-term intervention, and a low dose must be maintained to reduce the adverse side effects[131] at a cost of reduced efficacy. However, due to the poor bioavailability and retention of the drug on the ocular surface, the therapeutic benefit for the patient is not optimized[131,225].

2.11.3 Phenylboronic Acid Modified Mucoadhesive Polymer Micelles

Liu et al. have developed a self-assembled block copolymer micelle composed of a hydrophobic PLA core and dextran corona. The corona is functionalized with APBA which forms covalent bonds with diols of sialic acid residues on mucin fibers of the ocular mucosa. The particle structure and this interaction is visualized in Illustration 2.1. In vivo ocular retention studies were performed on male New Zealand White rabbits with dextran functionalized with APBA and cyanine 7.5 hydrazide (a fluorescent label). Dextran functionalized with only cyanine was used as the control. APBA modified dextran was retained for up to 6 h whereas unmodified dextran was negligible on the ocular surface after 3 h[225]. Additionally, a near infrared dye (indocyanine green) was encapsulated within the MNPs and free dye was used as control. Fluorescent ocular imaging revealed free dye was removed from the ocular surface within 3 hours, while the labelled MNPs were observed beyond 24 h. Additionally, indocyanine green loaded nanoparticles[225].

This drug delivery platform was used to investigate the improvement in CsA efficacy in rats with induced dry eye. In vivo studies were performed on female C57BL/6 mice. CsA loaded MNPs (CsA-MNPs) were administered once a week with concentrations ranging from 0.005 and 0.01 wt% CsA and compared with Restasis® thrice daily. Both CsA-MNP formulations resulted in recovery of the ocular surface and elimination of inflammation. Restasis® only eliminated inflammation, and goblet cell recovery was not observed. Liu et al. reported this to be equivalent to 50- to 100-fold reduction in dosage compared to Restasis® which would greatly reduce the potential for adverse side effects. Tear production and histopathology analysis revealed that recovery of the ocular tear film and goblet cells, whereas the control revealed changes in epithelium and lamina propria which are consistent with the disease[225].

This mucoadhesive drug carrier is a promising platform to improve the bioavailability of encapsulated therapeutics on the ocular surface. The reduced dosing frequency is also expected to improve the patient compliance and quality of life due by alleviating discomfort and adverse side effects. Nanomedicine has been predicted to enable the market entry of therapeutic agents which have thus far suffered in conventional formulations[230]. As previously mentioned, the majority of drugs are lipophilic in nature, and this platform has the potential for improving their efficacy.

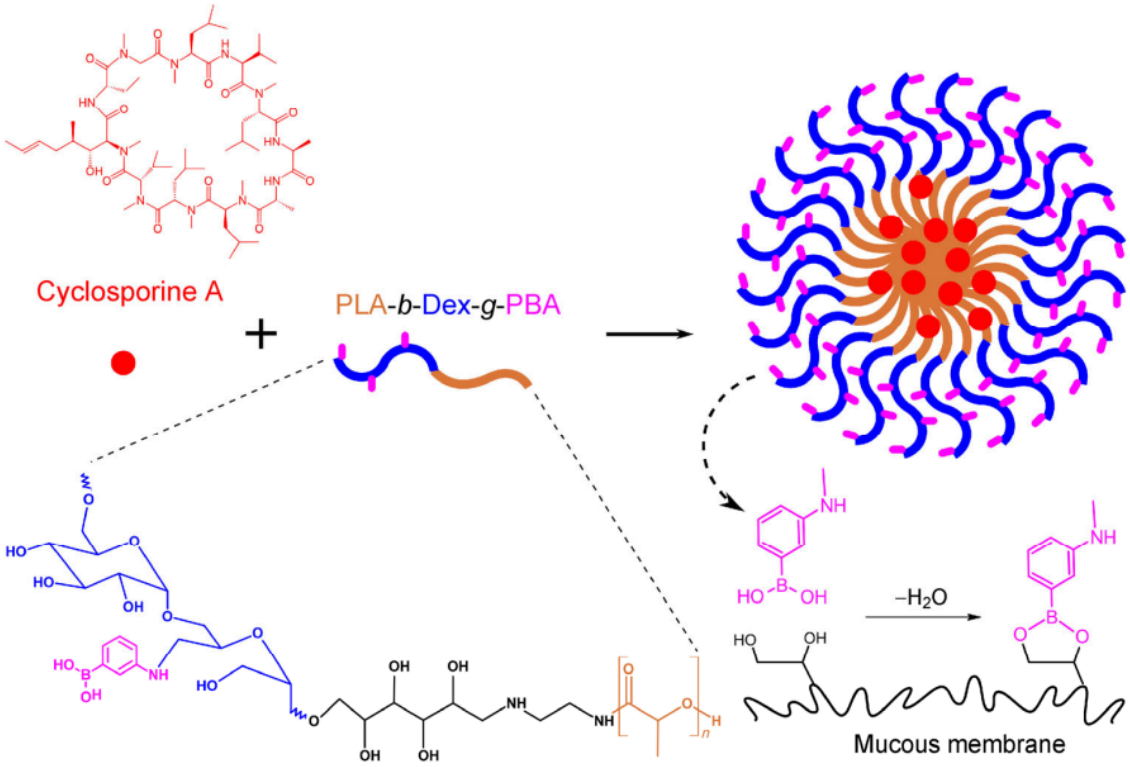

Illustration 2.1: Schematic illustrating the phenylboronic acid functionalized block copolymer, micelle structure, and mode of action (binding to sialic acid residues of the mucus membrane)[131].

Chapter 3
Optimization of APBA Conjugation onto PLA-*b*-Dex Nanoparticles for Ophthalmic Preparations

3.1 Summary

Mucosal drug delivery platforms facilitate targeted drug delivery in several regions of the body and improve bioavailability of therapeutics at the target site. The regeneration rate of mucosa varies between the different regions in the body; hence, the optimal mucosal drug delivery platform is flexible to facilitate adequate residence time for the encapsulated therapeutic. Phenylboronic acid functionalized polymer associates with the sialic acid residues of mucin fibers. Herein, the reductive amination mechanism through which APBA is conjugated onto the backbone of dextran is investigated to develop regression models which allows for the targeted conjugation.

3.2 Introduction

PBAs are Lewis acids with pK_a ranging between 8.2 – 8.86 which can be further reduced via the conjugation of electronegative groups and exists in equilibrium with the charged (hydrophilic) and uncharged (hydrophobic) forms[231]. Both forms have demonstrated ability to interact with 1,2-*cis*-diols, with the charged form being more stable[231]. This property has been used for the synthesis of PBA-polymer derivatives, cross-linked PBA-based hydrogels and glucose-responsive materials[231,232].

As discussed in Section 2.5, mucin is the primary component of mucus membranes protecting soft tissue and organs. About 25% of the amino acids are glycosylated with the carbohydrate chains terminated in fucose or sialic acid (*N*-acetylneuraminic acid)[9,13,32]. PBA has been found to have unusually high affinity and selectivity towards the sialic acid groups[233]. Under physiological conditions covalent bonds can form between the *cis*-diol groups of PBAs with the diol groups found in sialic acid[233].

Mucosal drug delivery is a proven approach to increase the retention time of novel drug carriers at the target site thereby improving the bioavailability of the drug at the site of action. In the context of ocular drug delivery, free drugs are cleared within minutes of administration resulting in only 5% of the administered dose reaching the target tissue. The refresh time of the ocular mucosa is significantly longer than that of the aqueous layer. Hence, using PBA functionalized polymer micelle nanoparticles

as drug carriers to target the ocular mucosa improves retention on the ocular surface and improves drug bioavailability.

The composition and properties of mucus membranes vary between the various regions. Areas with faster mucus turnover would require a higher density of mucoadhesive ligands, and regions of low turnover or those with fewer barriers would require lower ligands. This polymer micelle nanoparticle has demonstrated application as a drug carrier for the management of ophthalmic diseases. However, the technology's portfolio may be further expanded to other regions of the body which contain mucus membranes. This is an important consideration in the pharmacoeconomic evaluation of this technology as a commercially viable product. The ability to fine tune the drug carriers to target different mucus membranes and within different populations can allow these particles to improve several existing therapies.

PLA-b-Dex nanoparticles are composed of biodegradable polymer blocks of PLA and dextran. Both polymers have been previously approved by the FDA for applications in pharmaceuticals. Phenylboronic acid and its many derivatives have not yet been approved for consumer application and require further pharmacokinetic and toxicity data. Upon further investigation in the toxicology and pharmacokinetics of the PBA derivatives, the FDA may propose limitations on the conjugated ligand.

Furthermore, since free mucoadhesive polymer has been explored as a lubricant, for example for chronic dry syndrome, the study on mucoadhesive dextran alone provides insights into product development into this field. To address these three opportunities, control over conjugation of the phenylboronic acid ligands onto dextran is critical. In this study, we aimed to functionalize 3-aminophenylboronic acid to dextran via reductive amination while varying the two major factors, ligand and reducing agent concentration. Firstly, the conjugation of the ligand onto free dextran is explored and the conclusions of this study are used to develop the second study which investigates the conjugation of PBA onto the block copolymer.

3.3 Experimental Section

3.3.1 Materials

Acid-terminated poly(D,L-lactide) (PLA; Mw ~ 20 kDa), dextran from *Leuconostoc mesenteroides* (M_n = 9-11 kDa), boric acid, sodium chloride (NaCl), sodium hydroxide (NaOH), hydrochloric acid (HCl), sodium periodate ($NaIO_4$), ethylenediamine (EDA), sodium cyanoborohydride ($NaCNBH_3$), *N*-(3-Dimethylaminopropyl)-*N*′-ethylcarbodiimide hydrochloride (EDC), *N*-Hydroxysulfosuccinimide, sodium salt (NHS), 3-Aminophenylboronic acid monohydrate (APBA), glycerol, deuterium oxide (D_2O), methanol and dimethyl sulfoxide (DMSO) were purchased from Millipore Sigma. Liquid nitrogen was dispensed from the University of Waterloo Chem Stores.

3.3.2 Oxidation of Dextran

Dextran was dissolved in a 0.03 M solution of $NaIO_4$ prepared with deionized water (DI; >15 MΩ) at a concentration of 25 mg/ml. The reaction vessel was sealed and covered with aluminum foil due to the light sensitivity of $NaIO_4$. After 24 hours, the sample was transferred to regenerated cellulose dialysis tubing (MWCO: 3.5 kDa) and dialyzed against 10 times excess of DI water to remove dextran monomers and $NaIO_4$ from the solution. The media was changed eight times during the dialysis period of 48 hours. The oxidized dextran (Dex-Ox) was frozen with liquid nitrogen and freeze-dried to remove water and extract the dry polymer which was stored at -20 °C and thawed prior to use.

3.3.3 Conjugation of APBA onto Dextran

In methods previously described in literature by our group, the oxidized and dialyzed dextran is used directly for conjugation. However, the concentration can vary with the influx of medium into the tubing during dialysis. To control the concentration of dextran, and to ensure consistency between the trials by removing error resulting from inaccuracies in the concentration.

Dex-Ox was thawed at room temperature and dissolved in 0.1 M borate buffer (adjusted with 0.1 M NaOH and 1M HCl) at a concentration of 25 mg/ml. Solutions of APBA were prepared in DMSO and $NaCNBH_3$ in 1N NaOH as per Table 3.1. Following the dissolution of Dex-Ox, 0.3 ml of the APBA solution. The solution was stirred for two hours (previously determined as a sufficient duration for maximal Schiff base formation) and 53 µl of the $NaCNBH_3$ were added and the reaction proceeded for another four hours. The solution was transferred to regenerated cellulose dialysis tubing (MWCO:

3.5kDa) and dialyzed against 100 times excess of DI water to remove unreacted reagents from the solution. The media was changed four times during a dialysis period of 24 hours, and the modified dextran was frozen with liquid nitrogen and lyophilized to remove water and isolate the dry polymer.

3.3.3.1 Two Factor, Three Level, Factorial Design

A factorial study was performed on the reductive amination method of APBA with three replicates. The center point values represent the existing ratio of $NaCNBH_3$ and APBA to dextran in the reaction mixture and was also synthesized in triplicate. The corner points were selected at equal distance from the center for both factors. This allowed for the use of an orthogonal design in the analysis with Minitab.

Table 3.1: Factors and levels for APBA conjugation optimization

	Levels		
Factors	**Low (-1)**	**Center (0)**	**High (1)**
$NaCNBH_3$:Dextran (mol/mol%)	0.200	0.356	0.512
APBA:Dextran (mol/mol%)	0.040	0.065	0.090

3.3.4 Synthesis of Amine Terminated Dextran

Borate buffer was prepared by dissolving boric acid (3.1 g/L) in DI water (>15 MΩ) and adjusted to pH 8.2 with 1 N NaOH. Dextran was dissolved in the borate buffer at a concentration of 0.2 g/ml. The terminal dextran monomer exists in equilibrium as a open or ring structure. The alkaline conditions favor the open conformation which improves the reaction efficiency. EDA was added to the reaction mixture in 20 times excess of dextran (6 mmol) and allowed to react for 24 hours in a vessel shielded from light. After the first 24 hours, 300 µl of 5M $NaCNBH_3$ dissolved in 1N NaOH was added to the solution per day for 48 hours (total of two additions).

The aminated dextran (Dex-NH_2) was purified via methanol wash. Aliquots of the aqueous solution were topped with eight times excess of methanol in 50 ml conical centrifuge tubes. The mixture was vortexed to disperse the dextran and break apart any aggregated precipitates, and then centrifuged at

3,000 rpm, and the supernatant was discarded. The wash was repeated once more and air dried in a fume hood for 30 minutes prior to drying in a vacuum desiccator to remove residual methanol.

The dried polymer was analyzed for verification and quantification of amination via ^{1}H-NMR. The polymer was dissolved in D_2O at a concentration of 20 mg/ml. The dextran carbon 1 (C1) peak corresponds to the peak between 4.7 to 5 ppm. The $(CH_2)_2$ of the conjugated EDA has a chemical shift between 2.5 to 2.7 ppm. The ratio of the peaks is used to quantify the conjugation. Only Dex-NH_2 with conjugation efficiency greater than 80% was used for subsequent reactions.

3.3.5 Purification of Acid Terminated Poly (lactic acid)

Acid terminated PLA was dissolved in DCM at a concentration of 0.24 g/ml and washed with 8 times excess methanol to remove monomers and small chains. The mixture was centrifuged, and the supernatant was decanted. The remaining PLA gel was purged with air prior to vacuum desiccation for 24 hours. The weight averaged molecular weight was determined by end group analysis via ^{1}H-NMR; the PLA-end CH had a shift at 4.13 ppm and was compared to the PLA CH in the backbone at 5.18 ppm.

3.3.6 Synthesis of Block Copolymer of Poly (lactic acid) and Dextran

The block copolymer was synthesized via carbodiimide chemistry. Dex-NH_2 and purified PLA were dissolved separately in DMSO at a concentration of 0.1 g/ml separately. The acid-terminated PLA was activated by adding Sulfo-NHS (0.46 mmol) and EDC (0.209 mmol) to the PLA. The dissolved dextran was added to the PLA mixture after dissolution of the EDC. The reaction mixture was purged with nitrogen and remained shielded from light for the duration of the experiment. The polymer was purified via dialysis using regenerated cellulose dialysis tubing (MWCO: 12 to 14 kDa) against 200 times the volume DI water for 48 hours with at least six media changes. The unconjugated Dex-NH_2 (Mn ~ 9 – 11 kDa) was removed into the dialysis media and discarded leaving only the conjugated block copolymer within the dialysis tubing. The polymer solution was frozen with liquid nitrogen and lyophilized to remove water and isolate the dry polymer.

The dry polymer was analyzed via ^{1}H-NMR for verification and quantification of block copolymer synthesis. The ratio of the PLA (CH) peak between 5 to 5.3 ppm was compared to the reference peak of dextran (C1) at 4.6 ppm. Only lock copolymer samples with conjugation greater than 90% were used for the studies.

3.3.7 APBA Modification of PLA-*b*-Dex

The dried PLA-*b*-Dex block copolymer was dissolved in anhydrous DMSO at a concentration of 30 mg/ml. Nine ml of the polymer solution was nanoprecipitated into 30 ml of DI water (>15 MΩ). The suspension was continuously agitated for 30 minutes to allow the nanoparticles to complete forming. The reaction vessel was then shielded from light and 8.50 ml of a $NaIO_4$ solution (10 mg/ml) was added to the suspension to oxidize the dextran corona of the nanoparticles. After 20 minutes, 1 g of glycerol was added to react with the residual $NaIO_4$ as oxidation of glycerol would be favored over dextran. This was done to ensure the minimize the side reactions and consumption of the reducing agents. 120 mg of APBA was added, followed by 600 µ of a 5 M $NaCNBH_3$ solution prepared in 1 N NaOH. After 2 hours, the reaction mixture was dialyzed against 10 times excess DI water for 24 hours and lyophilized for 24 hours after being frozen with liquid nitrogen.

3.3.7.1 Two Factor, Two Level, Factorial Design

A factorial study was performed on the reductive amination method of Table 3.2 with three replicates. Deviations from the standard synthesis procedure outlined in Section 3.3.7 were used to reduce the variance between samples and replicates. APBA was first dissolved in DMSO at the concentrations specified in Table 3.2. This eliminated errors associated with the addition of dry APBA which can occur from i) accuracy limit of the balance, ii) human error in weighing out the material and adding slightly varied amounts allowing the study to remain orthogonal, and iii) eliminates potential for sample loss during addition (i.e dry powder sticking to the neck or walls of the reaction vessel).

Table 3.2: Factors and levels for APBA conjugation optimization

Factors	**Levels**	
	Low	**High**
[$NaCNBH_3$] (M)	2.5	5
[APBA] in DMSO (mg/ml)	40	60

3.3.8 Characterization of APBA Conjugation

The analysis of APBA conjugation was performed by reconstituting the dried Dex-APBA and PLA-*b*-Dex-APBA polymer in DMSO at a concentration of 1.25 mg/ml. Dex-Ox in DMSO at the same concentration was used the baseline. The absorbance was measured from 240 – 320 nm with a 1 nm step size using Tecan Infinite Pro 200 MPlex Multimode plate reader. The UV spectra from 210 – 500 nm is shown in (Figure 3.1) illustrating the high absorbance characteristic of DMSO prior to 240 nm. At 240 nm an increase in absorbance intensity is observed following the oxidation of dextran. The optimal wavelength for quantification of the phenylboronic acid derivative was 287 nm. Currently, the quality control protocol requires APBA conjugation between 5 to 20 mol/mol% (APBA/dextran monomer) for PLA-*b*-Dex polymer micelle nanoparticles.

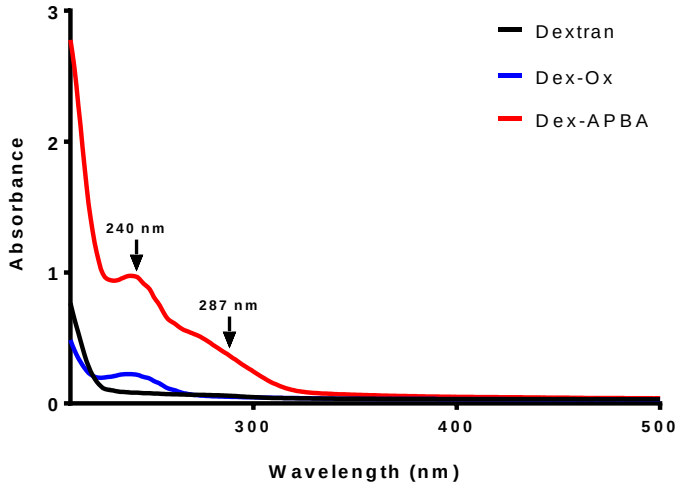

Figure 3.1: UV/Vis spectra for dextran, oxidized dextran (Dex-Ox), and phenylboronic acid functionalized dextran (Dex-APBA).

3.3.9 Characterization of Particle Size Following APBA Modification

The modified PLA-*b*-Dex-APBA polymer was dissolved in DMSO at a concentration of 6.818 mg/ml and nanoprecipitated into ten times excess of DI water (>15 MΩ). The suspension was stirred for 30 minutes. The suspension was transferred to regenerated cellulose dialysis tubing (MWCO: 3.5 kDa) and dialyzed against 1L of DI water for 3 hours to remove the excess DMSO. The dialyzed solution was then filtered with a 200 nm syringe filter. The particle was determined via DLS measurements using Brookhaven 90 Plus.

3.4 Results and Discussion

3.4.1 Conjugation of APBA onto Free Dextran

Dextran was used as the model for the purposes of the first study to investigate the effects of ligand (APBA) and reducing agent ($NaCNBH_3$) concentrations on the reductive amination pathway. This study was intended to develop the hypotheses for the study on APBA conjugation onto PLA-*b*-Dex block copolymer. Additionally, this study presents a strategy which may be utilized for the improvement of ocular lubricants. Suspensions of free dextran are commercially utilized but may be improved through the conjugation of APBA to yield a mucoadhesive, or long-lasting lubricant requiring a lower administration frequency. The reductive amination pathway for the conjugation of APBA onto the dextran backbone is depicted in Illustration 3.1.

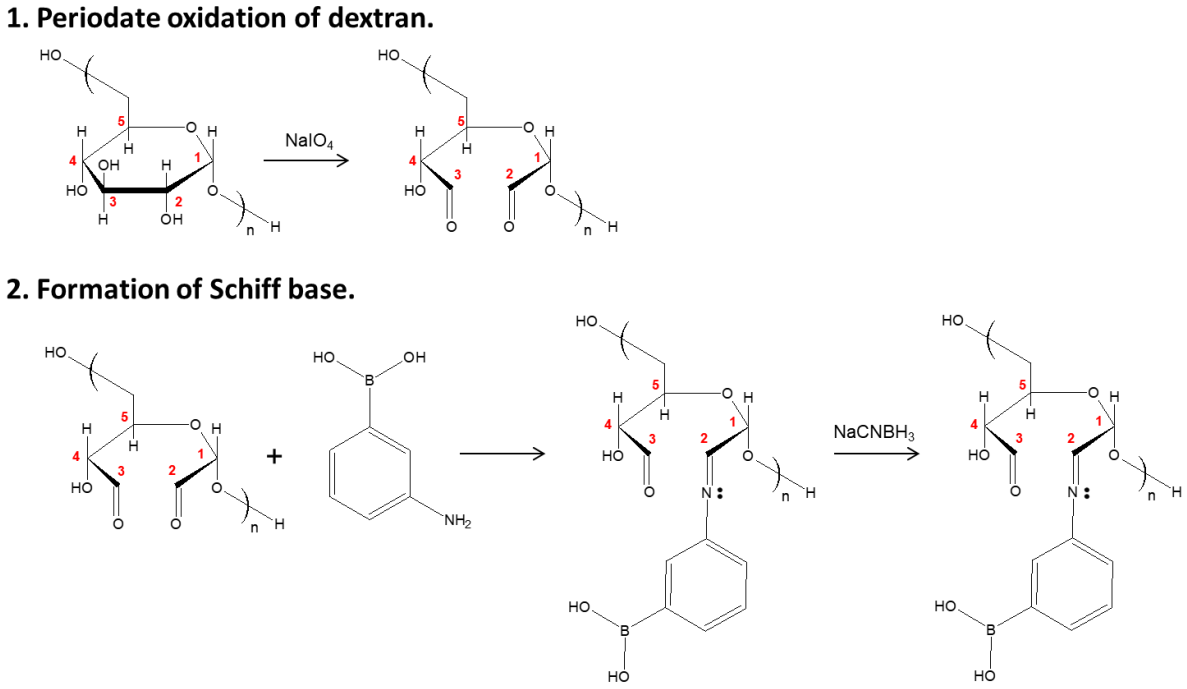

Illustration 3.1: Schematic of the reductive amination pathway for the conjugation of APBA onto the dextran backbone. Dextran is oxidized with sodium periodate yielding aldehydes on carbon 2 and 3 and opening of the ring. A Schiff base forms between the aldehydes and aminated phenyl boronic acid derivative. The reducing agent increases the reaction rate and stabilizes the structure to yield Dex-APBA.

Typical reductive amination reactions with imines reported in literature are carried out under slightly acidic conditions (pH 6 – 7). In this range, the imine (such as the Schiff base) is protonated to form the iminium ion which may be reduced to form the amide bond. However, the acidic conditions result in degradation of dextran. Dextran is first oxidized with $NaIO_4$ to which yields DexOx; the aldehyde groups of DexOx are more reactive in slightly basic conditions hence the reaction is carried out in borate buffer which is alkaline (pH 8 – 10). The buffer also helps to maintain the solution pH throughout the reaction especially since different concentrations of $NaCNBH_3$ (base) and APBA (acid) were added. The temperature was maintained at room temperature for this study because the goal is to optimization of APBA onto the dextran corona of the nanoparticles. Increased kinetic energy has been shown to destabilize colloidal systems. Furthermore, since the primary goal was to study the effect of the concentration and interaction between the reagents, additional heat could skew this interaction.

Results of the study are illustrated in Figure 3.2 which shows an increase in the conjugation of APBA to dextran monomers with an increase in APBA concentration. $NaCNBH_3$ however, appears to not have a significant effect on the conjugation. At the lower APBA level, a decrease in conjugation was observed as the $NaCNBH_3$ concentration was increased. This can be attributed to the side reactions associated with $NaCNBH_3$ which become more prevalent at higher concentrations. The rate of reduction for iminium ions is much faster than the rate of reduction for ketones and aldehydes. The current reaction mechanism depends on the adjacent hydroxyl groups of the glucopyranose ring being oxidized to generate two aldehyde groups. At higher $NaCNBH_3$ concentrations for a given reaction time, it is proposed that the carbonyl groups were preferentially reduced reducing the number of sites available for APBA conjugation.

Furthermore, the Schiff base is stabilized via chemical reduction with $NaCNBH_3$. In literature, Schiff bases have been reportedly used for the detection of cyanide. In the reaction vessel, the interaction with the Schiff base and cyanide is expected to reduce the conjugation. In aqueous environments, $NaCNBH_3$ produces cyanide as a byproduct under aqueous conditions[234]. This is also a potential reason for the reduction in the conjugation efficiency as the concentration $NaCNBH_3$ is increased.

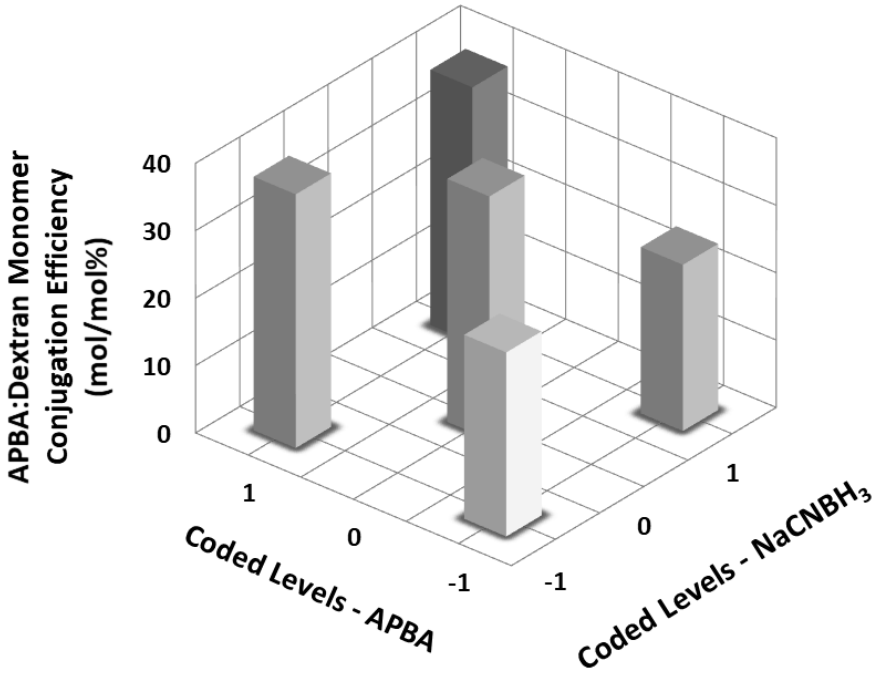

Figure 3.2: Results of APBA conjugation onto dextran via reductive amination.

It was hypothesized that increasing the concentration of the reducing agent would have a greater impact on the resulting conjugation efficient. An increase in ligand concentration was expected to increase the conjugation, but then plateau. These hypotheses were based on the low solubility of the APBA in aqueous environments. Thus, after reaching the maximum solubility limit, the ligand precipitates and the conjugation efficiency is no longer proportional to the ligand concentration in solution. From the results of this study, the converse was found to be true as shown in Figure 3.3. Increasing the APBA concentration has a significant effect on the conjugation efficiency. This conclusion, which is in contradiction to the hypothesis, may be a result of the concentration at the higher level not exceeding the solubility limit of APBA in the solution.

Moreover in Figure 3.3 curvature can be observed due to the placement of the center point in relation to the upper and lower levels used in the study. As previously mentioned, the primary interest of this study was the effect of NaCNBH3 and APBA concentration. Factors such as pH have been controlled, reaction volume, concentration and oxidation of dextran have been controlled. The curvature observed indicates the effect of other nuisance factors such as agitation rate, humidity, and exposure to light. Though the study was randomized and performed in triplicate, the inconsistencies between the stir

plates, and fluctuations in temperature in the laboratory environment may have been an influencing factor. The buffer used for this study was prepared every day and adjusted prior to use.

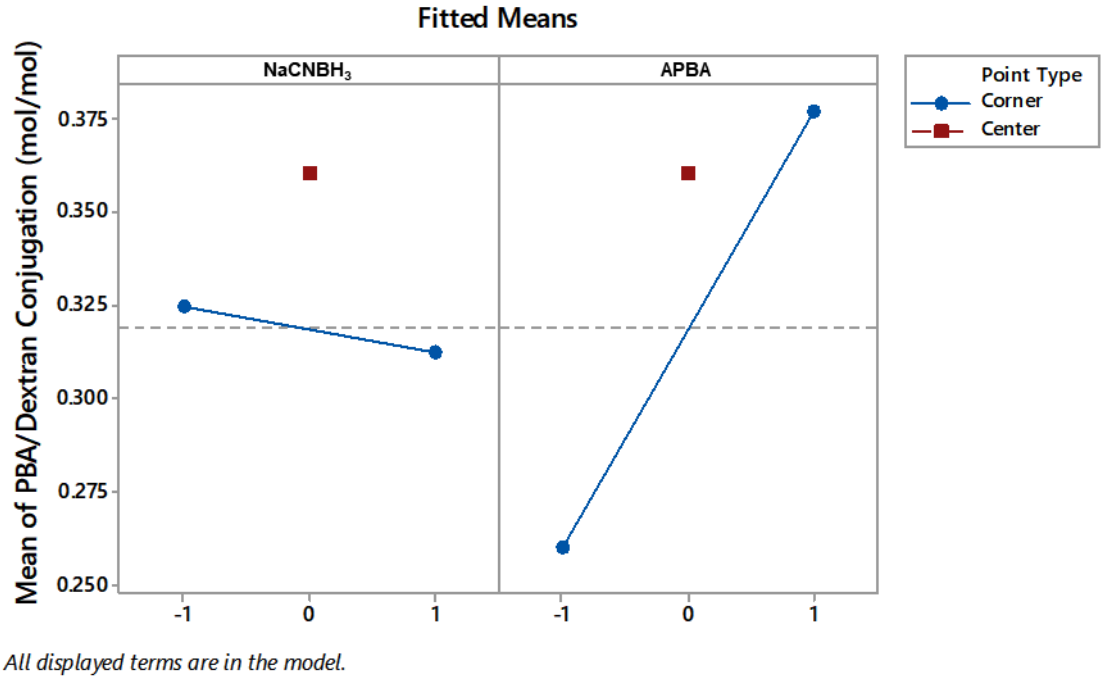

Figure 3.3: Main effects of design variables based on the fitted means of APBA/dextran monomer conjugation efficiency. APBA concentration in the reaction mixture has a more significant effect on the APBA/dextran monomer conjugation and has a positive correlation. $NaCNBH_3$ concentration is negatively correlated and has a less pronounced effect on the APBA/dextran monomer conjugation.

The interaction plot between the two main effects, shown in Figure 3.4, reveals that there is an effect of the interaction between the two concentrations. However, the interaction is not significant and outside of the working range. Investigation of the conjugation efficiency at significantly lower reducing agents may be explored in the future where the interaction will have a stronger influence on the conjugation efficiency. Hence, it can be concluded the APBA concentration is the major factor controlling the APBA conjugation onto dextran via reductive amination in the working range studied.

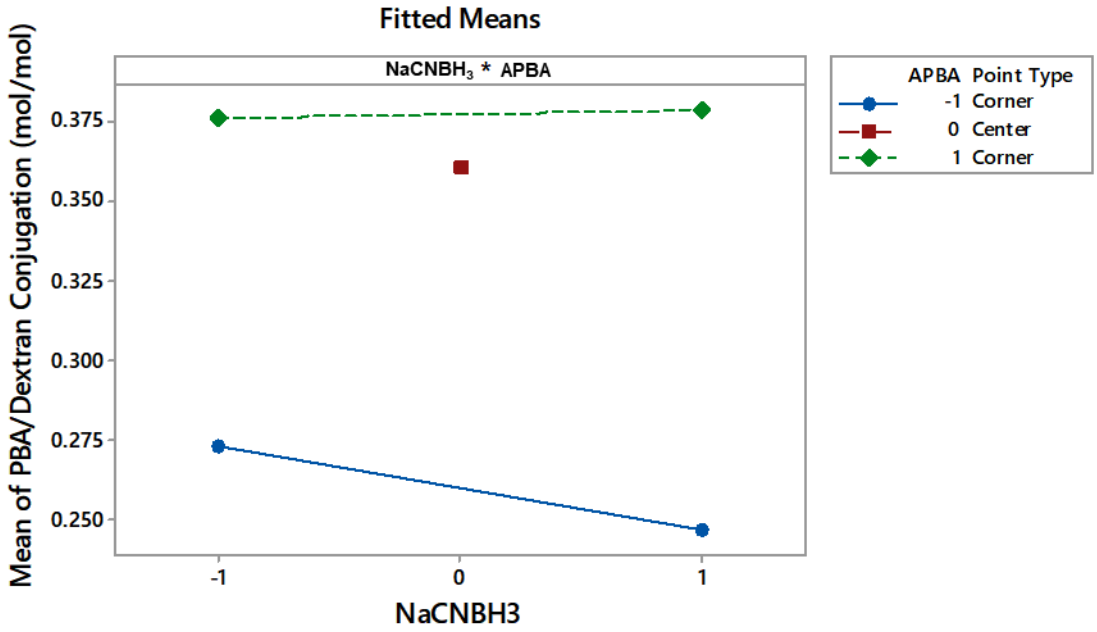

All displayed terms are in the model.

Figure 3.4: Interaction of design variables based on the fitted means of APBA/Dextran conjugation. There is no effect of the interaction between these two reagents in this working range.

To ensure consistency within the sample batches, the run order was randomized, and reagent solutions were prepared to eliminate error associated with the addition of dry mass. Figure 3.5 a) shows that the error follows the normal distribution, and Figure 3.5 b) confirmed there was no periodicity in the error resulting from the run order (i.e. the error is random). The eliminate the effect of nuisance variables, and to limit their contribution to the error the reaction was controlled as follows.

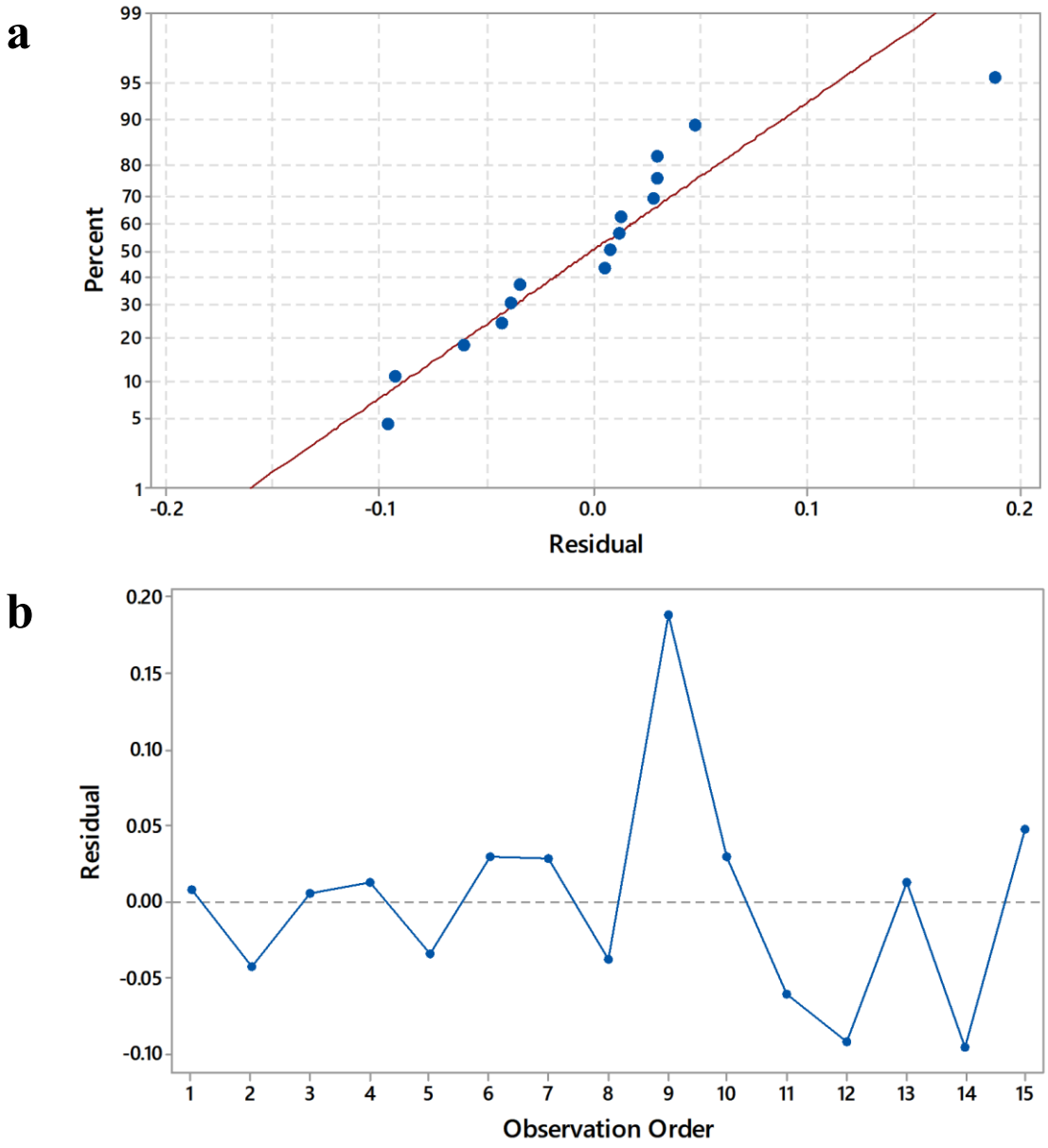

Figure 3.5: Residual plots indicating the error is normal. a) Normal probability plot for the APBA conjugation optimization study suggests that the errors in the response do indeed come from a normal distribution. b) Residuals versus run order for the APBA conjugation optimization study indicating that the study was indeed random as no distinct periodic pattern is visible.

3.4.1.1 Regression Model for APBA Conjugation onto Dextran

The model determined in this study (Equation 3.1) can be used to target a specific conjugation efficiency. C is the APBA/dextran monomer conjugation efficiency (mol/mol%), R is the molar concentration of the reducing agent solution (add 53 µl to reaction), and L is the molar concentration of the ligand solution (add 0.3 ml to reaction).

$$C = 0.3197 - 0.060R + 0.0588L + 0.0072RL \qquad \text{Equation 3.1}$$

3.4.2 Conjugation of APBA onto PLA-*b*-Dex Block Copolymer

This study focused on the same factors studied for the conjugation of APBA onto free dextran. The conclusions from the previous study were used to optimize this experiment and reduce the number of runs required due to the financial and time cost for the synthesis of PLA-*b*-Dex block copolymer. For the application of these mucoadhesive nanoparticles, it was important to prevent hydrolysis of the dextran backbone during the conjugation reaction. In the case of APBA conjugation onto free dextran, a buffered solution was used. However, the reduction amination of polymeric micelles is typically performed in DI water (>15 MΩ) (i.e. unbuffered aqueous environment) because salts, especially those of multivalent elements, destabilize the particles causing them to precipitate.

From the results of this study, shown in Figure 3.6, it can be concluded that an increase in the APBA concentration increases the conjugation efficiency. This agrees with the findings on APBA conjugation onto free dextran. However, in this study the effect of $NaCNBH_3$ is more significant. At the lower reducing agent level of 2.5 M, an increase in APBA concentration resulted in a reduction in conjugation. At the higher reducing agent level of 5 M and increase in APBA concentration resulted in an increase in the conjugation. This observation is attributed to the poor solubility of APBA in the reaction media (water). Upon addition of the concentrated 60 mg/ml stock of APBA in DMSO to the aqueous reaction media, aggregates are observed. The PLA-*b*-Dex block copolymer is insoluble in water, hence micelles are first created allowing the polymer to remain suspended in the reaction media and exposing the dextran corona to be available for reaction. Unlike the case with free dextran, fewer sites are available for conjugation due to the micelle structure which has a collapsed dextran corona. Furthermore, there is increased steric hinderance as the APBA conjugates to the dextran making the corona more hydrophobic and causing it to contract further.

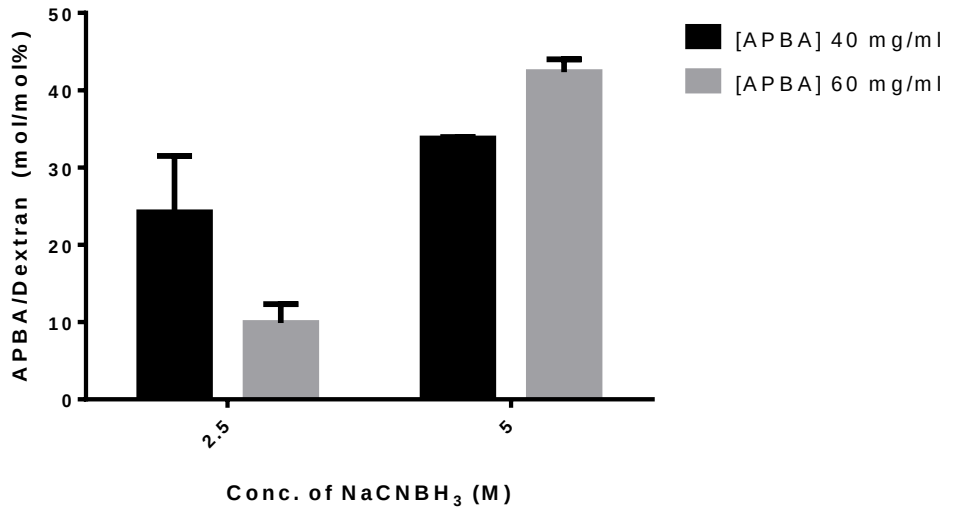

Figure 3.6: Effect of APBA and $NaCNBH_3$ concentrations on the APBA/Dextran conjugation onto PLA-*b*-Dex polymer micelle nanoparticles.

Upon addition of the 60 mg/ml APBA in DMSO solution to the reaction with 5M $NaCNBH_3$ the conjugation efficiency was the highest of all the samples. This environment is also more basic than the 2.5M solution, and the pH may have an impact on conjugation as this reaction was unbuffered. The conjugation efficiency of APBA/dextran monomer reached 42.3 (mol/mol%) as shown in Figure 3.6. This suggests that there is an interaction effect between the APBA and $NaCNBH_3$ during the conjugation of APBA onto PLA-*b*-Dex.

From the slope of the main effects in Figure 3.7 we can determine that the $NaCNBH_3$ concentration had a more significant impact on the conjugation efficiency. Furthermore, it can be concluded that the conjugation efficiency increases with reducing agent concentration. An increase in the ligand concentration resulted in decreased conjugation. Unlike in the case of APBA conjugation to free dextran, Figure 3.8 confirms that there is an interaction between the APBA and $NaCNBH_3$ in the operating region for conjugation to PLA-*b*-Dex. This interaction may be a direct consequence of the steric hinderance to the reaction which is not present with free dextran.

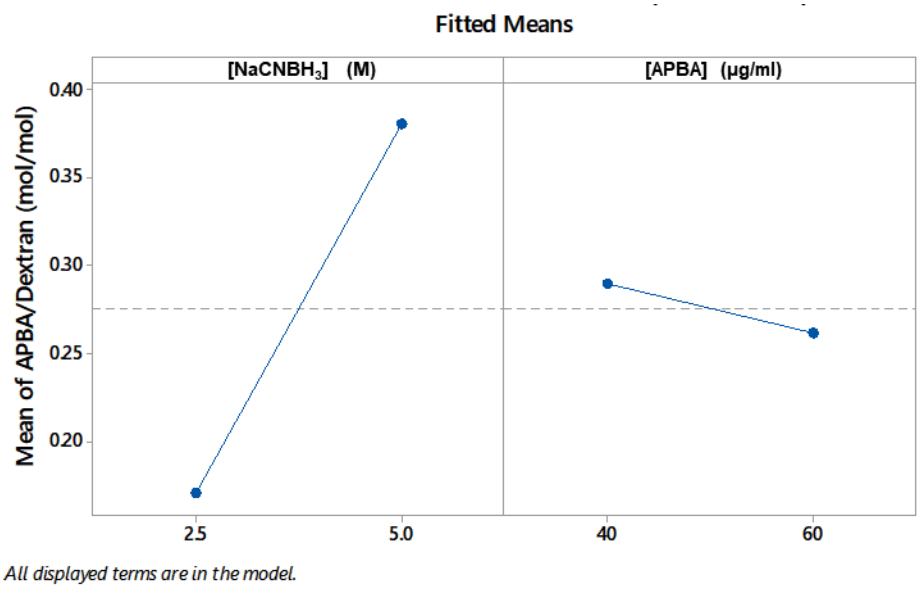

Figure 3.7: Plot of the main effects for APBA conjugation onto PLA-*b*-Dex polymer micelle nanoparticles showing the fitted means (mol/mol. The reducing agent has a more significant effect and is positively correlated with the conjugation efficiency. APBA is negatively correlated and has a less pronounced effect on the APBA/dextran conjugation.

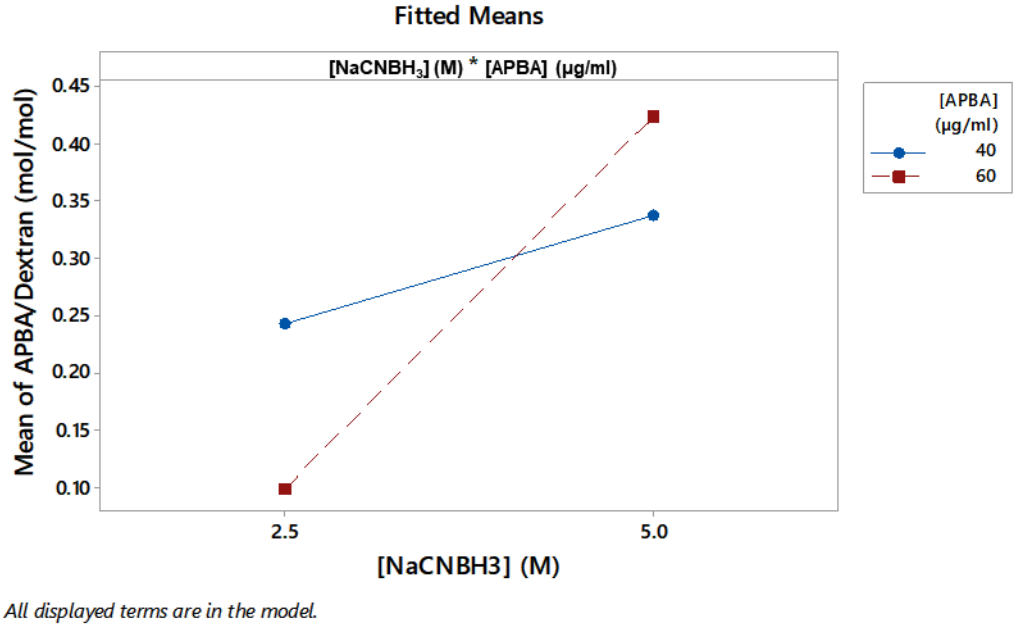

Figure 3.8: Interaction plot between the main effects in the conjugation of APBA to PLA-*b*-Dex block copolymer showing the fitted means and significant interaction in the operating region.

The pareto chart for the main effects and interactions (Figure 3.9) reveals that the APBA concentration was not a statistically significant factor at the 95% confidence level. The pareto chart also reveals that the concentration of reducing agent is a significant factor. More importantly the interaction between the concentration of $NaCNBH_3$ and APBA is concluded to have a statistically significant effect on the conjugation of APBA to the PLA-*b*-Dex block copolymer.

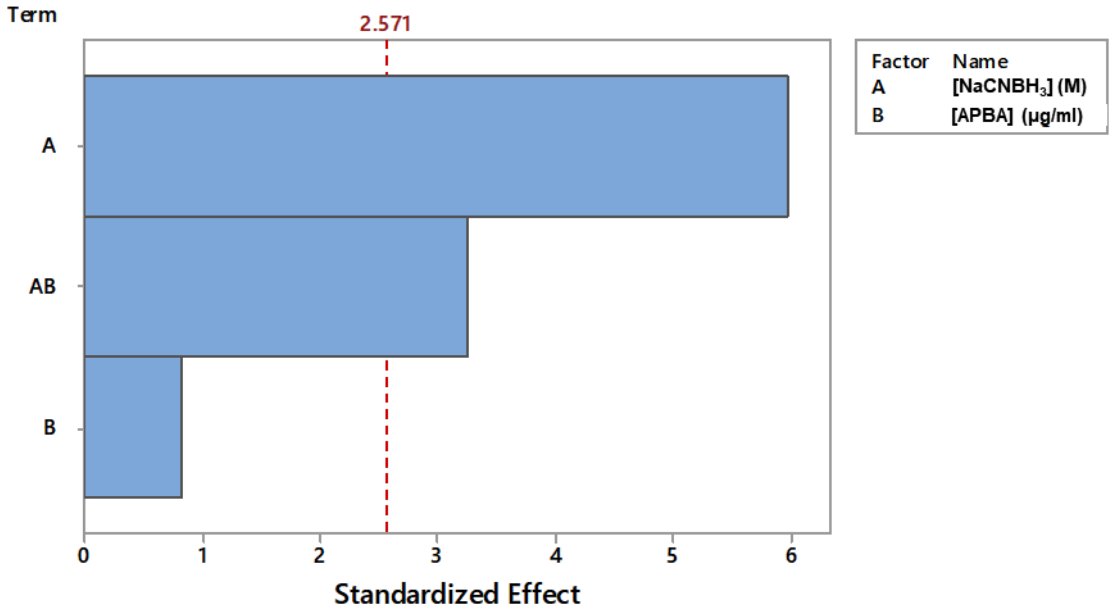

Figure 3.9: Pareto chart of the standardized effects. The response is APBA/dextran monomer conjugation (mol/mol%) with $\alpha = 0.05$. The significant factors in the conjugation of APBA to dextran onto the backbone of PLA-*b*-Dex were determined to be the reducing agent concentration and the interaction between the reducing agent and ligand.

The analyses shown in Figure 3.10 was conducted to ensure the error in the data followed a normal distribution. From Figure 3.10 a) and Figure 3.10 b) it can be concluded that the error follows the normal distribution at the 95% confidence interval. Figure 3.10 c) illustrates that the distribution follows a bell curve. Figure 3.10 d) reveals a random pattern indicating that the run order did not have an impact on the results. Since the samples were randomized and synthesized in batches over the course of a week, this suggests that nuisance factors were not significant factors between the randomized runs and batches.

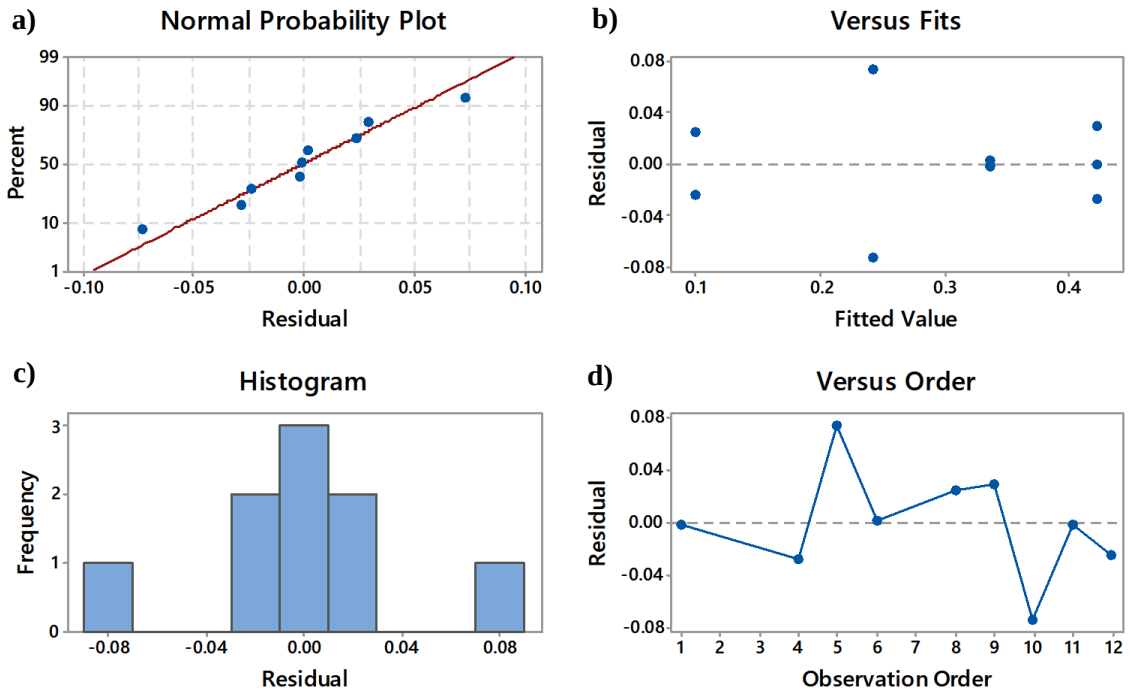

Figure 3.10: Residual plots for APBA/dextran monomer conjugation (mol/mol%) demonstrating the error follows a normal distribution. a) Normal probability plot of the residuals b) plot of residuals vs. response variable (APBA/dextran conjugation), c) a histogram of the residuals revealing a bell curve distribution, and d) a plot of residuals vs. run order.

3.4.2.1 Regression Model for APBA Conjugation onto PLA-b-Dex Polymer Micelles

Analysis of variance performed with Minitab's statistical package yielded a regression model with an R^2 value of 90.95%. This indicates a good fit but suggests that there are other factors which may influence the results, and this require further control. As shown in Figure 3.10 d) the run order and nuisance environmental factors such as humidity and temperature did not have a significant impact on the error.

This error is attributed to the oxidation stage of the reaction. The standard procedure for the conjugation involves the nanoprecipitation of PLA-*b*-Dex into aqueous media and is then followed by oxidation of the dextran backbone. Variance in the oxidation between runs and replicates would be a major contributor to the error in this model. This error can be eliminated via synthesis of PLA-*b*-DexOx block copolymer and subsequent purification to allow for consistent oxidation between runs. However,

the effect on stability and properties would need to be examined. Furthermore, PLA-*b*-Dex-Ox can be expected to have different solubility when nanoprecipitates due to a more hydrophobic corona. Lastly, there is need for a method for the accurate detection of oxidized monomers. ^{1}H-NMR analysis is unable to resolve the difference in the structure as the aldehyde groups of Dex-Ox and hydroxyl groups of dextran have the same relative chemical shift.

Nevertheless, the model determined in this study (Equation 3.2) has good correlation and may be used to approximately target a desired APBA/Dex conjugation as required by the application. C is the APBA/dextran monomer conjugation in units of mol/mol%, R is the molar concentration of the reducing agent stock solution (assuming 300 µl are added to the same reaction volume), and L is the concentration of the ligand stock.

$$C = 0.890 - 0.1449R - 0.01860L + 0.00458RL \qquad \text{Equation 3.2}$$

3.5 Conclusions

The utility of mucoadhesive platforms for drug delivery vehicles is well demonstrated in literature. Based on pharmacoeconomic analysis, the optimal mucoadhesive platform is one which may be easily customized for the different mucosal environments in the body. This study demonstrates that the conjugation of the mucoadhesive ligand can be modified by controlling the ligand and reducing agent concentrations. Two regression models were developed as a result of these studies to target APBA conjugation onto free dextran and PLA-*b*-Dex block copolymer micelles. The analyses presented provided insight into the reaction mechanism, interactions, and possible side reactions influencing the overall conjugation efficiency. The current quality control protocol calls for 5 – 20 mol/mol % conjugation of APBA onto dextran or PLA-*b*-Dex block copolymer. This wide range represents the variability in the reductive amination pathway. Through this work, sources of variance have been identified and thus can be controlled for improved reproducibility. Moreover, conjugation efficiencies as high as 42.3 mol/mol% have been achieved. Free dextran is currently utilized as an ocular lubricant; the mucoadhesive Dex-APBA explored in this chapter may be explored for the treatment of chronic dry eye as an ocular lubricant. These models may be utilized to diversify treatment regimens for varying severity as the mucoadhesive strength and retention time are related to the ligand conjugation. Optimization of this mucoadhesive platform can improve delivery and bioavailability of commercial therapeutics and enable market entry of molecules limited by their poor bioavailability.

Chapter 4
Co-Solvent Dehydration of BPBA onto Dextran Via Williamson Ether Synthesis Reaction Pathway

4.1 Summary

Carbohydrates are ubiquitous in drug delivery applications due to their biocompatibility and yield functional biomacromolecules upon modification. The complex and time-consuming chemistry often requires the use of solvents unsuitable for application in pharmaceuticals. Herein a reaction mechanism for the functionalization of dextran with a phenylboronic acid derivative is explored and the optimized. A conjugation efficiency of BPBA/dextran monomer of 42.6 mol/mol% was achieved with reaction conditions of 10 minutes and 110°C (significantly lower than conventional solid-state chemistry). By controlling the melt mixture in this third-order diffusion limited reaction and via the addition of water as a plasticizer the conjugation can be tuned. The resulting product is analogous to Dex-APBA explored in Chapter 3 and this process provides significant improvement over conventional reactions in solvent.

4.2 Introduction

Nanocarriers for drug delivery must be biocompatible, stable in physiological conditions, and be cleared from the body without toxic degradation products. Carbohydrates are the ideal materials for this application and they have already been utilized for numerous applications in medicine including tissue engineering and drug delivery[235,236]. Carbohydrates also have the added advantage of numerous functional groups present the backbone which allows for functionalization with various targeting moieties[237]. However, the long reaction times and multiple purification steps to remove organic solvents can be a significant drawback. Moreover, the stability of the nanoparticle, and loaded drug in some applications, may need to be considered when designing the process.

Solid-state chemistry presents a solvent-free and rapid reaction pathway alternative to conventional reactions performed in solvent. Conventional solid-state reactions are performed by combining powdered reagents and accelerated with heat (often 1000°C or above) to allow the reaction to proceed in an appreciable rate. The resulting viscous state is referred to as the melt. Typical reaction conditions such as the elevated temperature would result in irreversible degradation of the carbohydrate (or caramelization) yielding an unusable product.

Herein, a co-solvent dehydration method is utilized to modify dextran with 4-(bromomethyl)-phenylboronic acid (BPBA) to yield a functional carbohydrate (Dex-BPBA) similar to Dex-APBA explored in Chapter 3. The reaction scheme is based on Williamson ether synthesis, in the absence of organic solvent and thus a simplified purification process. Instead a small fraction of water is added to the reagent powders to improve homogeneity of the reactants in the mix. Unlike organic solvents such as acetone which are sometimes utilized during the mixing process, the water does not volatize. During the reaction, the water acts as a plasticizer improving the diffusion in the melt, and reduces the effective temperature thereby preventing degradation of the dextran. To further mitigate the degradation of the carbohydrate, the co-solvent dehydration method discussed herein is performed at much lower temperatures. This work investigates the melt composition, temperature and reaction time and their effects on the conjugation efficiency and kinetics.

This chapter contains co-authored material with Dr. Shengyan (Sandy) Liu. His thesis entitled 'Development of a topical ocular drug delivery system using polymeric nanoparticles' presents findings on the reaction conditions for this co-solvent dehydration mechanism. This thesis expands on the effect of the reaction conditions with a full factorial study and analysis on the reactant concentrations, as well as the reaction kinetics.

4.3 Experimental Section

4.3.1 Materials

Dextran from *Leuconostoc mesenteroides* (Dex; M_n = 9-11 kDa), sodium tert-butoxide (tBuONa), 4-(bromomethyl)phenylboronic acid (BPBA), N-Hydroxysulfosuccinimide (Sulfo-NHS), sodium hydroxide (NaOH), dimethyl sulfoxide (DMSO), deuterium oxide (D_2O) were purchased from Millipore Sigma. Liquid nitrogen was dispensed from the University of Waterloo Chem Stores.

4.3.2 Co-Solvent Dehydration of BPBA onto Dextran

Dextran, tBuONa, and BPBA were combined in a mortar and mixed with a pestle to uniformly distribute the powders. Water was then added dropwise at a 1.25:1 ratio of water:dextran on a mass basis while mixing to create a paste. The mixture was then transferred to a borosilicate scintillation vial with a sealed cap and placed inside a pre-heated oven at varied temperatures and durations. After the reaction time had elapsed, the vial was removed from the oven and purged with cool air to terminate

the reaction. Once at room temperature, the product dissolved in DI water (>15 MΩ) and dialyzed for 24 hours to remove any unreacted reagents or degraded product. The dialyzed solution was freeze-dried by freezing the solution with liquid nitrogen and dried using Labconco Freezone 2.5L at -54°C at 0.013 mPa for 24 hours or until the water had been removed. The modified dextran was characterized via ^{1}H-NMR; the characterization sample was prepared in D_2O at a concentration of 20 mg/ml. This procedure is visualized in Illustration 4.1..

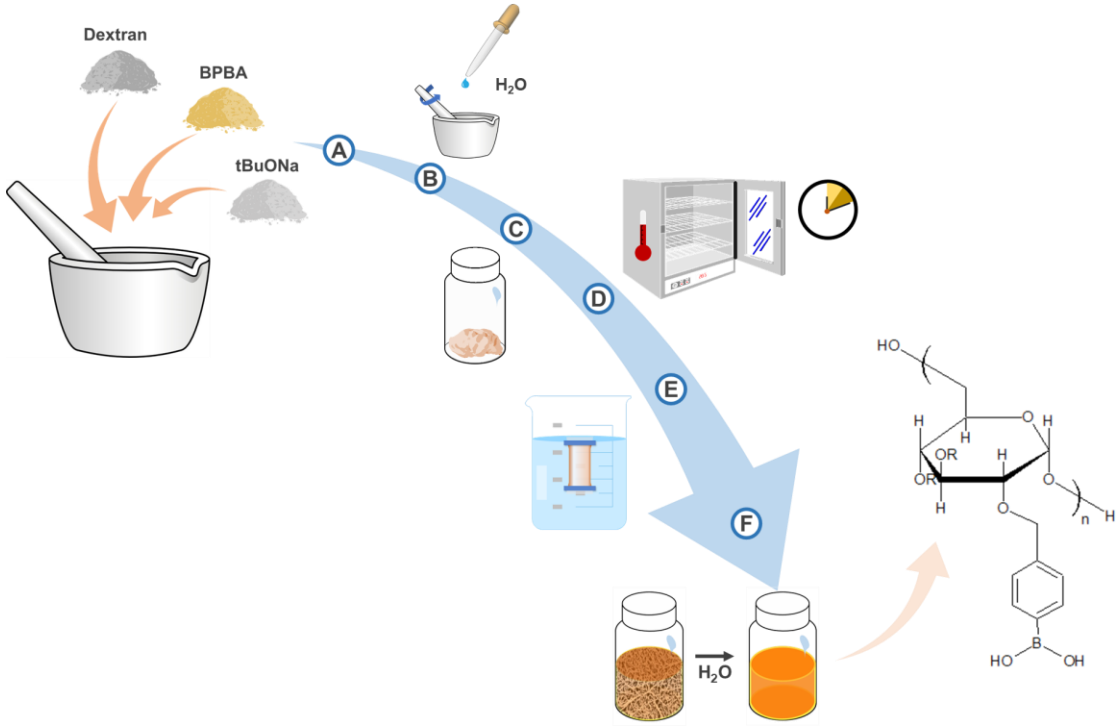

Illustration 4.1: Procedure for co-solvent dehydration of BPBA onto dextran. A) the reagents are combined, and B) water is added dropwise and mixed to create a paste which is C) transferred to a borosilicate vial. D) the vial is placed into a preheated oven for 10 minutes, and E) the product is dialyzed and freeze-dried to yield the final product F) Dex-BPBA.

4.3.3 Williamson Ether Synthesis for Modification of Dextran with BPBA in Solvent

Dextran was acclimated at room temperature, and 500 mg were dissolved in 10 ml of a solution comprising of DI water (> 15 MΩ) and DMSO with a mix ratio of 2:8. The mixture was vortexed until the dextran had dissolved, then stirred in a water bath at 45°C to raise the temperature of the solution. 1 ml of NaOH (30 w/v% in water) was added dropwise to the solution and the solution was equilibrated

for 30 minutes. BPBA (one molar equivalent) was added to the solution, the reaction vessel was sealed and shielded from light with aluminum foil, and the reaction proceeded for six hours. The product was purified via dialysis against DI water and freeze-dried. The modified dextran was characterized via ^{1}H-NMR; the characterization sample was prepared in D_2O at a concentration of 20 mg/ml.

4.4 Results and Discussion

4.4.1 Semi Solid-State Modification of Dextran with BPBA

The semi solid-state reaction performed was a co-solvent dehydration reaction based on the Williamson ether synthesis mechanism shown in Illustration 4.2. The conjugation efficiency was determined as a ratio of BPBA to dextran monomers via ^{1}H-NMR (Figure 4.1) after removing the unreacted BPBA from the mixture. Chemical shifts corresponding to carbon 1 (C1) of the dextran monomer were observed near 4.8 ppm, and shifts corresponding to the phenyl ring of BPBA were observed near 7.25 ppm (C2 and C6) and 7.6 ppm (C3 and C5).

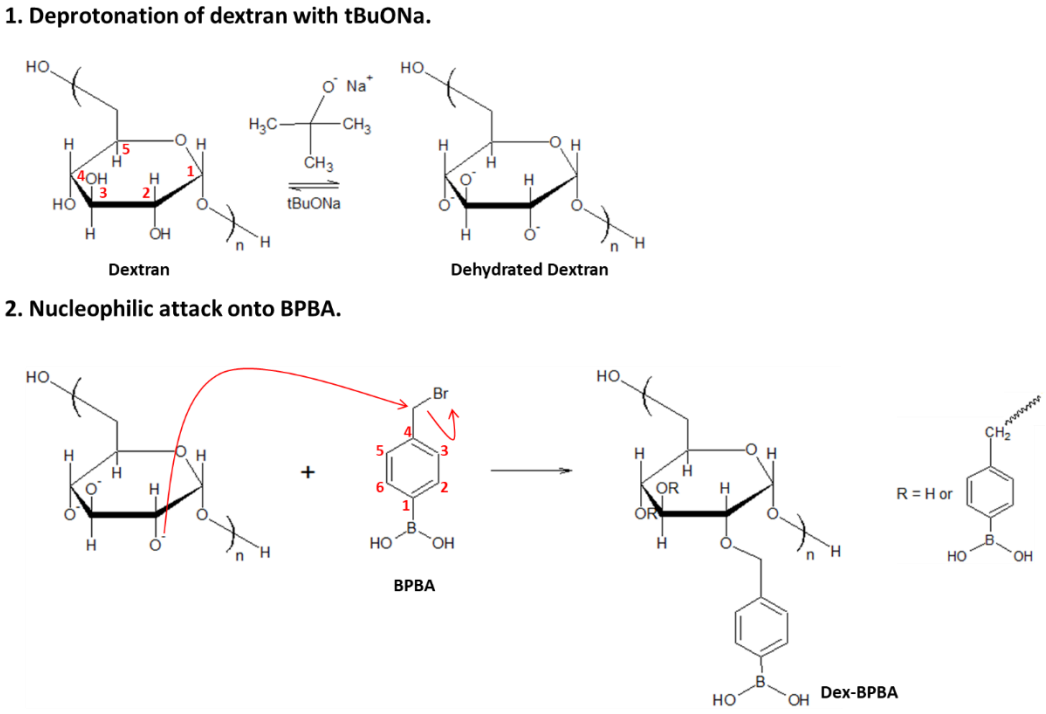

Illustration 4.2: Williamson ether synthesis mechanism for the conjugation of BPBA to dextran.

Effect of reaction conditions on BPBA/dextran conjugation efficiency

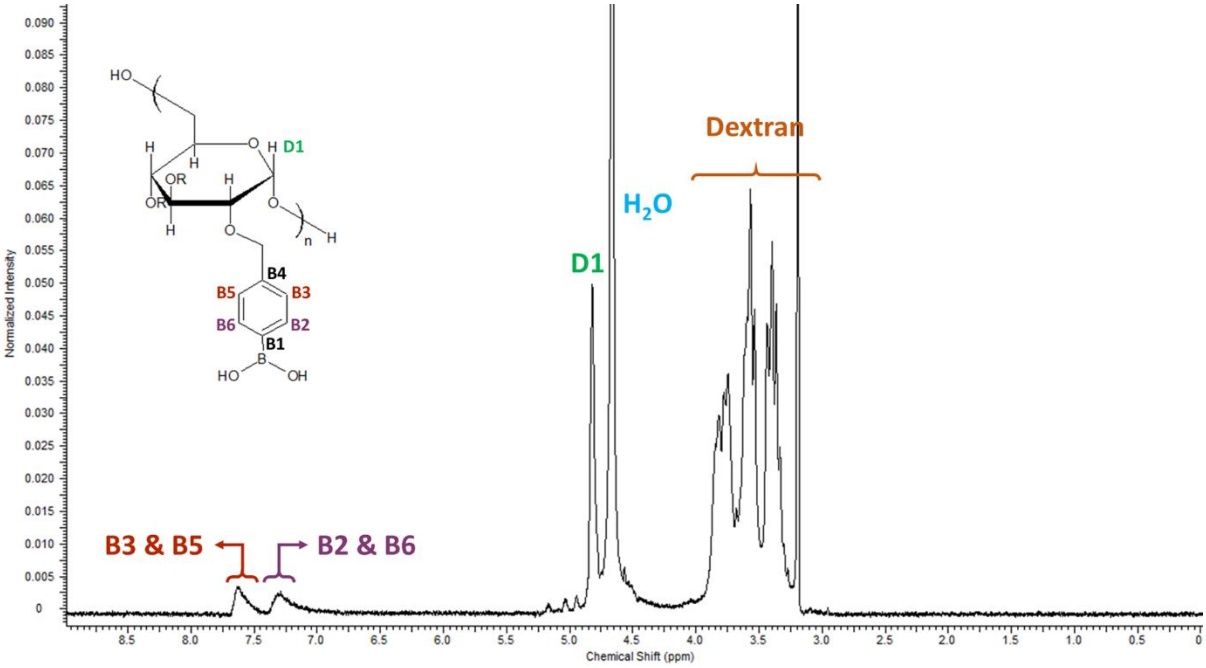

Figure 4.1: ^{1}H-NMR spectra confirming conjugation of BPBA to dextran.

To study the effects of the solid-state reaction process on the co-solvent dehydration of BPBA onto dextran, the reaction was performed at various temperatures and times. The reaction mixtures were prepared in a 1:1:1 ratio of dextran:tBuONa:BPBA on a molar basis with 1.25:1 ratio of water:dextran on a mass basis. Water is added as a plasticizer and to reduce effective reaction temperature the mixture was placed in an oven held at 70, 90, 110, or 130°C for 10, 30, 60, and 120 minutes. As seen in Figure 4.2, the study at 130°C was terminated after 30 minutes as the product had caramelized indicating degradation of the dextran. As reported in literature, the conjugation efficiency of BPBA onto dextran increased with reaction temperature[238]. An increase in time however did not significantly increase the efficiency of the conjugation (student t-test: $p < 0.05$). After just 10 minutes at 110°C the conjugation of the phenylboronic acid derivative onto dextran was similar to the desired conjugation of APBA onto PLA-*b*-Dex nanoparticles utilized for ophthalmic drug delivery. Thus it was concluded that 110°C was the optimal temperature for this process of co-solvent dehydration.

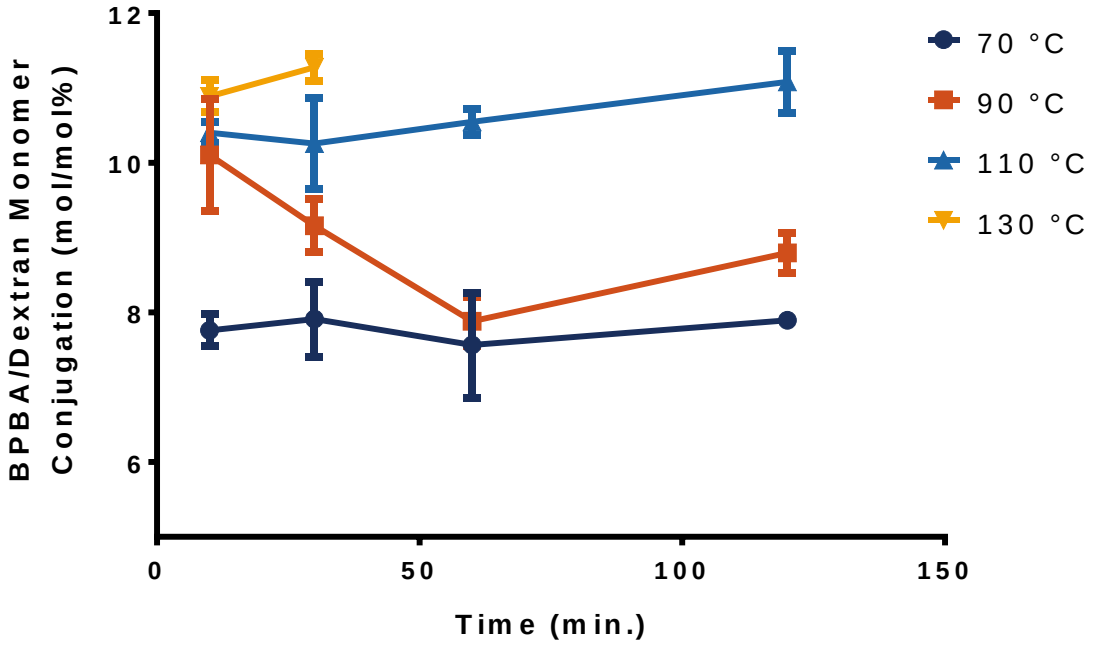

Figure 4.2: Effect of temperature and time on the BPBA/dextran conjugation efficiency

4.4.2 Effect of the Mix Ratio of Reagents on the BPBA/Dextran Conjugation Efficiency

To study the effects of reactants in the mix on the resulting conjugation efficiency a factorial study was performed in triplicate by varying the concentration of BPBA and tBuONa; these are represented as molar ratios to dextran. The reaction conditions of 10 minutes at 110°C, determined to be optimal in Section 4.4.1, were used.

As seen in Figure 4.3 increasing the concentration of tBuONa (catalyst) resulted in an increase in the conjugation efficiency for all BPBA ratios. This is attributed to increased deprotonation of the dextran C2, C3, and C4 hydroxyls enabling the formation of ether linkages with BPBA. When the tBuONa fraction was held constant and BPBA was increased, the increase in conjugation efficiency was not significant. Conversely when holding the tBuONa:dextran ratio constant at 2:1 an increase in BPBA conjugation was observed with increasing BPBA fraction. We attribute this to the high reactivity of tBuONa with water; at low tBuONa concentrations the side reactions with water are favoured decreasing the fraction of tBuONa available to deprotonate dextran. Furthermore, the dextran used for a linear macromolecule with M_n = 9 – 11 kDa and the steric hinderance and poor melt diffusion may

contribute to lower conjugation efficiencies at low tBuONa concentrations. When tBuONa is present in sufficient excess, the BPBA:dextran ratio becomes the limiting factor.

Increasing the concentration of BPBA in the reaction mixture did increase the conjugation efficiency however, the effect was not as significant as that of tBuONa. BPBA may undergo reactions with themselves and form trimeric anhydrides, boroxines, especially under dehydrated conditions[239], such as those used in this reaction mechanism. Excess BPBA can promote these side reactions over ether linkage formation with hydroxyl groups of dextran due to reduced steric hindrance.

The fraction of water added was constant throughout, but mixtures with low tBuONa:dextran and BPBA:dextran ratios formed softer pastes as a result of less dry material whereas mixtures with high ratios were stiff and dry. This difference in consistency is likely to have an effect on the melt and diffusion of the reactants during the reaction. This may have contributed to the results observed for this study. Furthermore, excess water may reduce the conjugation efficiency due to side reactions. This is also an important consideration for reactions at low temperatures where the water may not have evaporated. This would have resulted in greater side reactions with the tBuONa (preferential deprotonation of water instead of dextran) and therefore a reduced conjugation efficiency.

With a ratio of tBuONa:dextran of 2:1, we achieved a conjugation efficiency of 42.6 mol/mol%. In comparison, the Williamson ether synthesis mechanism in solvent conditions (7-hour process) yielded an efficiency in the range of 1-3 mol/mol%. Thus, this method of carbohydrate modification results in faster reaction times, may be performed at lower temperatures than conventional solid-state reactions, and yields higher conjugation efficiencies than reactions in solution. Furthermore, the results from the factorial study provide us with flexibility in tuning the conjugation of the ligand for various applications.

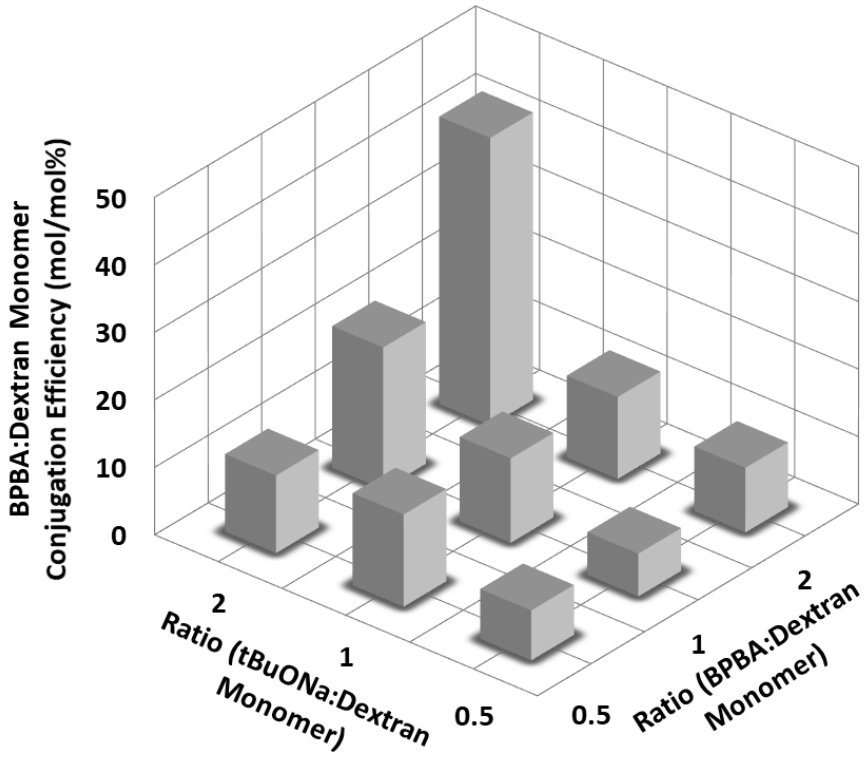

Figure 4.3: Effect of tBuONA:dextran and BPBA:dextran ratios in the mixture on BPBA/dextran conjugation efficiency (mol/mol%)

4.4.3 Co-Solvent Dehydration Reaction Kinetics

Reaction kinetics of typical solid-state reactions are determined via thermogravimetric analysis (TGA) or differential scanning calorimetry (DSC). Both techniques may be used to generate conversion curves as the dry mix is exposed to high temperatures and analyzed in situ. However, in the co-solvent dehydration reaction, a small fraction of water is added to as a plasticizer to prevent the degradation of the dextran polymer. The addition of water to the reactant mixture generates heat and initiates the reaction with tBuOna even prior to placing the mixture into the oven. Differences in time required to sample the mixture for measurement would be a source of variance in these methods. Additionally, the small mass required for TGA and DSC measurements impose additional restraints due to the precision of instruments available as well as the inability to mix the reagents. Consequently, TGA and DSC measurements could not be utilized in the determination of conversion and reaction kinetics as the study

would have significant variability. For the abovementioned reasons, ^{1}H-NMR measurements were used to determine the conversion fraction and draw conclusions on the reaction kinetics.

Solid-state kinetics are generally non-homogenous and vary in their rate limiting steps: nucleation, geometric contraction, diffusion, and rate order[240,241]. Several mathematical models have been proposed to determine the rate limiting step and corresponding the rate constants. Samples were prepared at constant temperatures with reactions times varying between 10 and 120 minutes to yield data on isothermal conversion with a constant BPBA:tBuONa:dextan ratio of 1:1:1. isothermal model fitting as described by Khawam et al. to determine the governing mechanism and rate constant [240]. The conversion data (conjugation efficiency) was used with various models in literature to determine the best fit. A linear plot of $g(a)$ vs. the reaction time is used to determine the appropriate model for the reaction. In Equation 4.1 $g(a)$ is the general integral form of the model, α is the conversion, k is the reaction constant with units of min^{-1}, and t is the reaction time in minutes. Models for 1D, 2D, and 3D diffusion in integral form are given by Equation 4.2, Equation 4.3, and Equation 4.4 respectively. After comparing the conversion fractions to these models, we propose that this semi solid-state reaction is 3D diffusion limited as shown in Figure 4.4. The largest contributing factor is likely the limited diffusion of BPBA and tBuONa in the viscous melt and the collapsed confirmation of dextran in this state restricting availability of conjugation sites. Thus, we propose that this semi solid-state reaction between dextran, tBuONa and BPBA is 3D diffusion limited, with a BPBA/dextran conjugation rate of $1.87 \times 10^{-6} \frac{(mol/mol\%)}{min}$.

$$g(a) = kt \qquad \text{Equation 4.1}$$

$$g(\alpha) = \alpha^2 = kt \qquad \text{Equation 4.2}$$

$$g(\alpha) = \big((1-\alpha)\ln(1-\alpha)\big) + \alpha = kt \qquad \text{Equation 4.3}$$

$$g(\alpha) = \left(1 - (1-\alpha)^{\frac{1}{3}}\right)^2 = kt \qquad \text{Equation 4.4}$$

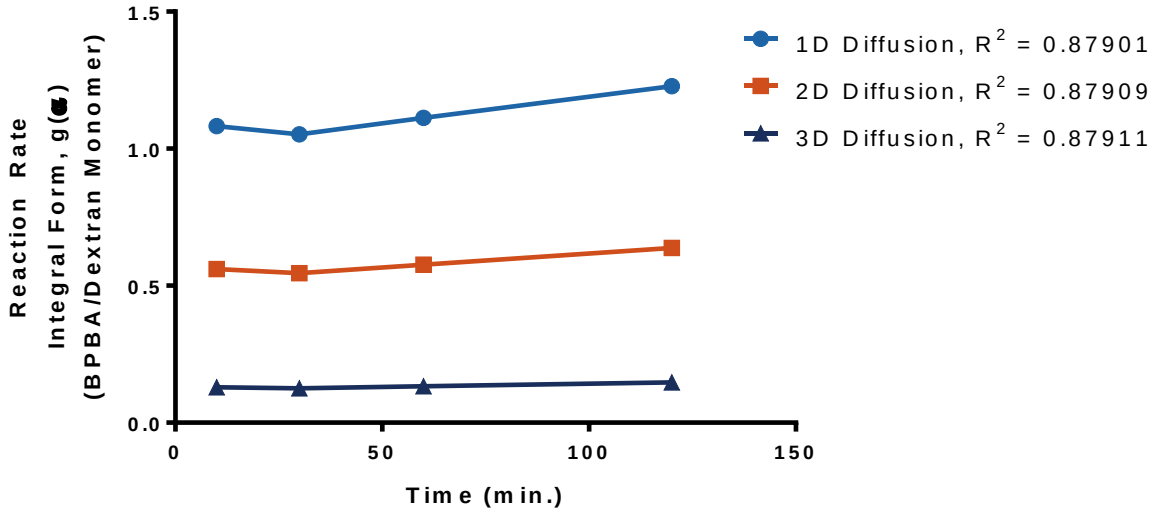

Figure 4.4: Diffusion models for semi solid-state conjugation reaction between BPBA and dextran.

4.5 Conclusion

Carbohydrates have proven utility in biomedical applications and are ideal materials for nanocarriers due their biocompatibility. They offer numerous functional groups for modification with targeting moieties such as the case with mucoadhesive PLA-*b*-Dex-APBA block copolymer micelles. However, the conventional modification processes require numerous complex steps and organic solvents which are undesirable for biomedical applications. A co-solvent dehydration method borrowing from principles of solid-state chemistry was utilized to functionalize dextran with a phenylboronic acid derivative. A small volume of water was used to prevent degradation of the carbohydrate and act as a plasticizer. The optimal reaction temperature was determined to be 110°C which is significantly lower than the temperatures typical in literature for solid-state chemistry. Reaction time was determined not to be a significant factor, and 10 minutes was sufficient in order to achieve a conjugation efficiency of 42.6 mol/mol% by modifying the concentration of reactants in the melt. The optimal ratio for dextran:tBuONa:BPBA was determined to be 1:2:1, yielding a conjugation similar to the reductive amination of APBA onto PLA-*b*-Dex block copolymer micelles. This conjugation can be achieved within 10 minutes as compared to the 24-hour reaction period for dextran, or nine hours for PLA-*b*-Dex micelles.

Chapter 5
Optimizing Stability and Long-Term Nanoparticle Storage

5.1 Summary

Colloidal drug delivery platforms have proven utility in overcoming the physical and chemical challenges to drug delivery. A major hurdle to commercialization to many of these systems is the short shelf-life due to long-term instability in their aqueous environments. Cryogenic and freeze-dried (or lyophilized) states have long been utilized by the pharmaceutical industry to isolate therapeutics and extend their shelf life. These techniques can also be utilized to extend the shelf-life of colloidal suspensions, such as the PLA-*b*-Dex-APBA polymer micelle nanoparticles, making them viable for commercialization. Herein, factors affecting the particle stability are discussed and optimal formulation design are discussed. A suspension containing 2 wt% of trehalose as a protectant was found to be the optimal formulation for freeze-drying and resuspension of MNPs. A self-cryopreservation property was also identified, and the components of the formulation were studied to determine the underlying cause.

5.2 Introduction

Colloidal systems have low stability and will aggregate or degrade overtime rendering the functional properties void[209]. This is one of the key challenges which must be addressed before formulations comprised of nanoparticles for drug delivery may become commercially viable[209]. The PLA-*b*-Dex block-copolymer is a biodegradable macromolecule designed to breakdown in the physiological conditions without toxic degradation products. As such, the intermolecular bonds are susceptible to hydrolysis. The resulting self-assembled micelles continue to release drug in aqueous media if a diffusion gradient exists, but also as they breakdown. This results in a short shelf-life as compared to other ophthalmic preparations in the market.

The purification of many pharmaceutical active ingredients is performed via freeze-drying. The stresses produced during this process can destabilize the colloidal suspension. However, once optimized for the formulation this technique does not damage the nanoparticle and results in effective removal of water from the system. In the dried form, the API has prolonged stability are not susceptible to deactivation in aqueous environments. This approach can be utilized to remove the drug loaded nanoparticles from their aqueous life, thus extending their shelf-life and commercial viability[209].

The ideal solution would encompass a facile and rapid preservation and reconstitution process which preserves the physiochemical properties of the suspension. In the interest of PLA-*b*-Dex-APBA nanoparticles as mucoadhesive drug carriers for ophthalmic drug delivery, the properties of interest are the particle size and drug entrapment. This work investigates properties of the nanoparticles under the stress of cryogenic conditions and lyophilization and proposes recommendations for formulation design. The freeze-drying process and the effect on the particles in suspension is shown in Illustration 5.1.

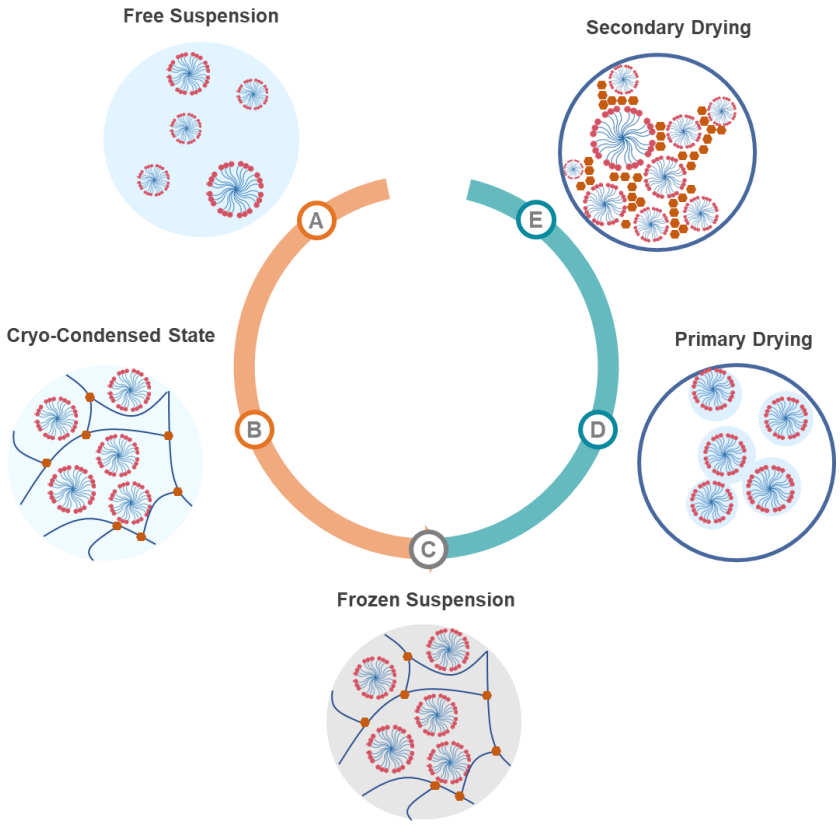

Illustration 5.1: Freeze-drying process and the effect of protectants on the particle stability. During the freezing process A) the free micelle in suspension B) concentrates into a 'cryo-condensed state' as the bulk of the water freezes. Micelles may aggregate or be disrupted due to the formation of large ice crystals. The presence of cryoprotectant C) results in the formation of smaller crystals less likely to disrupt the particles. During the primary drying D) bulk of the water is sublimed, and during E) secondary drying 'bound water' or molecules associated with the particles are sublimed. This process may drive aggregation of the micelles.

Trehalose had been previously determined to be effective in preserving the size and properties of the PLA-*b*-Dex and PLA-*b*-Dex-APBA polymer micelle nanoparticles. However, in literature, they are often used in concentrations which are unacceptable for ophthalmic preparations due to the osmolarity limit imposed by the regulatory bodies and as described in the USP. The first phase of this study investigated the effect of trehalose concentration on the stability of the preserved formulations. It has been shown in literature that the stabilization is proportional to the concentration of sugars when used in this role[209]. For the formulation to be commercially viable in accordance to the guidelines established by the regulatory bodies for ophthalmic preparations, it is critical to reduce the concentration of protectant required.

Alternate cryoprotectants were also investigated and compared to trehalose to determine if another molecule could provide better protection, particularly at comparable or lower concentrations. The protectants were selected based on excipients commonly used for commercially available ophthalmic preparations. This would result in faster regulatory approval for the nanoparticle formulation as the pharmacokinetics of the excipients would not have to be further investigated.

Lastly, trehalose has been successful as both a cryoprotectant and a lyoprotectant in literature. However, the efficacy of a protectant has be investigated for each formulation on the basis of trial and error. Furthermore, some therapeutics are frozen instead of being stored in liquid media or dried as a powder. As freezing is a much more cost effective than freeze-drying, this method and the role of protectants was also explored.

5.3 Experimental Section

5.3.1 Materials

Acid-terminated poly(D,L-lactide) (PLA; Mw ~ 20 kDa), dextran from *Leuconostoc mesenteroides* (M_n = 9-11 kDa), poly(ethylene glycol) methyl ether-block-poly(L-lactide-co-glycolide) (PLGA-*b*-PEG; $M_{n,PEG}$ 5,000; $M_{n,PLA}$ 25,000; lactide:glycolide 50:50), sodium periodate ($NaIO_4$), ethylenediamine (EDA), sodium cyanoborohydride ($NaCNBH_3$), *N*-(3-Dimethylaminopropyl)-*N′*-ethylcarbodiimide hydrochloride (EDC), *N*-Hydroxysulfosuccinimide, sodium salt (NHS), 3-Aminophenylboronic acid monohydrate (APBA), glycerol, deuterium oxide (D_2O), and D_2O with 1 w/w % 3-(Trimethylsilyl)-1-propanesulfonic acid-d6 (D_2O with DSS-D_6), methanol and dimethyl sulfoxide (DMSO) were purchased from Millipore Sigma. Liquid nitrogen was dispensed from the University of Waterloo Chem Stores.

5.3.2 Synthesis of Amine Terminated Dextran

Borate buffer was prepared by dissolving boric acid (3.1 g/L) in pure water (>15 MΩ) and adjusted to pH 8.2 with 1 N NaOH. Dextran was dissolved in the borate buffer at a concentration of 0.2 g/ml. The terminal dextran monomer exists in equilibrium as a open or ring structure. The alkaline conditions favor the open conformation which improves the reaction efficiency. EDA was added to the reaction mixture in 20 times excess of dextran (6 mmol) and allowed to react for 24 hours in a vessel shielded from light. After the first 24 hours, 300 µl of 5M $NaCNBH_3$ dissolved in 1N NaOH was added to the solution per day for an additional 48 hours (total of two additions).

The aminated dextran (Dex-NH_2) was purified via methanol wash. The aqueous solution was topped with eight times excess of methanol and vortexed to disperse the dextran and break apart any aggregated precipitates. The mixture was centrifuged at 3,000 rpm, and the supernatant was discarded. The wash was repeated one additional time prior to drying in a vacuum desiccator to remove residual methanol.

The dried polymer was analyzed for verification and quantification of amination via ^{1}H-NMR. The polymer was dissolved in D_2O at a concentration of 20 mg/ml. The dextran C1 peak corresponds to the peak between 4.7 to 5 ppm. The $(CH_2)_2$ of the conjugated EDA has a chemical shift between 2.5 to 2.7 ppm. The ratio of the peaks is used to quantify the conjugation. Only Dex-NH_2 with conjugation efficiency greater than 80% was used for subsequent reactions.

5.3.3 Purification of Acid Terminated PLA

Acid terminated PLA was dissolved in DCM at a concentration of 0.24 g/ml and washed with 8 times excess methanol to remove monomers and small chains. The mixture was centrifuged, and the supernatant was decanted. The remaining PLA gel was purged with air prior to vacuum desiccation for 24 hours. The weight averaged molecular weight was determined by end group analysis via ^{1}H-NMR; the PLA-end CH had a shift at 4.13 ppm and was compared to the PLA CH in the backbone at 5.18 ppm.

5.3.4 Synthesis of PLA-*b*-Dex

The block copolymer was synthesized via carbodiimide chemistry. Dex-NH_2 and purified PLA were dissolved separately in DMSO at a concentration of 0.1 g/ml separately. The acid-terminated PLA was activated by adding Sulfo-NHS (0.46 mmol) and EDC (0.209 mmol) to the PLA. The dissolved dextran was added to the PLA mixture after dissolution of the EDC. The reaction mixture was purged with nitrogen and remained shielded from light for the duration of the experiment. The polymer was purified via dialysis using regenerated cellulose dialysis tubing (MWCO: 12 to 14 kDa) against 200 times the volume DI water for 48 hours with at least six media changes. The unconjugated Dex-NH_2 (Mn ~ 9 – 11 kDa) was removed into the dialysis media and discarded leaving only the conjugated block copolymer within the dialysis tubing. The polymer solution was frozen with liquid nitrogen and lyophilized to remove water and isolate the dry polymer.

The dry polymer was analyzed via ^{1}H-NMR for verification and quantification of block copolymer synthesis. The ratio of the PLA (CH) peak between 5 to 5.3 ppm was compared to the reference peak of dextran (C1) at 4.6 ppm. Only lock copolymer samples with conjugation greater than 90% were used for the studies.

5.3.5 Synthesis of PLA-*b*-DexOx

The dried PLA-*b*-Dex block copolymer was dissolved in anhydrous DMSO at a concentration of 30 mg/ml. Nine ml of the polymer solution was nanoprecipitated into 30 ml of pure water (>15 MΩ). The suspension was continuously agitated for 30 minutes to allow the nanoparticles to complete forming. The reaction vessel was then shielded from light and 8.50 ml of a $NaIO_4$ solution (10 mg/ml) was added to the suspension to oxidize the dextran corona of the nanoparticles. After 20 minutes, 1 g of glycerol was added to react with the residual $NaIO_4$ as oxidation of glycerol would be favored over dextran. The

reaction mixture was dialyzed against 10 times excess DI water for 24 hours and lyophilized for 24 hours after being frozen with liquid nitrogen.

5.3.6 APBA Modification of PLA-*b*-Dex

The dried PLA-*b*-Dex block copolymer was dissolved in anhydrous DMSO at a concentration of 30 mg/ml. Nine ml of the polymer solution was nanoprecipitated into 30 ml of pure water (>15 MΩ). The suspension was continuously agitated for 30 minutes to allow the nanoparticles to complete forming. The reaction vessel was then shielded from light and 8.50 ml of a $NaIO_4$ solution (10 mg/ml) was added to the suspension to oxidize the dextran corona of the nanoparticles. After 20 minutes, 1 g of glycerol was added to react with the residual $NaIO_4$ as oxidation of glycerol would be favored over dextran. This was done to ensure the minimize the side reactions and consumption of the reducing agents. 120 mg of APBA was added, followed by 600 µL of a 5 M $NaCNBH_3$ solution prepared in 1 N NaOH. After 2 hours, the reaction mixture was dialyzed against 10 times excess DI water for 24 hours and lyophilized for 24 hours after being frozen with liquid nitrogen.

5.3.7 Characterization of APBA Conjugation

The analysis of APBA conjugation was performed by reconstituting the dried PLA-b-Dex-APBA copolymer in DMSO at a concentration of 1.25 mg/ml. Dex-Ox in DMSO at the same concentration was used the baseline. The absorbance was measured from 240 – 320 nm with a 1 nm step size using Tecan Infinite Pro 200 MPlex Multimode plate reader. The current protocol for quality control requires APBA conjugation between 5 to 20 mol/mol% (APBA/dextran monomer) for PLA-b-Dex polymer micelle nanoparticles.

5.3.8 Preservation of Polymer Micelles via Flash Freezing and Freeze-Drying

Polymer solutions were prepared in DMSO at concentrations of 6.818 mg/ml and nanoprecipitated into 10 times excess of DI water (>15 MΩ). The polymers investigated included PLA-*b*-Dex, PLA-*b*-Dex-APBA, and PLGA-*b*-PEG. The solution continuously agitated for 30 minutes. The nanoparticle suspension was dialyzed against 1 L of DI water for 3 hours. The particles were then filtered through a 200 nm syringe filter and the initial DLS particle size measurement was recorded using a Brookhaven 90 Plus.

The remaining solution was aliquoted into four vials each with a volume of 2 ml of the suspension. Protectants were added to two of the four suspensions at 2 wt%, and the mixture was vortexed to dissolve them. The vials without protectant were also vortexed to mimic the turbulence to ensure that did not contribute any error. Herein, flash freezing refers to the process of freezing nanoparticle suspensions in a bath of liquid nitrogen. The aliquots were frozen in liquid nitrogen by placing the uncapped vial in a shallow pool of liquid nitrogen, and crackling noises indicative of the freezing process was observed. The vials were removed when the cracking stopped. One vial with protectant and one without were immediately placed into a freezer at -20°C for storage (flash frozen samples). The remaining vials were freeze-dried in a Labconco® Freezone 4.5 L at -89°C abd 0.003 mPa until the ice and moisture had been completely removed, approximately 24 hours (freeze-dried samples). The samples were stored at -20°C until reconstitution for particle size measurements.

Particle size was measured after flash freezing and freeze-drying to determine the effects of the protectants and formulation stability. Analysis was performed with Brookhaven 90 Plus in triplicate. Flash frozen samples were thawed at room temperature and freeze-dried samples were reconstituted by adding DI water (>15 MΩ) equivalent to the original aliquot volume. Measurements were first performed without filtering the thawed or reconstituted suspensions. The same samples were then filtered and another DLS reading was recorded.

The studies with PLGA-*b*-PEG utilized trehalose, mannitol, and dextran (Mn ~ 10 kDa and 70 kDa) as protectants. Studies with PLA-*b*-Dex and PLA-*b*-Dex-APBA block copolymers involved the use of trehalose. Studies on the effects of PLA-*b*-Dex and PLA-*b*-Dex-APBA block copolymer concentration in suspension were performed with initial polymer solutions of 30 mg/ml, 15 mg/ml, 7.5 mg/ml, and 3.25 mg/ml.

5.3.9 Determination of Protectant Size in DLS Measurements

A 2 wt% solution was prepared in DI water (>15 MΩ) was prepared for each common cryoprotectants/lyoprotectants to be tested. Aliquots of solution (2.5 ml) were added to DLS cuvettes and a Brookhaven 90 Plus was used to determine the particle size.

5.3.10 Investigation of Particle Corona and Effect on Suspension Stability

Polymer solutions of PLA-*b*-Dex, PLA-*b*-DexOX, PLA-*b*-Dex-APBA were prepared in DMSO at concentrations of 6.818 mg/ml and nanoprecipitated into 10 times excess of DI water (>15 MΩ). The solution continuously agitated for 30 minutes. The nanoparticle suspension was dialyzed against 1 L of DI water for 3 hours. The particles were then filtered through a 200 nm syringe filter and the initial DLS particle size measurement was recorded using a Brookhaven 90 Plus.

The remaining solution was aliquoted into four vials each with a volume of 2 ml of the suspension. Trehalose was added to two of the four suspensions at 2 wt%, and the mixture was vortexed to dissolve them. The vials without trehalose were also vortexed to mimic the turbulence to ensure that did not contribute any error. The aliquots were frozen in liquid nitrogen by placing the uncapped vial in a shallow pool of liquid nitrogen, and crackling noises indicative of the freezing process was observed. The vials were removed when the cracking stopped. One vial with protectant and one without were immediately placed into a freezer at -20°C for storage (flash frozen samples). The remaining vials were freeze-dried in a Labconco® Freezone 4.5 L until the ice and moisture had been completely removed, approximately 24 hours (freeze-dried samples). The samples were stored at -20°C until reconstitution for particle size measurements.

Particle size was measured after flash freezing and freeze-drying to determine the effects of the protectants and formulation stability. Analysis was performed with Brookhaven 90 Plus in triplicate. Flash frozen samples were thawed at room temperature and freeze-dried samples were reconstituted by adding DI water (>15 MΩ) equivalent to the original aliquot volume. Measurements were first performed without filtering the thawed or reconstituted suspensions. The same samples were then filtered and another DLS reading was recorded.

5.3.11 Preparation of TEM Samples

TEM samples were prepared on 300 mesh copper grids coated with 10 nm formvar and stabilized with 1 nm carbon. A 7.5 µl drop of the nanoparticle suspension was placed on top of the grid and allowed to dry for 24 hours. The grid was then stained with a 20 mg/ml phosphotungstic acid (PTA) solution for 15 seconds; the excess volume was absorbed from the bottom of the grid, and the grid was then dried for 24 hours before imaging with a Philips CM10 TEM.

5.3.12 Quantification of DMSO Content via ^{1}H-NMR

The method for quantification of DMSO via ^{1}H-NMR analysis was adapted from work by Lehr et al. to suppress the peak corresponding to H_2O in the sample[242]. One dimensional Nuclear Overhauser Effect Spectroscopy (NOESY) was conducted on a Bruker Avance 600 MHz with 1024 acquisitions per FID. All NMR samples contained a volume of 700 µL consisting of 90% of the nanoparticle suspension and 10% D_2O with DSS-D_6. Spectra were analyzed with the ACD software suite using the methyl groups of DSS-D_6 at a chemical shift at 0 ppm as the integration reference for determination of DMSO concentration at 2.7 ppm.

5.4 Results and Discussion

5.4.1 Effect of Trehalose on PLA-*b*-Dex-APBA Polymer Micelle Nanoparticles

Freeze-dried samples under both conditions exhibited a significant increase in particle size. The sample with trehalose however, is tolerable by the ocular surface. Furthermore, the filtered sample is not significantly different than the unfiltered sample, suggesting the particles can simply be rehydrated and administered as necessary. Freeze-drying without trehalose offered no advantage and resulted in irrecoverable particles upon rehydration. Macroscopic aggregates were visible and are unacceptable for drug delivery as they would immediately induce a foreign body experience, inflammation, and increased nasolacrimal drainage.

Suspensions of MNP were preserved under different conditions with and without trehalose as a protectant. The results are shown in Figure 5.1. Flash frozen samples without trehalose (filtered and unfiltered) were statistically similar to the initial filtered sample. In the presence of trehalose there was an increase in particle size in the unfiltered sample which is statistically different than the initial sample. However, this size is well within the tolerable range of particle size for ocular drug delivery. The filtered sample with trehalose however, was not significantly different than the initial. This suggests that the MNP suspension can be frozen and thawed prior to administration as needed. The DLS technique averages particle sizes, resulting in the slight decrease in effective diameter upon filtering of aggregates.

In literature, formulations destabilize upon freezing due to the formation of ice crystals and a cryo-condensed state which induces aggregation. This behaviour is not observed for the PLA-*b*-Dex-APBA polymer micelles. As shown in Figure 5.1 the protectant does not have a significant impact on the stability of the solution. APBA is hydrophobic and thus it was hypothesized that this is a consequence

of the APBA conjugation onto the dextran corona. This results in a more collapsed structure and fewer water molecules would form hydrogen bonds with the corona and therefore the crystallization of ice would not destabilize the particles. To verify this hypothesis, the same test was carried out with PLA-*b*-Dex polymer micelles (Section 5.4.2).

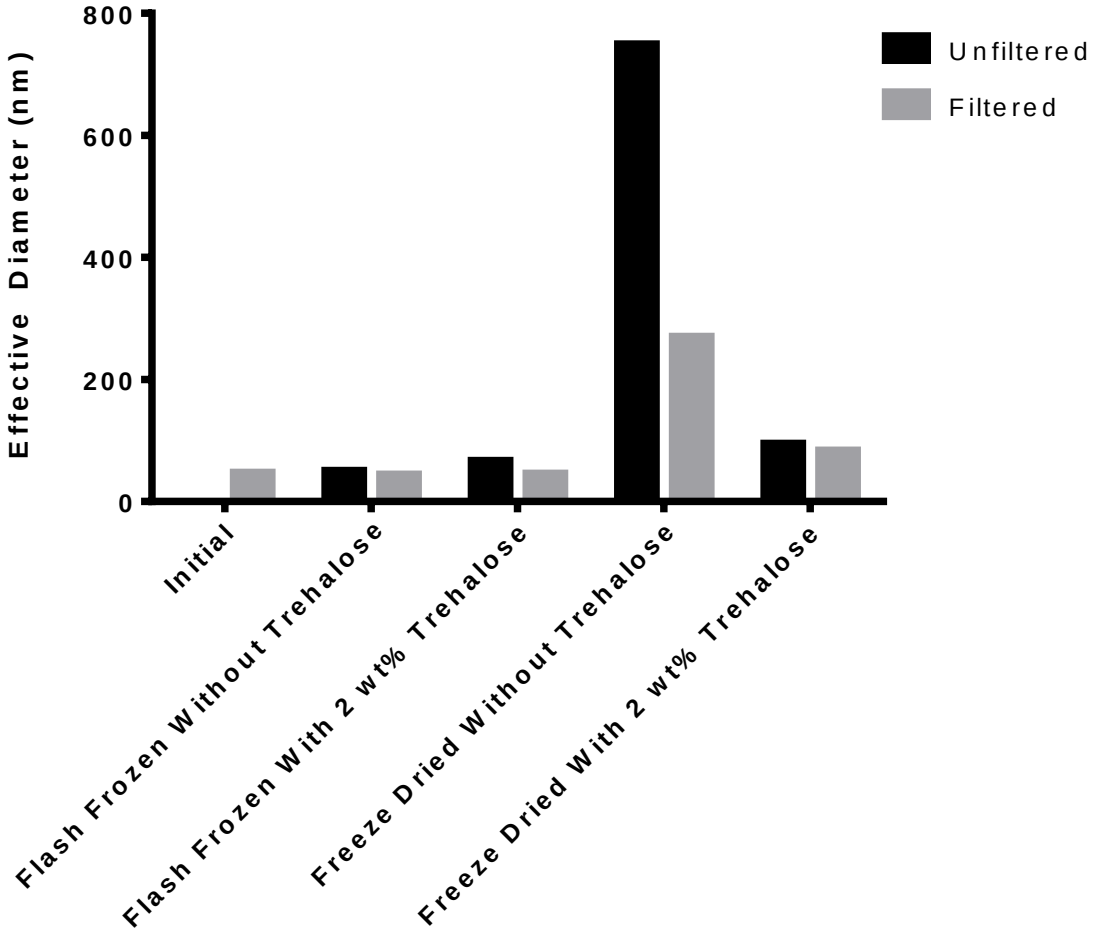

Figure 5.1: Effect of trehalose on flash frozen and freeze-dried PLA-*b*-Dex-APBA polymer micelle nanoparticles

TEM images were used to visualize the effects of the preservation techniques. The particles prior to preservation treatments were imaged and show good correlation with the DLS size (Figure 5.2). Though the flash frozen nanoparticles in the absence of trehalose were similar to the initial sample, the TEM images revealed a higher degree of polydispersity (Figure 5.3a). The sample with 2 wt% trehalose appears to be more monodisperse and the particles are well dispersed on the sample grid showing little evidence of aggregation. The freeze-dried sample even without trehalose had some dispersed nanoparticles comparable to the initially prepared sample prior to preservation treatments. However, there is clear evidence of aggregation of the particles into clusters as shown in Figure 5.3c) which gives rise to the larger DLS effective diameter. This aggregation is not present in the same extent in the sample freeze-dried with 2 wt% trehalose, Figure 5.3d).

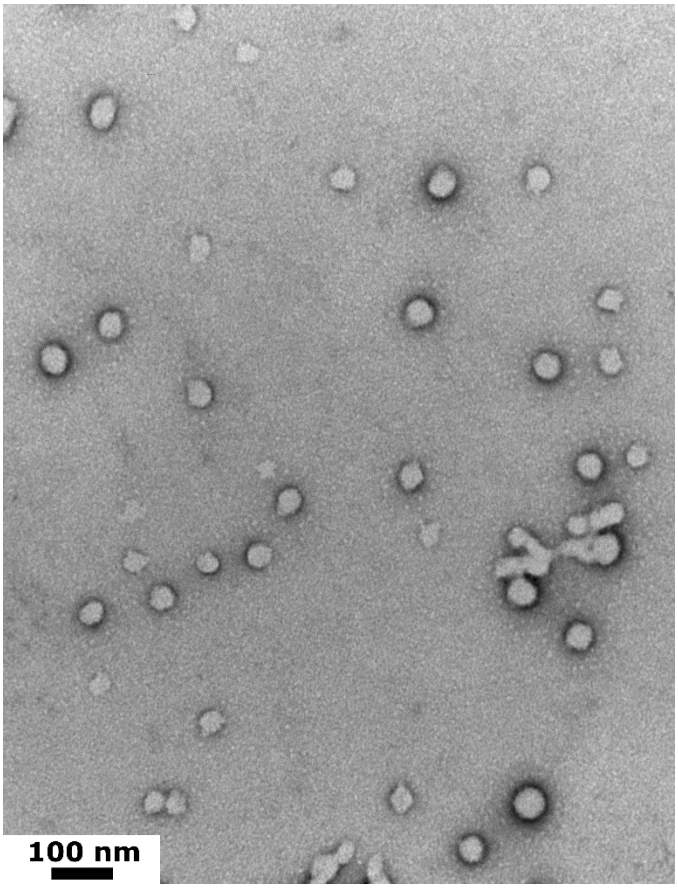

Figure 5.2: TEM image of PLA-*b*-Dex-APBA nanoparticles prior to preservation treatments.

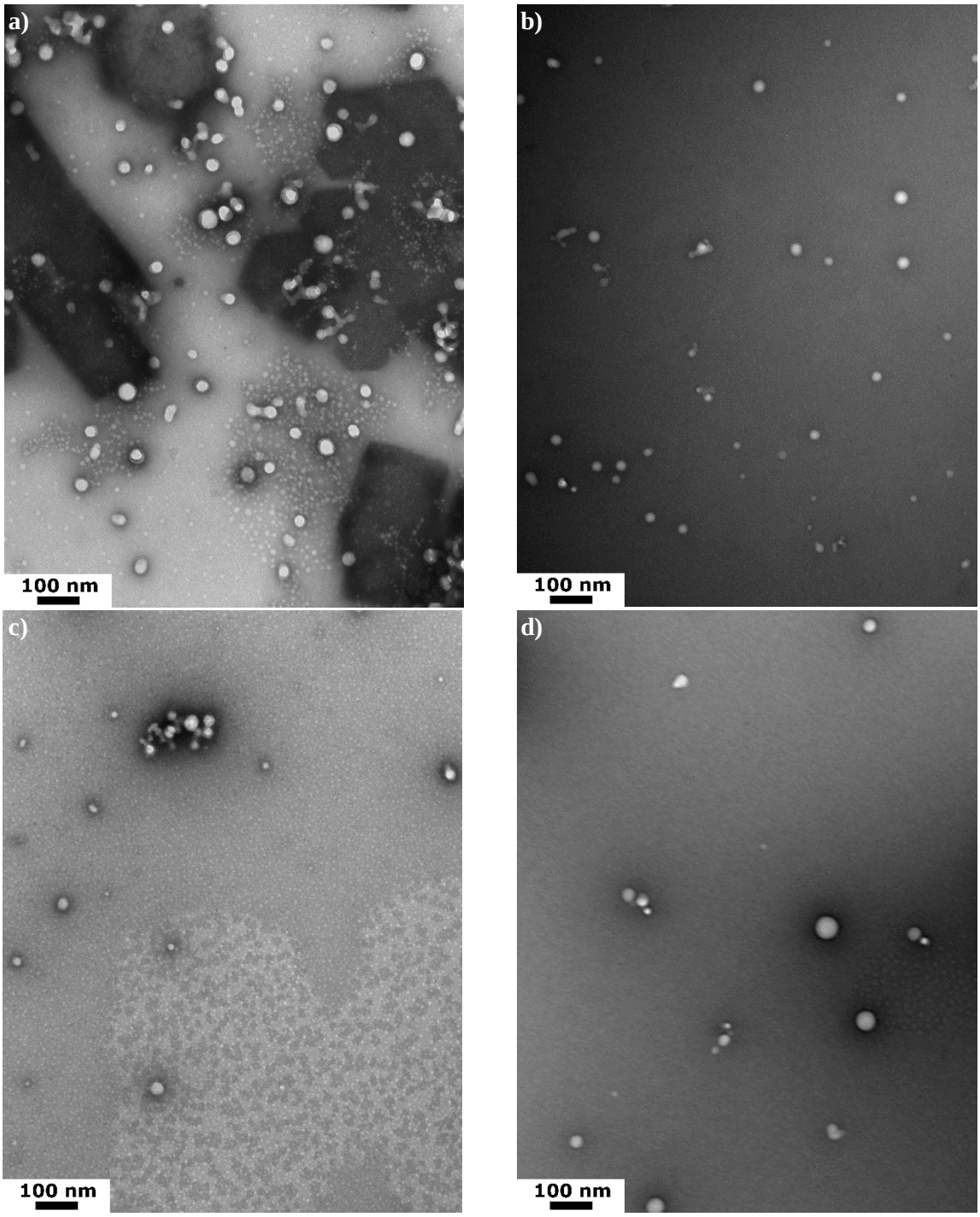

Figure 5.3: TEM images of PLA-*b*-Dex-APBA nanoparticles after preservation treatment: a) flash freezing without trehalose, b) flash freezing with 2 wt% trehalose, c) freeze-drying without trehalose and d) freeze-drying with 2 wt% trehalose.

In literature, the cryopreservation properties of trehalose are attributed to the formation of a glassy matrix which prevents the aggregation and destabilization of the nanoparticles. The protectant acts as an intercalator separating the particles and preventing them from coming into contact. This was evident through TEM as suspensions with trehalose appear to have more distance between the nanoparticles and also show a reduction in the size change. The increase in effective diameter appears to be a result of an increased hydrodynamic radius. However, the nanoparticles forming the cluster appear to be similar in size to the original sample.

5.4.2 Effect of Trehalose on PLA-*b*-Dex Polymer Micelle Nanoparticles

PLA-*b*-Dex nanoparticles were flash frozen and freeze-dried with and without trehalose. Flash frozen samples with and without trehalose show an initial increase in the unfiltered size which than the initial filtered sample (Figure 5.4). The filtered sample was not significantly different than the initial sample, but a decrease in the particle size was observed.

Freeze-dried particles without trehalose had a significant increase in the particle size and had a large polydispersity and aggregation in the filtered sample. It should be noted that the aggregation for these particles was not as sever as what was observed for MNPs (Figure 5.1). In the presence of trehalose, unfiltered freeze-dried sample was not significantly different than the flash frozen sample with trehalose. The filtered sample with trehalose shows a small decrease from the unfiltered sample but is still larger than the unfiltered sample.

The self-cryopreservation property observed for the PLA-*b*-Dex-APBA polymer micelles was also observed for PLA-*b*-Dex micelles. Initially, it was hypothesized that the cause of this stability is the presence of APBA which makes the particles more hydrophobic. However, from this study it evident that APBA actually contributes to the destabilization as indicated by the severe aggregation.

The dextran conjugated with APBA is also oxidized which results in a loss of hydroxyl groups capable of hydrogen bonding with water. This “bound water” is removed at a slower rate and is believed to be the main cause of aggregation and damage to the nanoparticle structure. To determine if the Dex-Ox may be contributing to the preservation property, PLA-*b*-Dex-Ox nanoparticles were synthesized, and studied with the same preservation conditions (Section 5.4.3). Additionally, dextran is used as a cryoprotectant in literature. A different particle composition had to be used to determine if the dextran

did in fact impede formation of large ice crystals and improve stability. To further evaluate dextran, PLGA-PEG particles were used in a study (Section 5.4.5) and dextran was added as a protectant.

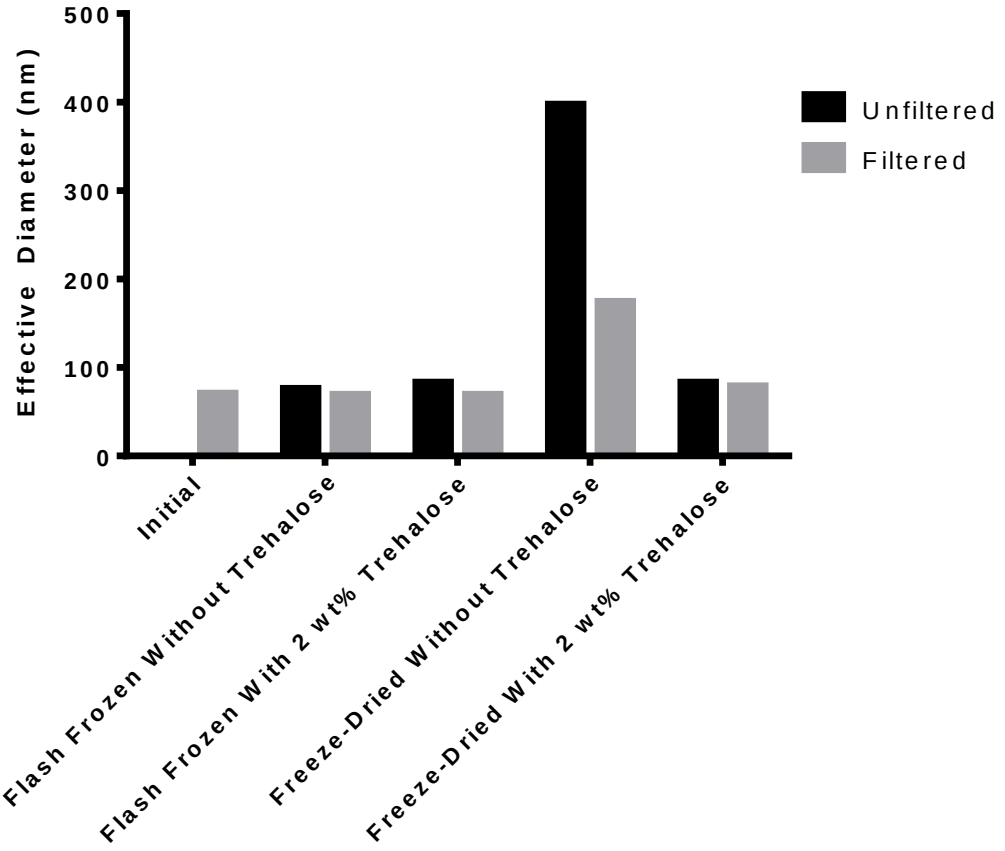

Figure 5.4: Effect of trehalose on flash frozen and freeze-dried PLA-*b*-Dex polymer micelle nanoparticles

5.4.3 Effect of Polymer Micelle Corona on Preservation Techniques

From Figure 5.5 it was observed that upon oxidation the particle size decreased significantly from 70 nm to 48 nm and then 45 nm upon functionalization with APBA. This suggests that the oxidation stage is more critical in imparting a hydrophobic character to the nanoparticles. However, upon flash freezing the PLA-*b*-Dex-Ox nanoparticles had a significant increase in particle size whereas the PLA-*b*-Dex and PLA-*b*-Dex-APBA nanoparticles remained relatively stable both with and without trehalose. The oxidized corona did not improve stability. The recovery from this stage and return of the self-

cryopresvation is a result of the APBA conjugation which results in a loss of the aldehydes. Thus, it was concluded that oxidized dextran was not the cause of this property.

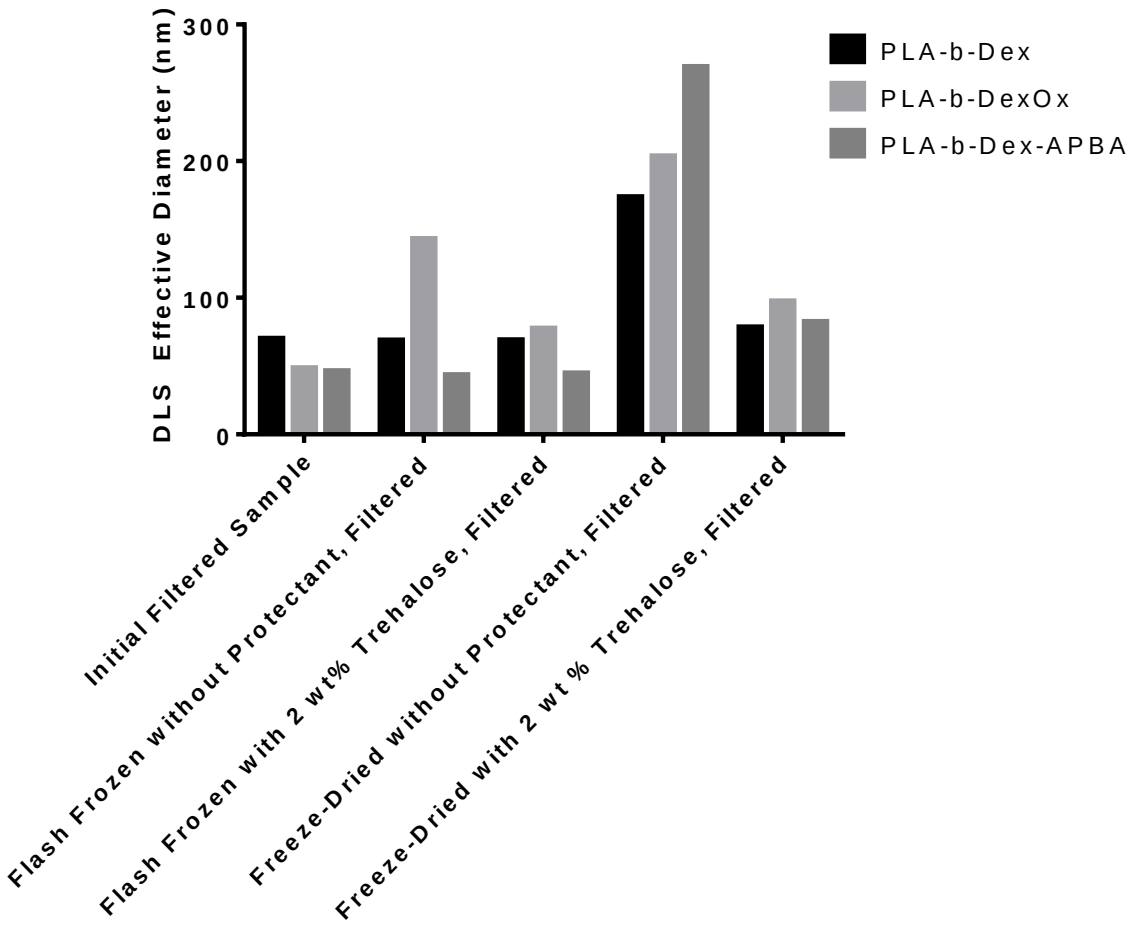

Figure 5.5: Effect of oxidized dextran corona on the particle size and cryopreservation

5.4.4 Effect of Protectant Size on DLS Measurements for Effective Diameter (nm)

This study was conducted to determine if the particle size of the protectant would influence the resulting particle size during measurement. The protectants selected for trehalose, mannitol, dextran polymer with Mn ~ 10 and 70 kDa. Trehalose is the most successful cryoprotectant and lyoprotectant in literature and has demonstrated efficacy for preservation of PLA-*b*-Dex and PLA-*b*-Dex-APBA polymer micelles nanoparticles. Mannitol is a common excipient in ophthalmic formulations to control the solution osmolarity, and hence would serve a dual purpose if shown to be effective as a protectant for

our nanoparticles. To test the self-cryopreservation property, constituents of the block copolymer had to be investigated. In literature, some dextran nanopartibles have exhibited this property, and dextran as been used a commercial cryoprotectant. Hence, dextran of different molecular weights was investigated.

As the length of the dextran chain increased (Figure 5.6) we observe an increase in particle size due to a larger hydrodynamic diameter. Upon filtering the majority of dextran (Mn ~ 70 kDa) was removed from. The disaccharides which are smaller than the macromolecular dextran appeared to have larger particle size. This is an error and results from scattering of artifacts in or on the cuvette (dust or cracks), as dissolved sugars of this size do not scatter light. The count rate observed for these samples was also significantly low. This study was primarily conducted to conclude that high molecular weight dextran would not skew the data if added to a suspension of nanoparticles to act as a protectant. Sugar monomers dissolve and do not scatter light which can be detected by the detector. Polymers on the other hand may if they are not solvated and take on a closed conformation. The only protectant which may be a factor will be dextran (Mn ~ 70k) due to its size. Fortunately, the cryoprotectant can be filtered and this can be used to protect the nanoparticles and easily filtered out.

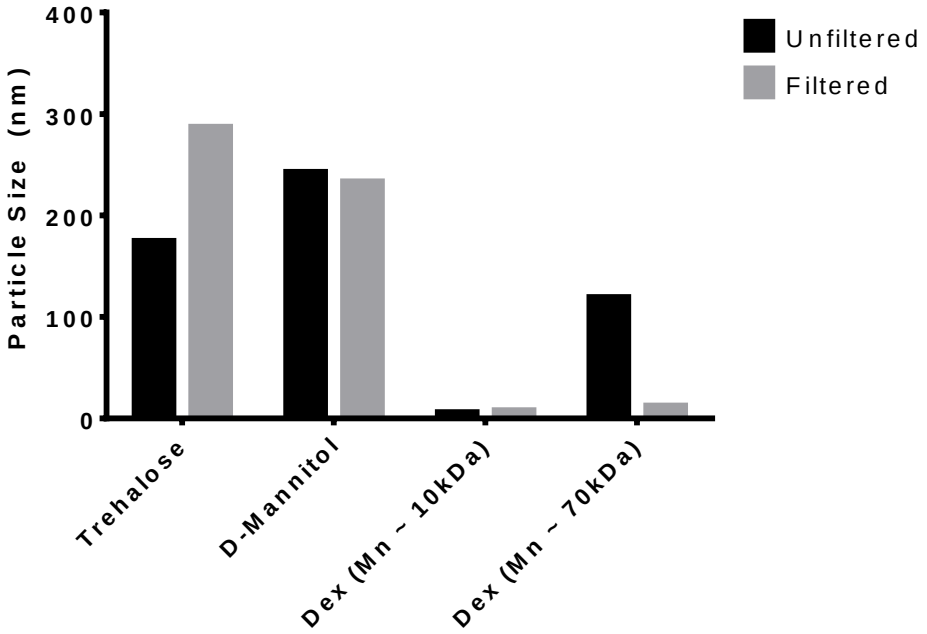

Figure 5.6: DLS effective diameter (nm) evaluating the size of protectants in water.

5.4.5 Effect of Various Protectants on PLGA-PEG Polymer Micelles

The freeze thawed samples were acclimated at room temperature prior to being transferred to a DLS cuvette for measurement. freeze-dried samples were reconstituted with an equal volume of pure water as the aliquot after acclimation at room temperature. The vessel was gently agitated to dislodge the nanoparticle film from the walls of the vial. The particle size was first measured unfiltered, and then passed through a 200 nm syringe filter and measured again. Freeze-dried samples without protectant did not have usable results due to the aggregation and are omitted.

From Figure 5.7 it is evident that nanoparticle suspensions subjected to cryogenic and lyophilization stress undergo some aggregation. The aggregation for the freeze-dried sample prior to filtering was too large hindering measurement of the particle size. However, the flash frozen sample without the addition of D-mannitol had a smaller increase in particle size or aggregation as compared to the sample freeze thawed with protectant. Furthermore, upon filtering both the freeze-dried and thawed sample without the presence of D-mannitol were comparable in particle size whereas the freeze thawed sample with protectant had a statically significant increase in size.

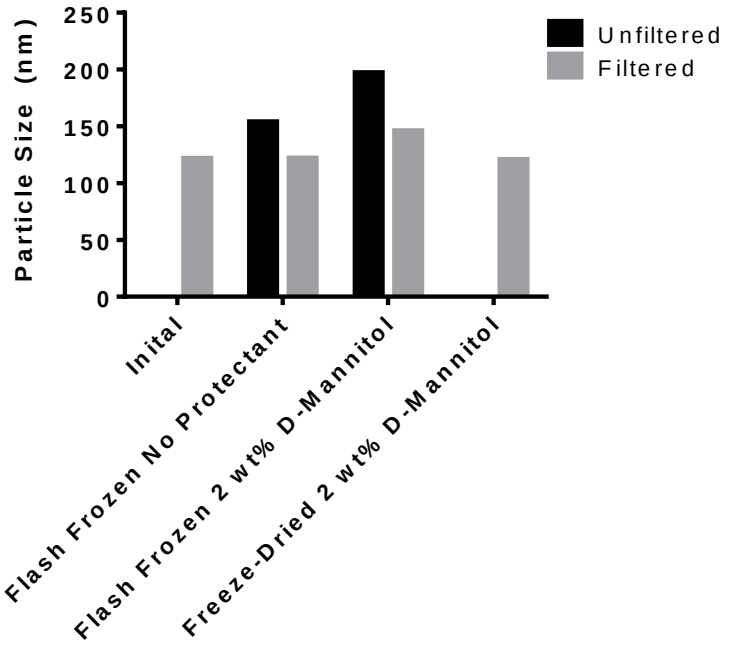

Figure 5.7: Effect of D-Mannitol as a cryoprotectant and lyoprotectant on PLGA-PEG polymer micelle nanoparticles.

Samples freeze-dried with trehalose show recovery to particle sizes statistically similar to the initial sample. When the sample was freeze-dried without trehalose however, the aggregation of PLGA-*b*-PEG micelles was severe. The aggregate could not be resuspended for measurement. Freeze drying the particles without protectant also resulted in similar particles by size upon filtering. The results are shown in Figure 5.8.

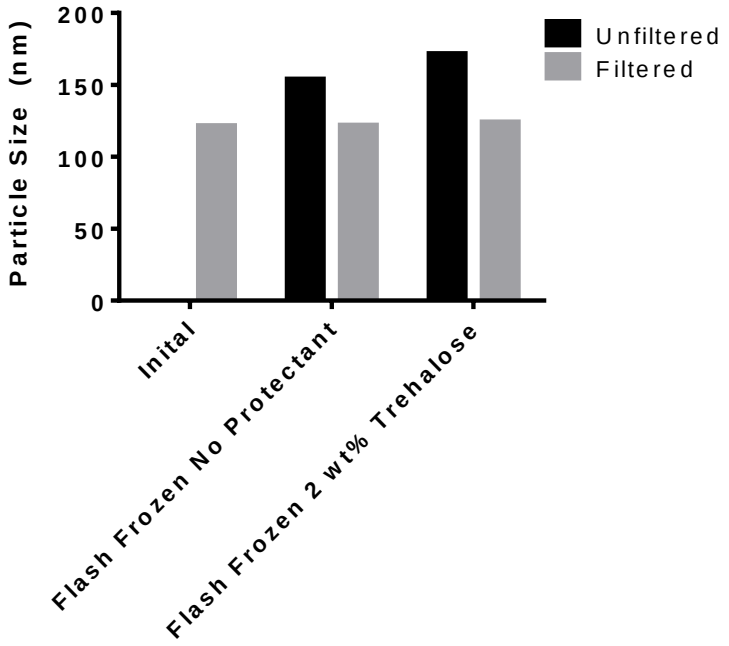

Figure 5.8: Effect of trehalose as a cryoprotectant and lyoprotectant on PLGA-PEG polymer micelle nanoparticles.

With dextran (Mn 10 kDa) shown in Figure 5.9 the effect of the aggregation was even more pronounced than the disaccharides especially for the freeze-dried sample. This is likely due to the free polymer entangling during the cryo-condensed state formed during freeze-drying and further contractions during the drying process. Both treatments with the dextran as a protectant appear to have an increase in the particle size but are similar.

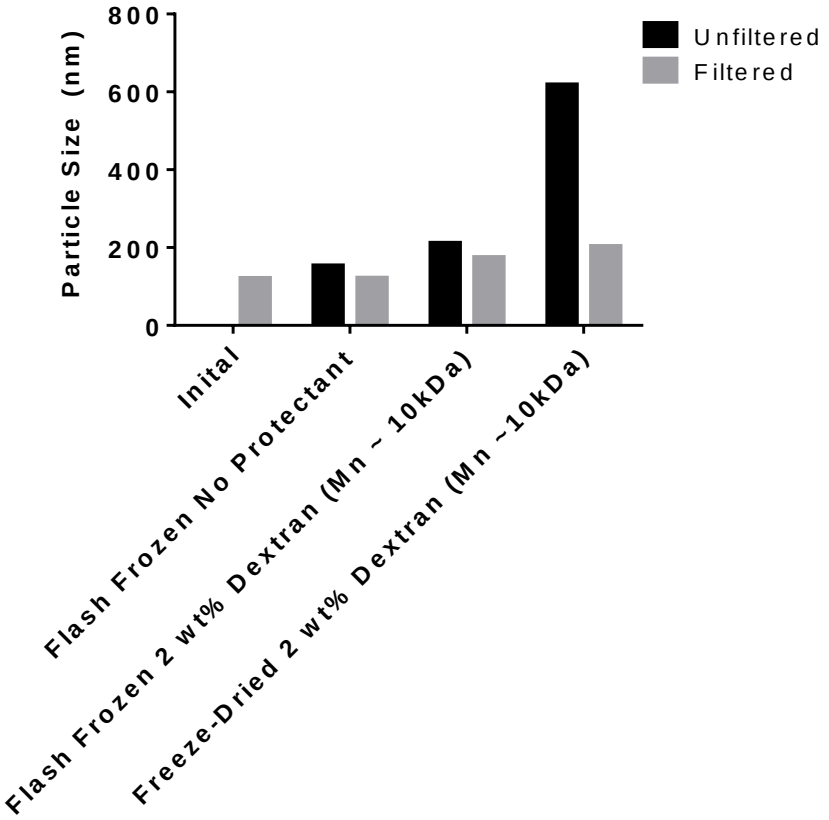

Figure 5.9: Effect of dextran (Mn ~ 10 kDa) as a cryoprotectant and lyoprotectant on PLGA-PEG polymer micelle nanoparticles.

In the case of (Mn ~ 70 kDa) shown in Figure 5.10 a similar trend is observed. The freeze thawed sample resulted in a smaller particle size after filtering. This is attributed to significant loss of sample and residual polymer and smaller particles in the suspension resulting in the decrease in particle size. The freeze-dried sample is consistent in the particle size increase.

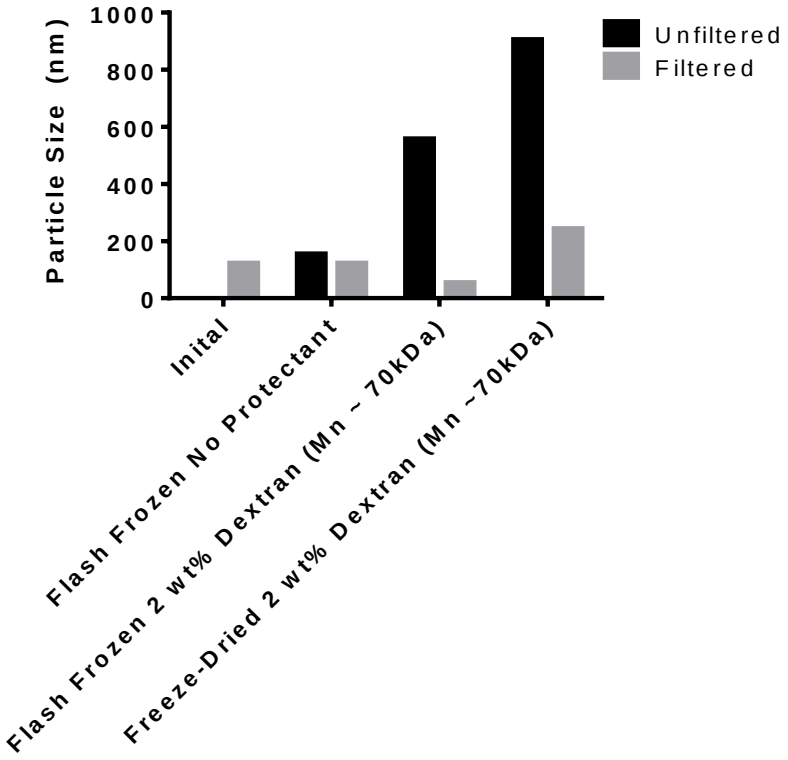

Figure 5.10: Effect of dextran (Mn ~ 10 kDa) as a cryoprotectant and lyoprotectant on PLGA-PEG polymer micelle nanoparticles.

5.4.6 Effect of Polymer Concentration on the Preservation of Polymer Micelles

As shown in Figure 5.11 the particle size continues to increase with the polymer concentration, however the effect is more pronounced the polymer functionalized with APBA. This could be a result of increased hydrophobicity and therefore instability in aqueous media causing the micelles which form to become larger.

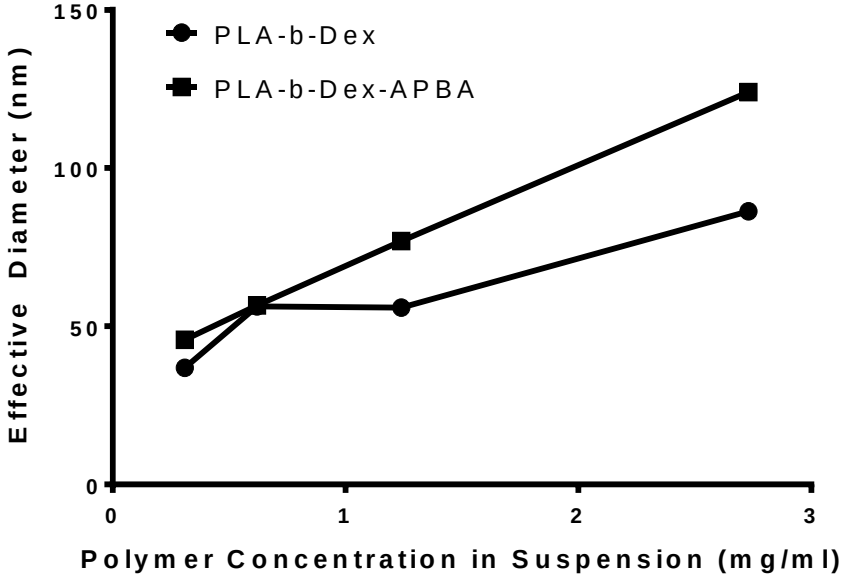

Figure 5.11: Effect of polymer solution in suspension on micelle size

PLA-*b*-Dex polymer solutions were prepared DMSO at various concentrations. 1 ml of the polymer solution was nanoprecipitated into 10 ml of pure water. As shown in Figure 5.12 the samples flash frozen with and without trehalose retained their particle size without significant variance except for 0.62 mg/ml. This result may have been influenced by some error, as no significant trend can be concluded of the polymer concentration. In the case of the freeze-dried sample, the unfiltered sample have a decrease in aggregation with an increase in particle size. This effect is significant and may be suggesting that and increasing in particle concentration correlates with an increase in cryopreservation. The freeze-dried sample with trehalose shows similar particles and preservation for all samples except for 0.31 mg/ml which also had the highest aggregation of the unfiltered sample.

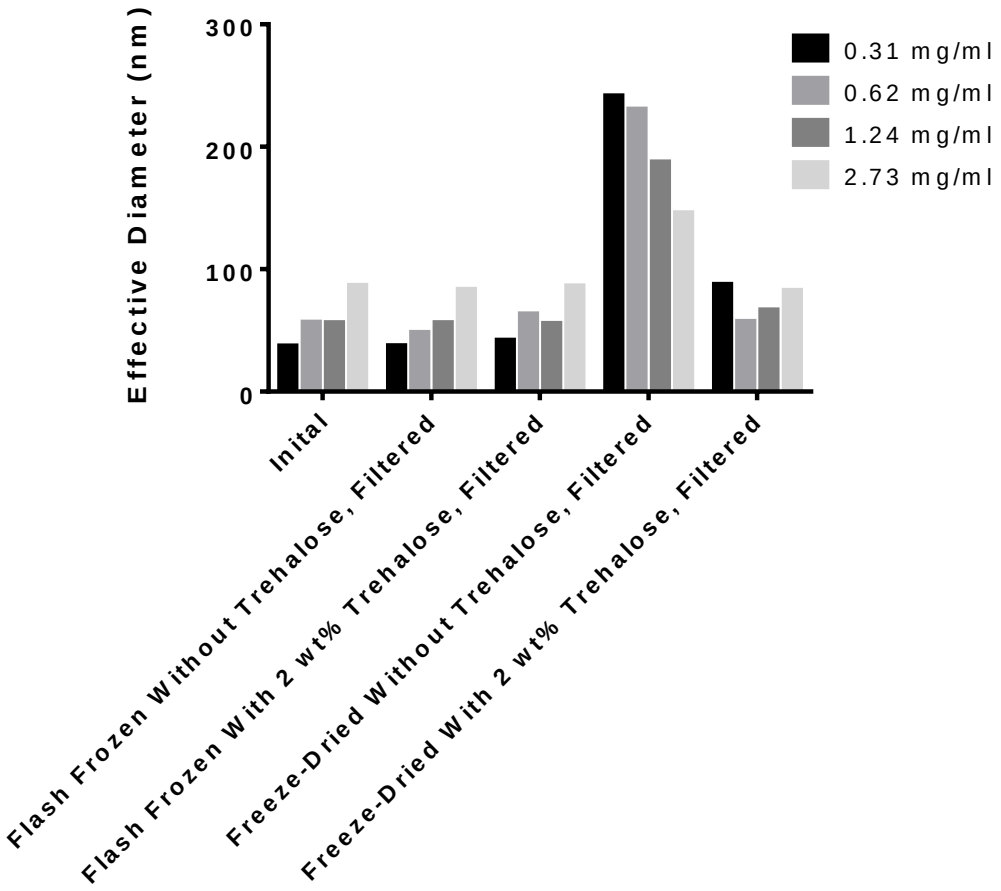

Figure 5.12: Effect of polymer concentration on the particle size and cryopreservation of PLA-*b*-Dex micelle nanoparticle

The same study was conducted with PLA-*b*-Dex-APBA polymer micelles. As shown in Figure 5.13 an increase in the polymer concentration results in an increase of the initial particle size. This trend, for the working range for this experiment was determined to be linear. Upon flash freezing the particle size remained consistent and significantly similar except for the sample at 0.31 mg/ml which had a slight increase in particle size. With trehalose, all of the flash frozen samples were statistically similar to their respective initial samples. The freeze-dried samples revealed a trend similar to the PLA-*b*-Dex samples which show a decrease in the aggregate size when freeze-dried without trehalose. With trehalose however, the particle size is greater than the initial sample for all concentrations except for the most concentrated sample at 2.73 mg/ml. This sample remained consistent for all treatments except when

freeze-dried without trehalose. This result suggests that the polymer concentration does have an impact on the particle size, but also on the preservation of the particles under cryogenic and lyophilization stresses.

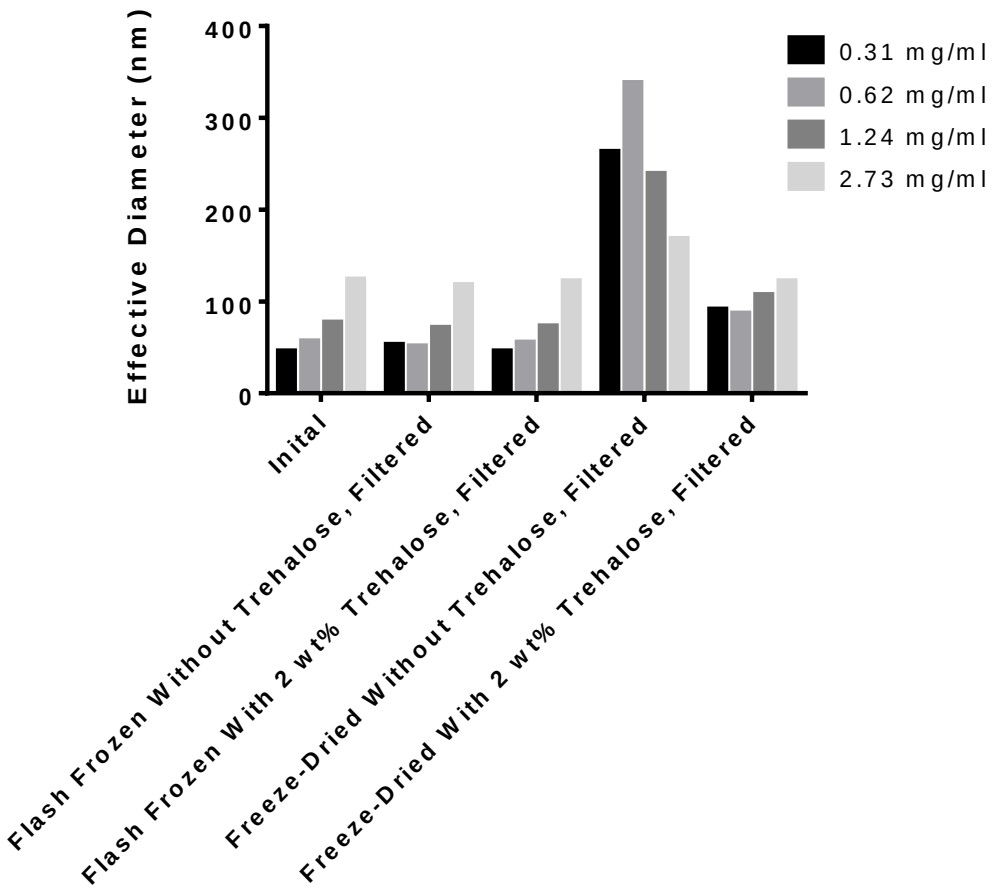

Figure 5.13: Effect of polymer concentration on the particle size and cryopreservation of PLA-*b*-Dex-APBA micelle nanoparticles

5.4.7 Determination of Residual DMSO Content

The nanoparticles described are prepared via precipitation of the polymer dissolved in an oil phase (DMSO) into an aqueous phase (water). The high solubility of DMSO in water makes it a difficult to remove solvent. The current synthesis process involves dialysis to remove the DMSO however, residual DMSO may still remain in the formulation. Previous animal studies have not shown signs of irritation of histopathological change. Furthermore, DMSO is approved for use as an excipient in pharmaceutical formulations, organic solvents can cause inflammation on the ocular surface.

In the context of preservation, DMSO is often used for cryopreservation of cells and biological systems. The DMSO molecules disrupt the formation of ice crystals resulting in smaller domains which are less likely cause cell death. After investigation of the particle corona, the DMSO was hypothesized to the cause of the self-cryopreservation property. ^{1}H-NMR NOESY spectra (shown in Figure 5.14) were used for quantification of trace quantities of DMSO in the nanoparticle suspension to determine the residual fraction after purification of the suspension, and to determine if DMSO has an effect on the preservation of the particles. Chromatography techniques were also investigated, however complete isolation the DMSO signal could not be achieved. As shown in Figure 5.15 this method revealed a strong linear correlation between the integrated area and the known DMSO concentrations in the calibration solutions.

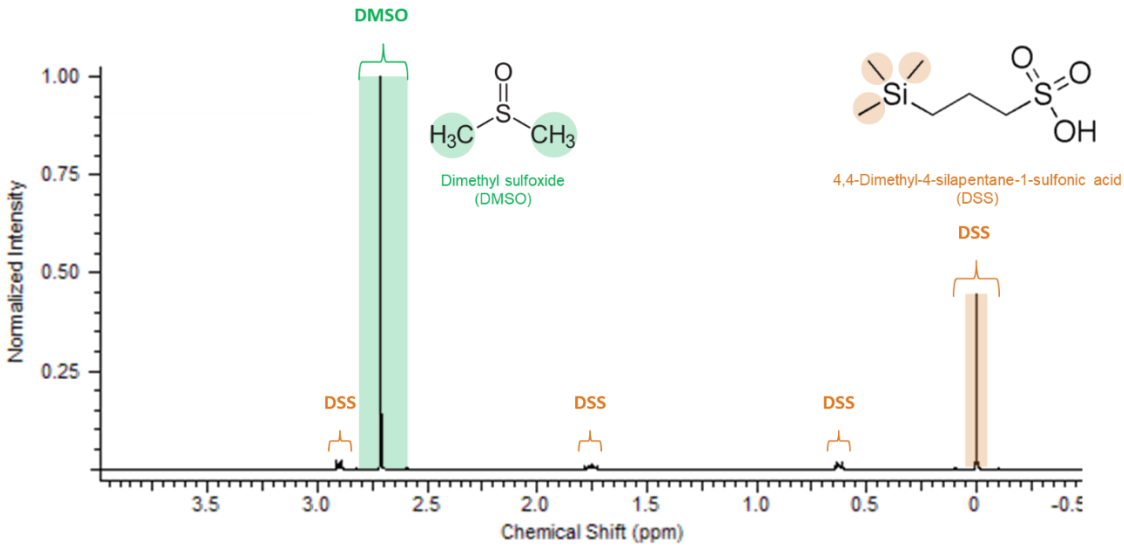

Figure 5.14: ^{1}H-NMR NOESY spectra for the determination of trace DMSO content with DSS as an internal reference.

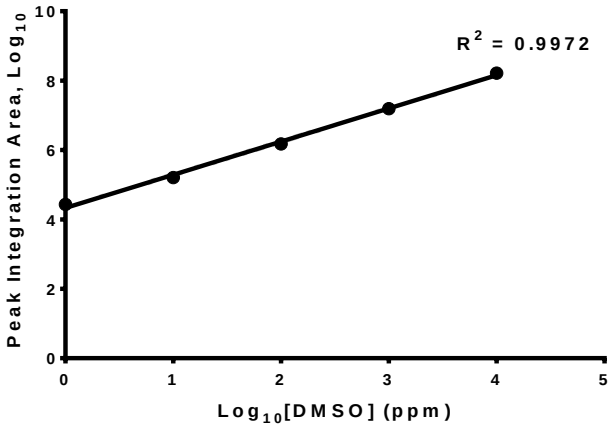

Figure 5.15: DMSO calibration curve generated from ^{1}H-NMR NOESY spectra for determination of trace quantities in nanoparticle suspension.

To determine the effect of trehlose on DMSO retention, suspensions of PLA-*b*-Dex polymer micelles were dialyzed for 3 hours and then freeze-dried with varying concentrations of trehalose. Upon rehydration, the particles were then filtered using an Amicon® centrifuge filter. The free volume is collected in the shaft of the centrifuge tube and was analyzed to determine the residual DMSO free in suspension (Figure 5.16). This concentration may also be the result of disrupted micelles which released the small fraction of encapsulated DMSO during freeze-drying. Figure 5.17 shows the residual DMSO present in the particles. The retentate was resuspended in order to quantify this. As shown by these two figures, an increase in the trehalose concentration restuled in an increase in DMSO retention.

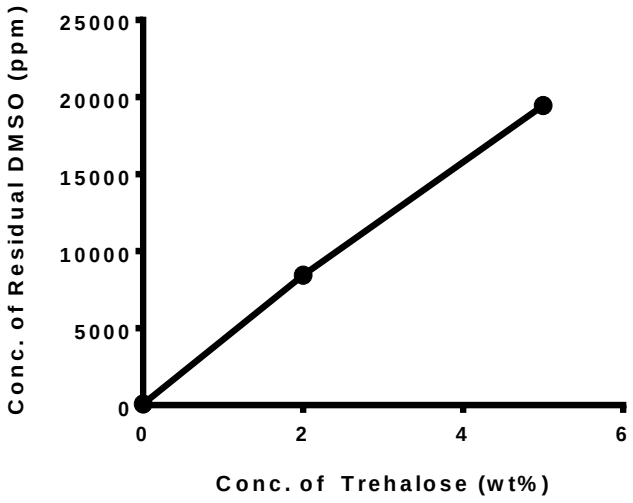

Figure 5.16: Residual concentration of DMSO in the Amicon® filtrate increases with the concentration of trehalose added as a protectant for freeze-drying.

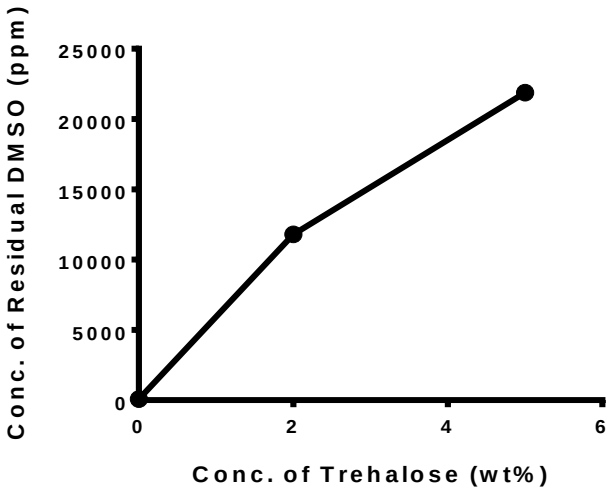

Figure 5.17: Residual concentration of DMSO in the Amicon® retentate increases with the concentration of trehalose added as a protectant for freeze-drying.

To demonstrate removal of DMSO from the MNP via dialysis, the particles were dialyzed for 24 hours, and then freeze-dried. As shown in Figure 5.18 as the fraction of trehalose added to the solution as a protectant resulted in an increase in the residual DMSO which remained after lyophilization. However, after this extended period of dialysis, the DMSO had been largely removed from the system. From the results of these studies, it was hypothesized that the trehalose is trapping the DMSO in the glassy matrix. This residual fraction, upon rehydration of the sample, contributes to the recovery of the particles. In flash frozen samples, the volume of DMSO remains unchanged, and thus we see that the addition of trehalose has no impact on the cryopreservation as formulations without any trehalose are statically comparable to the initial solution. To further confirm this, studies on 1% v/v solutions of DMSO in water were freeze-dried with varying concentration of trehalose.

The results shown in Figure 5.19 again reveal that increasing the amount of trehalose added to the formulation increases the retention of DMSO even in a solution void of particles. This can be attributed to the glassy trehalose matrix which may be trapping this residual DMSO. This effect may be two-fold because the trehalose and DMSO both acts to disrupt the ice crystal formation protecting the particles during the freezing step. However, the stability of the dried formulation may be a consequence of the trapped DMSO, which upon reconstitution can associate with the hydrophobic PLA and help to reduce the aggregation which is otherwise observed.

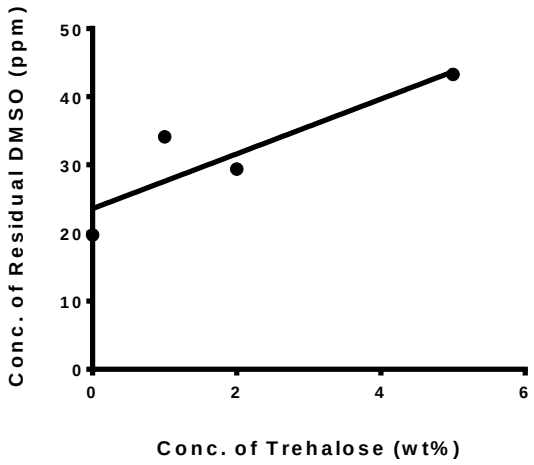

Figure 5.18 : Residual DMSO concentration in MNPs dialyzed for 24 hours. The DMSO fraction is reduced, but an increase in the trehalose concentration increases the DMSO retention.

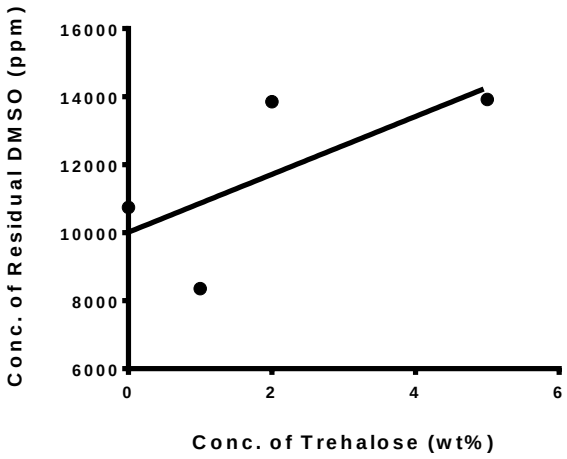

Figure 5.19: Residual DMSO concentrations increase with fractions of trehalose added to solutions of 1% v/v DMSO in water.

In order to conclude that the DMSO was the true cause of the self-cryopreservation property observed during freeze-drying, the nanoparticles were dialyzed for extended periods of time to essentially eliminate all detectable traces of DMSO. After about 3 hours (Figure 5.20), majority of the DMSO has been removed from the system, we observe the loss of the self-cryopreservation property. This again supports the hypothesis that the DMSO in solution acts as a cryoprotectant for the nanoparticles.

In all cases shown in Figure 5.20, the timepoint of -1 hour represents the initial measurement following nanoprecipitation and filtration through a 200 nm filter. The time point of 0 hours represents samples flash frozen or freeze-drying without dialysis. The remaining time points indicate the duration of dialysis with media changes every three hours.

Comparing Figure 5.20 a) and Figure 5.20 b) we find that there is no significant difference between the initial DLS reading at timepoint -1 hour and the preserved formulations without dialysis. As the dialysis time increased, the particle size increased dramatically for the flash frozen sample without trehalose. In the absence of DMSO and trehalose, ice crystals are not easily disrupted causing instability in the cryo-condensed state and aggregation. With the addition of 2 wt% trehalose the aggregation is not as pronounced at any of the time point as compared to the sample without trehalose as shown in Figure 5.20 b). The particle size under 200 nm is tolerable on the ocular surface and does not cause visual aberrations or foreign body experience.

The freeze-dried sample without trehalose is shown in Figure 5.20 c) and the instability resulting from the lack of protectant is evident. The formulation at the 0 hour timepoint resulted in average effective DLS diameter of 443 nm compared to the initial 47.2 nm. As the sample was dialyzed however, the stress of freezing and drying both resulted in significantly higher aggregation than all other formulations.

The freeze-dried sample with trehalose shown in Figure 5.20 d) also showed an increase in particle size with dialysis time. The increase from time point -1 hour to 0 hour was 47.2 nm to 114 nm which is less significant than the freeze-dried sample without trehalose. Even after prolonged dialysis and removal of DMSO, the freeze-dried formulation with trehalose remained more stable than the other preservation conditions explored.

This study confirms the observation that the DMSO present in the suspension, whether it be free or within the particles, contributes to the stability of the particles when frozen in order to increase the shelf life. Upon dialysis and removal of the DMSO, the particle suspension became unstable without the addition of a protectant, in this case trehalose. Freeze-drying with trehalose however appears to be a more stable and attractive method of improving the shelf life of the particles for commercial use.

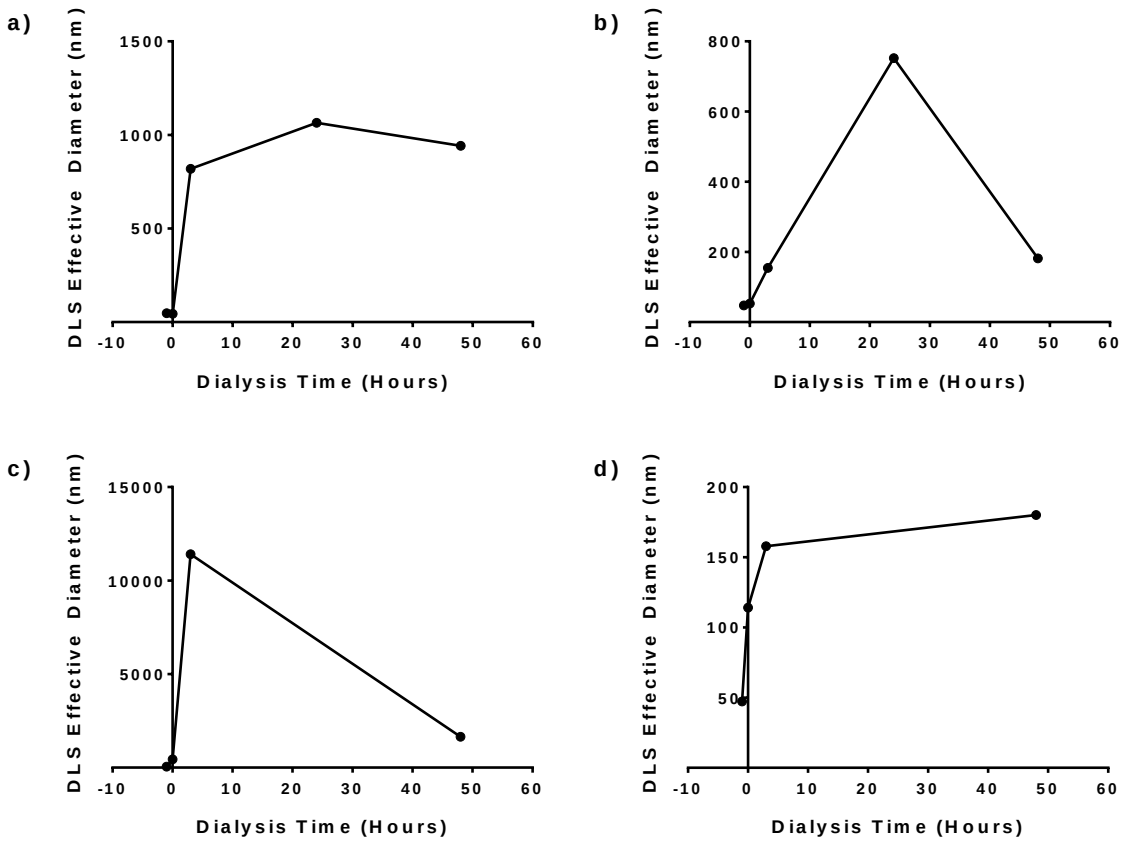

Figure 5.20: Effect of dialysis time on MNP preservation a) flash frozen without trehalose, b) flash frozen with 2 wt% trehalose, c) freeze-dried without trehalose, and d) freeze-dried with 2 wt% trehalose. The increased dialysis time results in destabilized particles.

5.4.8 Cryopreservation of MNPs

A drug loaded nanoparticle system comprising of PLA-*b*-Dex-APBA polymer micelles may be stable if frozen without the addition of protectant. This means that the overall osmolality of the solution may be reduced and maintained in the range accepted by the USP. This is critical as the addition of the protectant alone may exceed the allowable osmolarity. However, ophthalmic preparations typically require the addition of salts which buffer the pH of the solution and help preserve the drug molecule. This allows for more modifications and optimization of the commercial formulation. Furthermore, the lack of added excipients reduces the cost of the overall formulation and an additional step in the formation. Moreover, the exclusion of another excipient reduces the need for regulatory testing required to determine any possible adverse effects of the interaction of trehalose and nanoparticles on the ocular surface.

We also propose that the stabilization provided to PLA-*b*-Dex and PLA-*b*-Dex-APBA nanoparticles by trehalose is in part a result of hydrogen bond formation with the dextran corona. Under cryogenic conditions, destabilization is caused by the formation of large ice crystals which may penetrate the nanoparticle. Protectants like trehalose disrupt the crystal formation resulting in smaller crystalline domains. Secondly, the destabilization may occur via aggregation while the solution is in a cryocondensed state.

During the drying process, the removal of bound water (water molecules which have formed weak bonds with the nanoparticles) is the last step and likely to cause the most stress to the nanoparticles. Trehalose possesses several hydroxyl groups capable of displacing the water and forming hydrogen bonds with the Dextran corona of the nanoparticles. In literature, 20 wt% of cryo- or lyo-protectant is typically added to nanoparticle formulation and has been shown to result in complete recovery of the particles. However, this quantity of protectant is unacceptable for ophthalmic preparations due to the increased osmolarity of the suspension. With only 2 wt% of the protectant added to the formulation, we are able to achieve reproducible recovery and stabilization of the polymer micelles post freeze-drying as shown in Figure 5.21 and Figure 5.22.

Paired t-tests at a 95% confidence interval were used to compare the samples subjected to cryogenic and lyophilization stresses with the initial sample. It was concluded that both flash frozen samples were not significantly different than the initial filtered sample. This suggests that the protectant is not required to preserve the properties of the nanoparticle when freezing the particles for storage. However,

the lyophilized sample without trehalose was significantly different and even produced visible aggregates whereas with trehalose, the sample was similar to the initial. This suggests that the nanoparticle suspension is not stable under the lyophilization stresses without the addition of a cryoprotectant. Furthermore, the nanoparticles have displayed self-cryopreservation properties.

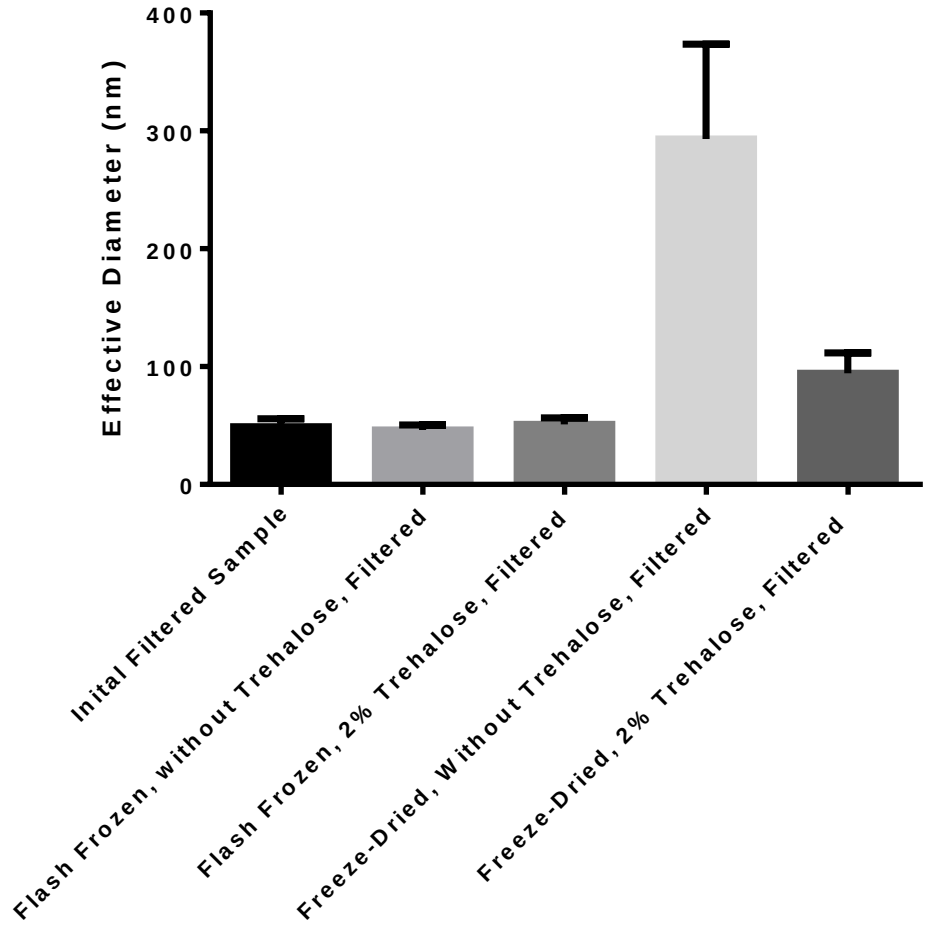

Figure 5.21: DLS particle size of MNPs before and after flash freezing and freeze-drying. The flash-frozen samples are statistically similar to the initial sample. Freeze-drying without trehalose results in destabilization of the particles. Hence, 2 wt% trehalose must be added to the suspension to preserve the particles.

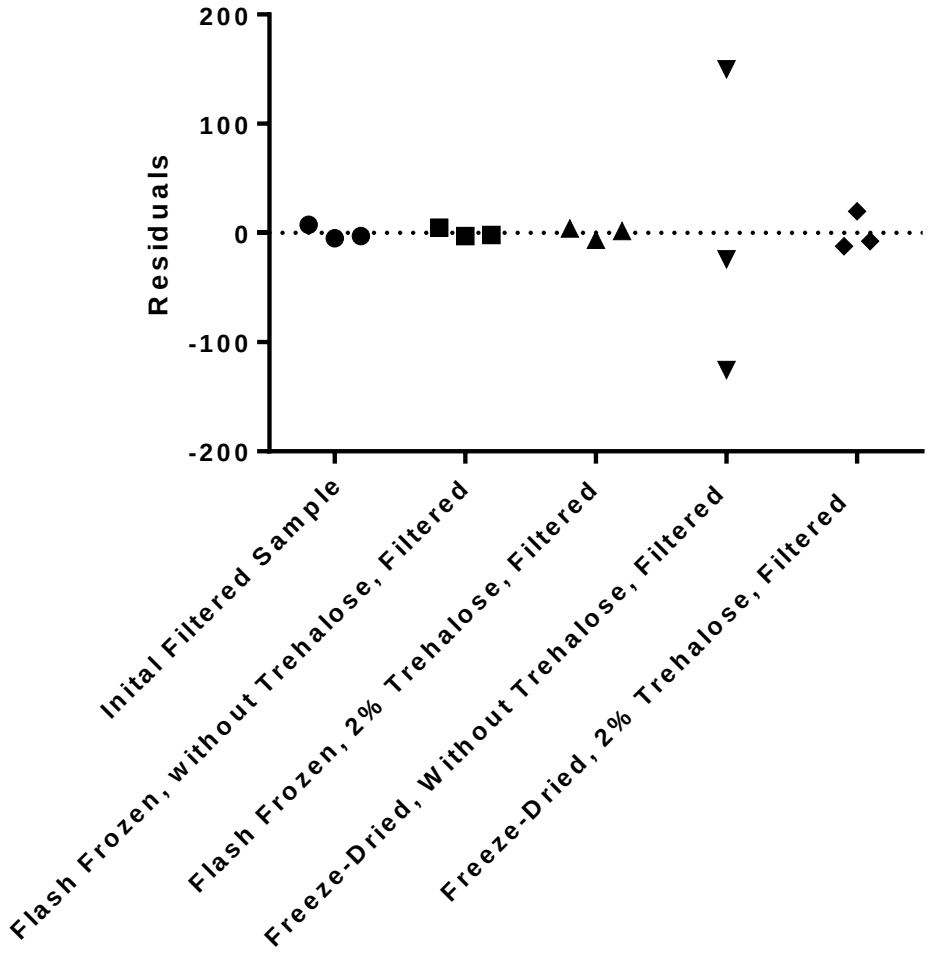

Figure 5.22: Residuals plot showing there is no trend or nuisance variable influencing the results.

The preservation of PLA-*b*-Dex and PLA-*b*-Dex-APBA nanoparticles with a 10 times reduction in the quantity of protectant can be attributed to two factors. First, the hydrogen bonding of trehalose with the corona which forms a tighter protective layer than it would with nanoparticles without the presence of such groups. Second, this self-preservation property is afforded to the MNPs due to the residual DMSO fraction. Together, in an optimized ratio, trehalose and small fraction of DMSO which is still

present after extended periods of dialysis, overcome the challenge of colloidal suspension preservation, and limitations imposed by the guidelines for ophthalmic preparation.

5.5 Conclusions

In conclusion, we have concluded that trehalose is the best cryoprotectant and lyoprotectant to improve the shelf-life of nanoparticles. A concentration of 2 wt% of trehalose provides adequate stability without exceeding the osmolarity limit for ophthalmic preparations. A self-cryopreservation property was observed as a result of these investigations. It was determined that the cause of this property was residual DMSO remaining in the formulation and disrupting the formation of large ice crystal domains similar to other protectants such as trehalose. Lastly, it was concluded that freeze-drying the nanoparticle suspension with 2 wt% trehalose results in retention of a residual DMSO fraction. Together these two preservation factors improve the shelf-life of the particles.

Chapter 6
Synthesis of MNPs Under Lyophilization Stress

6.1 Summary

At present, the commercialization strategy for MNP requires the use of freeze-drying to isolate the polymers micelles from aqueous media until required for administration. This is expected to drastically improve the shelf-life of the product. However, this process synthesizes the nanoparticles via nanoprecipitation, followed by freeze-drying to produce the final product. Herein, a method for the direct synthesis of a dried polymer micelle form is described using the stress induced during freeze-drying. This eliminates the need for a preliminary synthesis in aqueous media resulting in reduction in the synthesis time from 3.5 hours to about 10 minutes and reduction in synthesis complexity.

6.2 Introduction

A commercially viable pharmaceutical product must be stable in maintaining its potency, physical characteristics and purity over the shelf-life. A shorter shelf-life results in higher cost of the therapy and therefore affects the pharmacoeconomic evaluation. As described in Chapter 5 freeze-drying is a used approach in the pharmaceutical industry to isolate drug molecules from aqueous environments. The use of freeze-drying to preserve the physical characteristics of the PLA-*b*-Dex and PLA-*b*-Dex-APBA polymer micelles has also been demonstrated. Due to the biodegradable nature and being susceptible to hydrolysis, removal of the excess aqueous media is expected to significantly improve the shelf-life of the product.

At present, the self-assembly is first performed in aqueous media via nanoprecipitation of the polymer dissolved in an organic solvent into an excess of water. With agitation and energy input, an oil-in-water (o/w) emulsion is formed and the hydrophobic chains associate with dispersed droplets of the organic solvent, while the hydrophilic stabilizes the particle. The dispersion is then dialyzed, and then freeze-dried.

Work proposed by Dufrense et al. has showed self-assembly of amphiphilic block-copolymers into polymer micelles under the stress of lyophilization[208,243]. The polymer, drug, and solvent mixture with organic and aqueous fractions is combined and freeze-dried. The freezing step as described in the Chapter 5 creates a cryo-condensed state bringing the chains together causing them to associate. As the

formulation is dried, the removal of aqueous and organic solvent. This results in significant cost and time savings, as the final nanoparticle formulation for commercial use can be prepared directly via freeze-drying, bypassing the nanoprecipitation and dialysis steps. This, and the current process are shown in Illustration 6.1. This chapter describes the process developed for direct synthesis of MNPs.

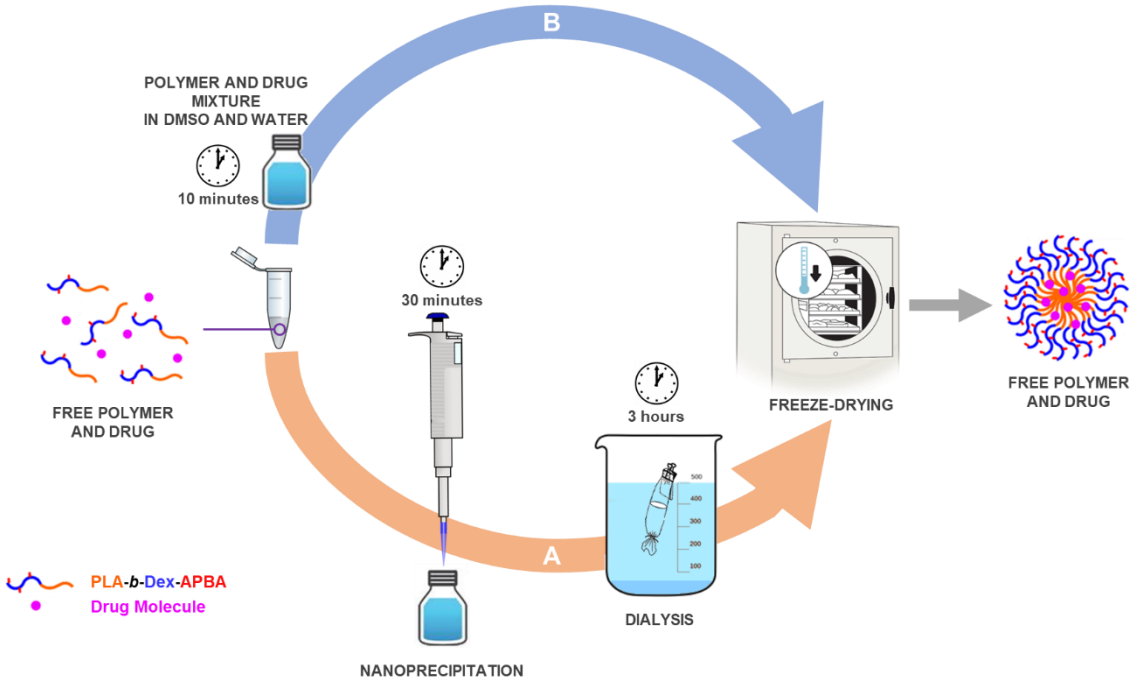

Illustration 6.1: Self-assembly of PLA-*b*-Dex-APBA polymer via A) the current process of nanoprecipitation and agitation for 30 minutes, followed by dialysis for 3 hours and freeze-drying and B) combining the components of the formulation and directly freeze-drying.

6.3 Experimental Section

6.3.1 Materials

Acid-terminated poly(D,L-lactide) (PLA; Mw ~ 20 kDa), dextran from *Leuconostoc mesenteroides* (M_n = 9-11 kDa), sodium periodate ($NaIO_4$), ethylenediamine (EDA), sodium cyanoborohydride ($NaCNBH_3$), *N*-(3-Dimethylaminopropyl)-*N′*-ethylcarbodiimide hydrochloride (EDC), *N*-Hydroxysulfosuccinimide, sodium salt (NHS), 3-Aminophenylboronic acid monohydrate (APBA), glycerol, deuterium oxide (D_2O), methanol and dimethyl sulfoxide (DMSO) were purchased from Millipore Sigma. Liquid nitrogen was dispensed from the University of Waterloo Chem Stores.

6.3.2 Synthesis of Amine Terminated dextran

Borate buffer was prepared by dissolving boric acid (3.1 g/L) in pure water (>15 MΩ) and adjusted to pH 8.2 with 1 N NaOH. Dextran was dissolved in the borate buffer at a concentration of 0.2 g/ml. The terminal dextran monomer exists in equilibrium as a open or ring structure. The alkaline conditions favor the open conformation which improves the reaction efficiency. EDA was added to the reaction mixture in 20 times excess of dextran (6 mmol) and allowed to react for 24 hours in a vessel shielded from light. After the first 24 hours, 300 µl of 5M $NaCNBH_3$ dissolved in 1N NaOH was added to the solution per day for an additional 48 hours (total of two additions).

The aminated dextran (Dex-NH_2) was purified via methanol wash. The aqueous solution was topped with eight times excess of methanol and vortexed to disperse the dextran and break apart any aggregated precipitates. The mixture was centrifuged at 3,000 rpm, and the supernatant was discarded. The wash was repeated one additional time prior to drying in a vacuum desiccator to remove residual methanol.

The dried polymer was analyzed for verification and quantification of amination via ^{1}H-NMR. The polymer was dissolved in D_2O at a concentration of 20 mg/ml. The Dextran C1 peak corresponds to the peak between 4.7 to 5 ppm. The $(CH_2)_2$ of the conjugated EDA has a chemical shift between 2.5 to 2.7 ppm. The ratio of the peaks is used to quantify the conjugation. Only Dex-NH_2 with conjugation efficiency greater than 80% was used for subsequent reactions.

6.3.3 Purification of Acid Terminated PLA

Acid terminated PLA was dissolved in DCM at a concentration of 0.24 g/ml and washed with 8 times excess methanol to remove monomers and small chains. The mixture was centrifuged, and the supernatant was decanted. The remaining PLA gel was purged with air prior to vacuum desiccation for 24 hours. The weight averaged molecular weight was determined by end group analysis via ^{1}H-NMR; the PLA-end CH had a shift at 4.13 ppm and was compared to the PLA CH in the backbone at 5.18 ppm.

6.3.4 Synthesis of PLA-*b*-Dex

The block copolymer was synthesized via carbodiimide chemistry. Dex-NH_2 and purified PLA were dissolved separately in DMSO at a concentration of 0.1 g/ml separately. The acid-terminated PLA was activated by adding Sulfo-NHS (0.46 mmol) and EDC (0.209 mmol) to the PLA. The dissolved dextran was added to the PLA mixture after dissolution of the EDC. The reaction mixture was purged with nitrogen and remained shielded from light for the duration of the experiment. The polymer was purified via dialysis using regenerated cellulose dialysis tubing (MWCO: 12 to 14 kDa) against 200 times the volume DI water for 48 hours with at least six media changes. The unconjugated Dex-NH_2 (Mn ~ 9 – 11 kDa) was removed into the dialysis media and discarded leaving only the conjugated block copolymer within the dialysis tubing. The polymer solution was frozen with liquid nitrogen and lyophilized to remove water and isolate the dry polymer.

The dry polymer was analyzed via ^{1}H-NMR for verification and quantification of block copolymer synthesis. The ratio of the PLA (CH) peak between 5 to 5.3 ppm was compared to the reference peak of Dextran (C1) at 4.6 ppm. Only lock copolymer samples with conjugation greater than 90% were used for the studies.

6.3.5 APBA Modification of PLA-*b*-Dex

The dried PLA-*b*-Dex block copolymer was dissolved in anhydrous DMSO at a concentration of 30 mg/ml. Nine ml of the polymer solution was nanoprecipitated into 30 ml of pure water (>15 MΩ). The suspension was continuously agitated for 30 minutes to allow the nanoparticles to complete forming. The reaction vessel was then shielded from light and 8.50 ml of a $NaIO_4$ solution (10 mg/ml) was added to the suspension to oxidize the dextran corona of the nanoparticles. After 20 minutes, 1 g of glycerol was added to react with the residual $NaIO_4$ as oxidation of glycerol would be favored over dextran.

This was done to ensure the minimize the side reactions and consumption of the reducing agents. 120 mg of APBA was added, followed by 600 µ of a 5 M $NaCNBH_3$ solution prepared in 1 N NaOH. After 2 hours, the reaction mixture was dialyzed against 10 times excess DI water for 24 hours and lyophilized for 24 hours after being frozen with liquid nitrogen.

6.3.6 Characterization of APBA Conjugation

The analysis of APBA conjugation was performed by reconstituting the dried Dex-APBA in Millipore water at a concentration of 1.25 mg/ml. Dextran was used as the baseline for the measurement. The absorbance was measured from 240 – 320 nm with a 1 nm step size using Tecan Infinite Pro 200 MPlex Multimode plate reader. The current protocol for quality control requires APBA conjugation between 5 to 20 mol/mol% (APBA/Dextran monomer).

6.3.7 Synthesis of *l*-MNP

The synthesis of *l*-MNPs was studied the effect of the stress of lyophilization on the synthesis of nanoparticles. As shown in earlier chapters, the presence of a protectant, namely trehalose was important for the stability of the particles. The nanoparticles were prepared in pure water (>15 MΩ) and a solution of trehalose in pure water.

5.7 ml of pure water and trehalose solutions were aliquoted in 20 ml borosilicate vials. Solutions of PLA-*b*-Dex-APBA were prepared in DMSO at various concentrations. 300 µl of the polymer solution was added to the aqueous media and the vial was immediately sealed and vortexed for 30 seconds. 3 ml of the suspension was extracted for dynamic light scattering to determine if the agitation from the vortex itself was enough for the synthesis of the nanoparticles. The remaining 3 ml of the suspension was immediately transferred to a well of liquid nitrogen to immediately freeze the particles. The liquid volume was sufficient to submerge the entire suspension; however, care was taken to ensure the nitrogen did not enter the vial. The vials were kept in the nitrogen until the ice formation had stopped; crackling noises are indicative of the ice crystal formation and the vials remained in the well for an additional 2 minutes after the noises stopped. The remaining samples were prepared in the same way. The starting concentration of the trehalose solution was 21.05 mg/ml to result in a 2 wt% final solution after the addition of the polymer. The initial samples aliquoted into DLS cuvettes were analyzed in triplicate with dyanimic light scattering (DLS) with a Brookhaven 90 Plus.

The frozen samples were dried using a Labconco Freezeone 4.5L freeze-drier at -89°C and 0.009 mPa for 24 hours to ensure all water was removed from the sample, and then stored at -20 °C. The samples were thawed at room temperature and resuspended in 3 ml of pure water (restoring the original volume of the sample). The film was fused to the walls of the vial and was slowly agitated for an hour to ensure the entire film had broken away from the vial. The suspension was transferred to the a DLS cuvette and the size was analyzed. The samples were then filtered with a 200 nm syringe filter to remove any aggregates and then measured again.

6.4 Results and Discussion

6.4.1 Synthesis of *l*-MNP in Pure Water

DLS measurements on the initial aliquoted samples confirmed that nanoparticles did not form immediately upon agitation of the synthesis mixture. Though precipitates were not observed, the solution remained translucent. DLS measurements were not conclusive for many samples and indicated particles greater than 300 nm for the rest. These results were attributed to the aggregation of polymer and it was concluded that MNPs did not form as a result of this agitation.

l-MNP were synthesized by freeze-drying the remaining solutions and rehydrating the particles with DI water (>15 MΩ). The freeze-dried samples were thawed at room temperature and reconstitute with the same amount of liquid was removed. DLS results are shown in Figure 6.1. The unfiltered freeze-dried samples reveal significant aggregation. Large visible shard like aggregates (> 1 mm) were still visible and not transferred to the cuvette for measurement. The DLS readings in this case however showed that samples prepared with polymer concentrations above 0.038 mg/ml were statistically similar. The lower concentration appeared to have significant aggregation upon freeze-drying. This may have occurred due to one of two reasons.

First, the volume of DMSO in each case was kept the same while the concentration of the polymer was varied. At the low polymer concentration, the excess DMSO may have been sufficient to stabilize the polymer inhibiting the formation of the nanoparticles during the stages of the freeze-drying process. Second, the polymer concentration may have been below the critical micelle concentration which would mean that there was insufficient polymer for the micellar structure to start forming and the polymer aggregated during freeze-drying instead. DLS measurements on the filtered *l*-MNP show that particles with a size below 200 nm with low polydispersion could be synthesized. The concentration of polymer

in the mixture did not appear to be a significant factor. Paired t-tests were conducted on measurements for each formulation which revealed there was a statistically significant difference between the means of the initial, freeze-dried unfiltered, and freeze-dried filtered samples. Unpaired t-tests between samples of the different conditions revealed that the freeze-dried filtered samples are statistically similar. There is no statistically significant trend for the initial unfiltered and freeze-dried unfiltered sample. The freeze-dried system consistently reveals aggregates when the suspension is unfiltered but are removed upon filtering. The count rate was maintained above 300 kcps suggesting that a significant fraction of the small nanoparticles exist in the suspension.

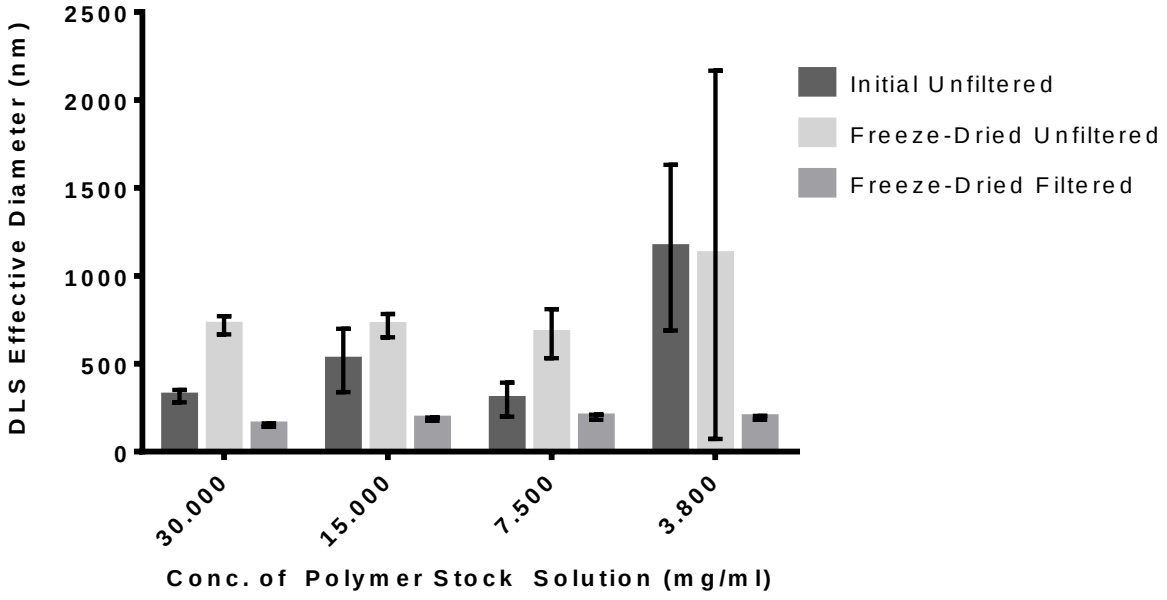

Figure 6.1: *l*-MNP Synthesized in Pure Water (>15 MΩ) at varied concentration of polymer stock solution.

The correlation and residual plots were the three treatment conditions were used to determine if there was an effect of polymer concentration on the resulting nanoparticle size. The correlation for the freeze-dried and unfiltered sample in Figure 6.2 c) was determined to not be significant. This is supported by the residual plot shown in Figure 6.2 d) revealing an unbiased but heteroscedastic pattern; the variance between the polymer concentrations is not equal. The heteroscedasticity is also observed for the initial unfiltered sample in Figure 6.2 b) suggesting higher variability at higher concentrations for this treatment condition. Though the correlation is poorly linear, the slope was determined to be non-zero

at a significance of $\alpha = 0.05$. Nevertheless, an increase in polymer concentration appears to correlate with smaller particle size.This trend was observed for the freeze-dried samples after filtering as shown in Figure 6.2 e). The residuals for this treatment show an unbiased and homoscedastic distribution indicating uniform variance between the treatments after filtering as shown in Figure 6.2 f). From this it can be concluded that the aggregates formed at lower concentrations were more polydisperse as compared to the samples at higher concentrations.

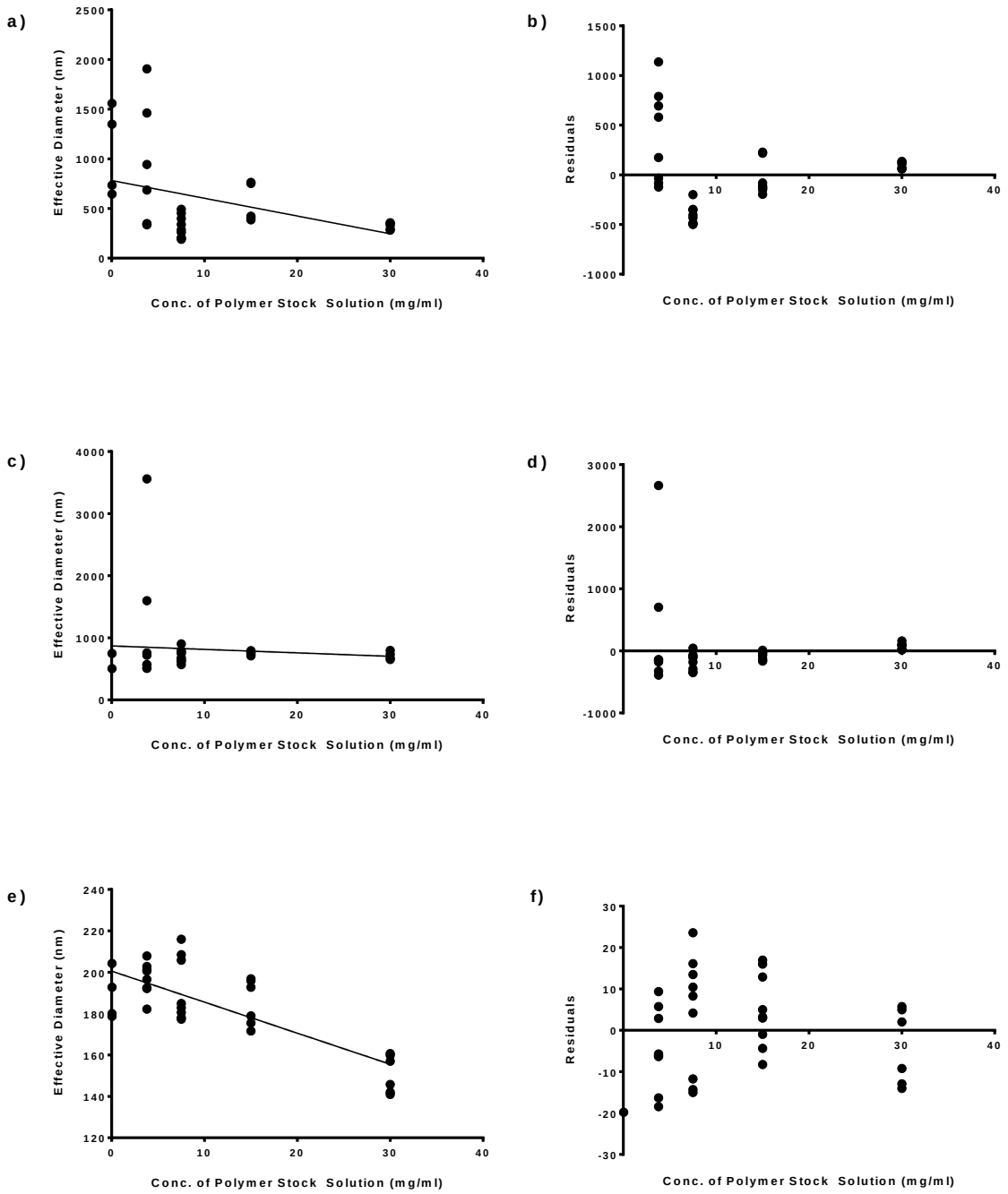

Figure 6.2: Correlation plots and residual plots for *l*-MNP synthesized in water: a) & b) initial unfiltered sample, c) & d) freeze-dried unfiltered sample, and e) & f) freeze-dried filtered sample.

6.4.2 Synthesis of *l*-MNP in a 2 wt% Trehalose Solution

Similar to the *l*-MNPs synthesized in pure water, the initial aliquots of agitated mixtures show no significant trend in particle size or aggregate formation. Upon freeze-drying however, the samples in DI water (>15 MΩ) show significant aggregation, whereas particles synthesized in the trehalose solutions do not for samples with polymer concentrations less than 0.3 mg/ml. In fact, the unfiltered freeze-dried particles synthesized in the trehalose solution were smaller than the freeze-dried filtered samples synthesized in water. These unfiltered particles would be tolerated by the eye without foreign body experience and acceptable according to the USP for ophthalmic preparations. The filtered freeze-dried particles similarly resulted in a decrease in particle size upon filtered, less than 100 nm for all concentrations less than 0.3 µg/ml. Furthermore, the filtered samples approach sizes typical of polymer micelles synthesized via nanoprecipitation with PLA-*b*-Dex. Though they are not statistically similar, there is no discernable trend as a function of concentration. These results are shown in Figure 6.3.

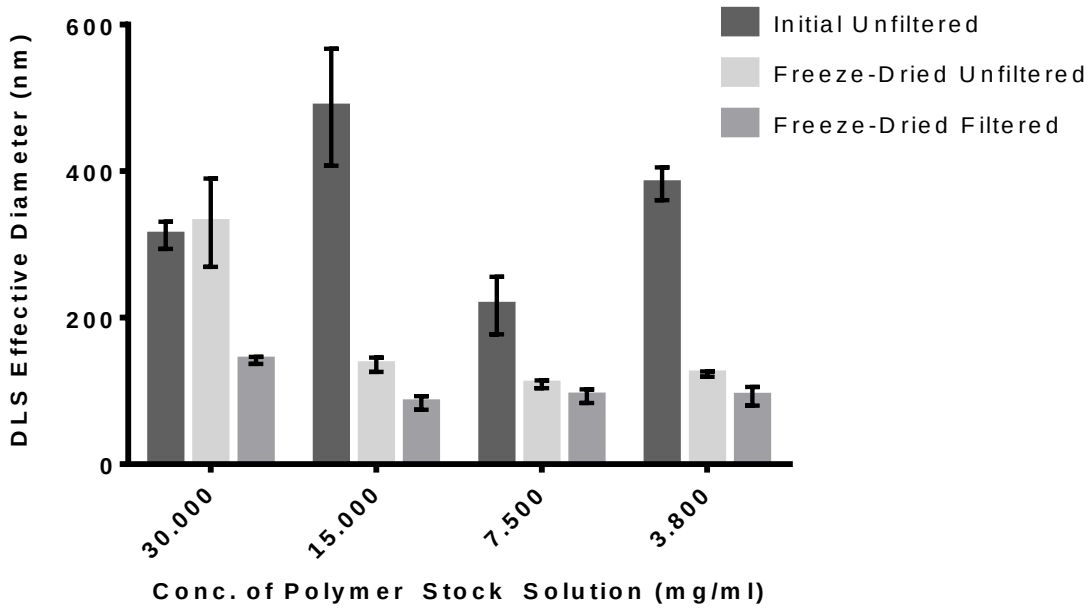

Figure 6.3: DLS effective diameter of *l*-MNPs synthesized in 2 wt% trehalose solution.

The presence of trehalose in the suspension has previously been shown to help preserve the properties of the nanoparticles upon freeze-drying. This was attributed to the formation of the glassy matrix and retention of DMSO as described in Chapter 5. *l*-MNPs synthesized in ultrapure water had a much larger particle size than those synthesized in a solution of trehalose. The mechanism for stabilization and production of smaller *l*-MNPs may also be a result of intercalation. Thus, it can be concluded that synthesis of *l*-MNP in a solution of 2 wt% trehalose is the preferred route to exploit this process. The optimal concentration for the polymer stock to be used in this method is 15 mg/ml. Resulting particles were consistently smaller and stable, and more similar to the nanoprecipitated sample.

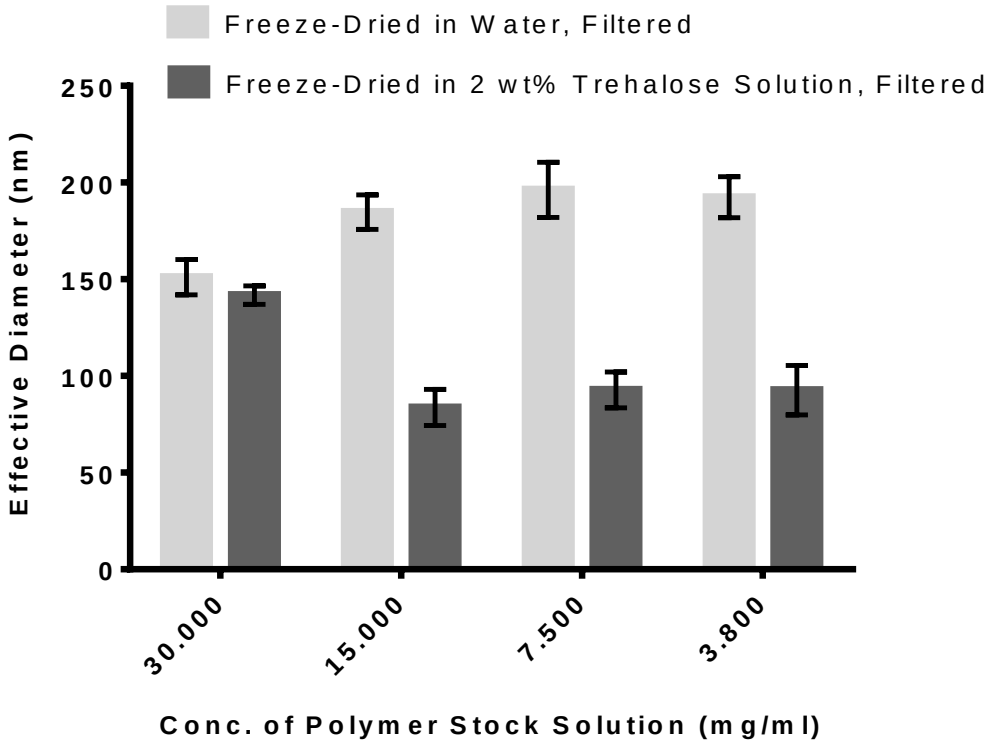

Figure 6.4: Effect of Trehalose on MNPs Produced Under Lyophilization Stress

The correlation and residual plots were the three treatment conditions were used to determine if there was an effect of polymer concentration on the resulting nanoparticle size. The initial unfiltered sample had no correlation, shown in Figure 6.5 a), and the slope was not significantly different from zero at a significance level of $\alpha = 0.05$. The residual Figure 6.5 b) shows unbiased variances in the different polymer concentrations.

Both freeze-dried samples, unfiltered and filtered, had a slop significantly different than zero at a significance level of $\alpha = 0.05$. Converse to the samples produced in pure water, the samples produced in 2 wt% trehalose solution were shown to have an increasing particle size with an increase in polymer concentration as shown in Figure 6.5 c) and Figure 6.5 e). Both residual plots for these samples also appear to have a parabolic distribution as shown in Figure 6.5 d) and Figure 6.5 f). This is generally an indication that a non-linear model may be a better fit. A non-linear model in this case may suggest the involvement of another factor other than polymer concentration also influencing the synthesis of the particles.

This study suggests that the method proposed by Dufrense et al. to synthesize polymer micelles under lyophilization stress is applicable for the synthesis of MNPs. This method can result in significant time savings for the manufacture of the commercial ophthalmic suspension. Currently, the drug-loaded nanoparticles would be synthesized via nanoprecipitation, dialyzed, and then freeze-dried and shipped as a dry formulation to the patient. Trehalose would need to be added to the formulation in both instances, and the study used an equal amount of trehalose in the solution to start. However, by adapting the method presented in this study, the dry formulation may be readily produced under the stresses produced via lyophilization. Overall this method would result in cost and time savings allowing for higher throughput.

To commercialize nanoparticles using this method, a dual chamber would be utilized which separates the dry nanoparticles and API from the aqueous vehicle for delivery. This method is currently utilized and packaging for consumer application have been developed. The dried polymer film would be further broken down to facilitate quick dissolution of the polymer in media. This was not performed for this proof-of-concept study. However, the impact of the mechanical stress and a trade-off with the reconstitution time may have to be reached.

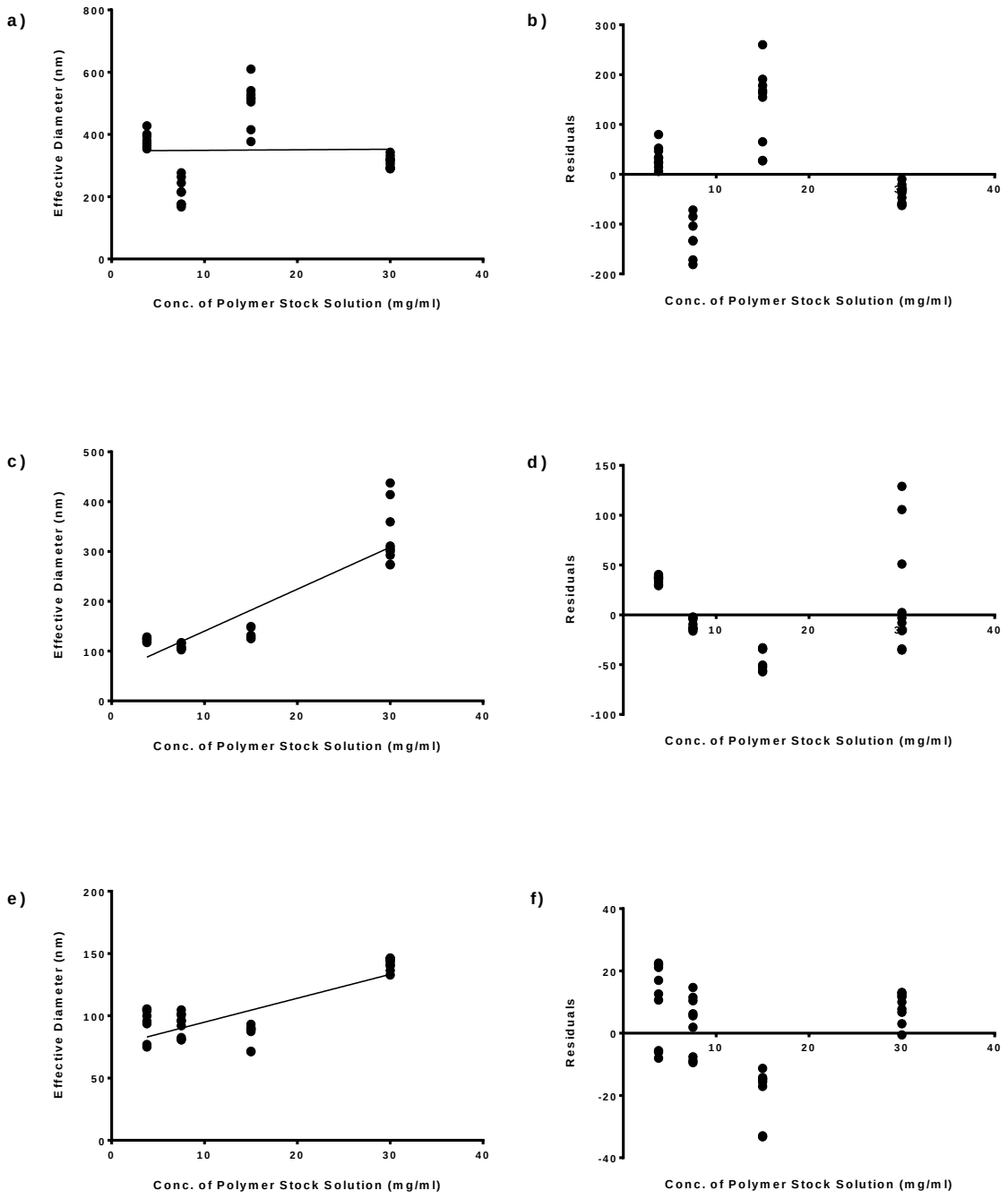

Figure 6.5: Correlation plots and residual plots for *l*-MNP synthesized in a solution of 2 wt% trehalose: a) & b) initial unfiltered sample, c) & d) freeze-dried unfiltered sample, and e) & f) freeze-dried filtered sample.

6.5 Conclusions

Freeze-drying polymer micelles is an attractive strategy to improve the shelf-life of the formulation and commercial viability. At present, the formulation is prepared via nanoprecipitation followed by dialysis prior to the freeze-drying. The commercial formulation will be reconstituted when needed and ready for administration. An alternate synthesis route was explored which combines the constituents of the formulations and by immediately freeze-drying the formulation yields a porous cake which forms particles upon reconstitution. This bypasses the initial nanoprecipitation and dialysis steps resulting in a reduction of manual work prior freeze-drying from 3.5 hours to 10 minutes producing the final formulation intended for market. A 2 wt% solution and a polymer stock concentration of 15 mg/ml are the ideal conditions for the synthesis of *l*-MNPs. The process of freeze-drying which has thus far been limited to the extraction of solutes from aqueous media for preservation, can also be utilized for the synthesis of block copolymer micelles.

Chapter 7
Conclusions and Future Works

7.1 Summary

MNPs have proven utility in the area of ocular drug delivery by targeting the ocular mucosa to overcome the physiological and anatomical challenges to conventional formulations. Many colloidal systems and strategies discussed in earlier chapters are also able to improve upon the incumbent in their niche application. However, these formulations face unique challenges of their own which have thus far limited the widespread commercialization of nanotechnology enabled medicine in the market. This work addresses some key challenges and opportunities for the MNP platform. The major conclusions and recommendations for future work are presented below.

7.2 Conclusions

The following are major conclusions of the work presented in this thesis.

1. The conjugation of mucoadhesive ligand has been investigated to optimize and better control the reaction. The current quality control standard for the synthesis of APBA functionalized dextran and PLA-*b*-Dex block copolymer requires a conjugation efficiency of 5 – 20 mol/mol%. This broad conjugation range cannot be tolerated for a commercial product as it would result in significant batch-to-batch variation. The work presented in Chapter 3 resulted in better control and understanding of the reaction.

    a) Statistically significant interactions between the reducing agent and ligand have been identified in the synthesis of PLA-*b*-Dex-APBA. It was also concluded that the reducing agent concentration was statistically significant, whereas the ligand concentration was not allowing for better synthesis planning.

    b) The variance between batches has been reduced demonstrating stronger control of the reaction conditions and reduced batch-to-batch variance.

    c) When studying the conjugation of APBA onto dextran, there was lower variance than when investigating the conjugation onto PLA-*b*-Dex polymer micelles.

2. In Chapter 4 an alternate reaction scheme for the conjugation of the mucoadhesive ligand BPBA borrowing principals of solid-state chemistry.

    a) This synthesis procedures results in a reduction in reaction time from 30 hours (reaction explored in Chapter 3) to 10 minutes. A maximum BPBA/dextran monomer conjugation efficiency of 42.6 mol/mol% was achieved in 10 minutes by tuning the melt mixture and at significantly reduced temperatures than conventional solid-state reactions.

    b) This method of carbohydrate modification was free of organic solvents and did not result in degradation of the macromolecule. The reaction chemistry is not specific to dextran and BPBA and can be used for the modification of other carbohydrates used in pharmaceutical applications.

3. The challenge of poor stability and shelf-life is a limiting factor in the commercialization of colloidal systems is explored in Chapter 5 in the context of PLA-*b*-Dex-APBA polymer micelles.

    a) Freeze-drying was determined to be an optimal solution to improve the shelf-life of the polymer micelle nanoparticles. Removing them from the aqueous media reduces the chances of particle aggregation as well as breakdown and hydrolysis of the biodegradable polymer before administration. This is likely to ensure a consistent dose and performance during batches.

    b) Trehalose added at 2 wt% of the solution was determined to be the optimal concentration of protectant in the system. This is a significant reduction from typical cryoprotectant and lyoprotectant concentrations used in literature (up to 20 wt%) which would exceed the osmolarity limit allowed for ophthalmic formulations as specified by regulatory bodies.

    c) During the experimentation, a self-cryopreservation property was demonstrated, i.e. suspensions frozen without cryoprotectant are statistically similar to the initial formulation. The addition of cryoprotectant was not necessary for the recovery of the nanoparticles.

4. As described in Chapter 5 freeze-drying is an attractive solution for improving the shelf-life of the PLA-*b*-Dex-APBA polymer micelle nanoparticles. The commercial product can be contained within a dual chamber package with the dried particle separated from aqueous media for resuspension. The current synthesis project requires the nanoprecipitation of PLA-*b*-Dex-APBA polymer into aqueous media and subsequent dialysis for the removal of DMSO and free drug. This process is then followed by freeze-drying.

    a) An alternate synthesis route was explored in which the freeze-dried formulation is prepared directly bypassing the nanoprecipitation and dialysis steps. This results in a time saving from 3.5 hours to 10 minutes prior to lyophilization resulting in time saving. The particles synthesized with the alternate route were similar in size suggesting that this method can directly produce the final desired product.

    b) A 2 wt% solution of trehalose should be used as the medium for *l*-MNP synthesis instead of water for the improved particle stability. A polymer stock concentration of 15 mg/ml in DMSO should be utilized as this consistently resulted in the smallest particles, which are most similar to those prepared via nanoprecipitation.

7.3 Recommendations for future work

The following are recommended tasks and avenues to explore based on the conclusions of this thesis.

1. The effect of reducing agent and ligand concentration on the conjugation efficiency of APBA on dextran were explored in Chapter 3. It is proposed that the regression models derived from these experiments be further validated by targeting arbitrary conjugation efficiencies within the working region and verifying the model with experimental observations. It is possible for the current model to have multiple solutions for a particular target, and this study will help to shift the weights associated with the main factor and interaction terms.

2. Solutions of biocompatible polymers such as dextran are used as lubricants for the alleviation of dry eye symptoms. Mucoadhesive dextran as described in Chapter 3 may provide prolonged relief thereby reducing the administration frequency. This would improve patient compliance and quality of life. Furthermore, the solution can be tuned by controlling the concentration of conjugated mucoadhesive ligand onto the polymer for varying stages of the disease. This should be explored

as an opportunity for commercialization especially since the investment into PBA pharmacokinetics and toxicology will have to be carried out for the mucoadhesive nanoparticles.

3. Pharmacokinetic and toxicology studies must be carried out on PBA which is the only constituent of the mucoadhesive block copolymer which is not yet approved by the FDA. Thus far, studies in rabbit models have shown that there is no irritation or change to the tissue structure. Long term studies should be performed on the eye as well as other organ systems to study their effects and distribution and clearance in the body. The effect of PBA conjugation on retention time should be analyzed in vivo to determine if the relationship is linear or if it plateaus to determine the optimal useful ligand concentration.

4. Chapter 4 explores a co-solvent dehydration reaction mechanism for the modification of carbohydrates. A reaction time of 10 minutes was determined to be optimal as the effect of time was not a significant factor in the conjugation rate. Shorter time scales should be investigated to determine the changes in composition up to 10 minutes. The effect of the water present should be explored at this time scales to determine a) when it evaporates and is removed from the system, and b) the impact of residual water on the conjugation efficiency.

5. Chapter 6 presents a proof-of-concept study demonstrating the direct synthesis of MNPs utilizing the stress induced during the freeze-dried process. As the next step in this development, it is recommended that drug molecules be incorporated into the nanoparticles. The effect of drug concentration in the stock solution on the encapsulation efficiency should be investigated. Lipophilic molecules are easily incorporated into the hydrophobic core of the PLA-*b*-Dex-APBA polymer micelles, thought they vary in loading efficiency. This method should be explored for potential improvements in the drug loading. Lastly, hydrophilic drug molecules are not well encapsulated within the core since the preparation method utilizes nanoprecipitation which is an o/w emulsion technique. This freeze-drying synthesis mechanism should also be explored for the entrapment of hydrophilic molecules. Literature indicates small volumes of DMSO can be removed via lyophilization, and the presence of water (which is the major component) allows the DMSO to remain frozen during the drying process. The process for complete removal is lengthy.As a pre-clinical study, the residual fraction of DMSO in the formulation after freeze-drying should be determined.

Bibliography

[1] Y. Weng, J. Liu, S. Jin, W. Guo, X. Liang, Z. Hua, *Acta Pharm. Sin. B* **2017**, *7*, 281.
[2] S. K. Sahoo, F. Dilnawaz, S. Krishnakumar, *Drug Discov. Today* **2008**, *13*, 144.
[3] M. S. Sridhar, *Indian J. Ophthalmol.* **2018**, *66*, 190.
[4] *Vis. Eye Inst.* **2017**.
[5] S. K. Sahoo, *Nanotechnology in Health Care*, Jenny Stanford Publishing, **2012**.
[6] S. M. Sharma, J. T. Rosenbaum, in *Ocul. Dis.* (Eds.: L.A. Levin, D.M. Albert), W.B. Saunders, Edinburgh, **2010**, pp. 642–653.
[7] G. Sunkara, U. B. Kompella, U. B. Kompella, "Membrane Transport Processes in the Eye," DOI 10.1201/9780203912072-6can be found under https://www.taylorfrancis.com/, **2003**.
[8] M. Hornof, E. Toropainen, A. Urtti, *Eur. J. Pharm. Biopharm.* **2005**, *60*, 207.
[9] A. Ludwig, *Adv. Drug Deliv. Rev.* **2005**, *57*, 1595.
[10] A. Patel, K. Cholkar, V. Agrahari, A. K. Mitra, *World J. Pharmacol.* **September 6**, *2*, 47.
[11] L. C. du Toit, V. Pillay, Y. E. Choonara, T. Govender, T. Carmichael, *Expert Opin. Drug Deliv.* **2011**, *8*, 71.
[12] J. F. Fangueiro, F. Veiga, A. M. Silva, E. B. Souto, *Curr. Pharm. Des.* **2016**, *22*, 1135.
[13] E. Fröhlich, E. Roblegg, *J. Nanosci. Nanotechnol.* **2014**, *14*, 126.
[14] M. Ali, M. E. Byrne, *Expert Rev. Clin. Pharmacol.* **2008**, *1*, 145.
[15] J. Fischbarg, F. Diecke, P. Iserovich, A. Rubashkin, *J. Membr. Biol.* **2006**, *210*, 117.
[16] R. Zhou, R. R. Caspi, *F1000 Biol. Rep.* **1**, *2*, 3.
[17] J. C. Tsai, in *Ocul. Dis.* (Eds.: L.A. Levin, D.M. Albert), W.B. Saunders, Edinburgh, **2010**, pp. 178–183.
[18] Y.-C. Tham, X. Li, T. Y. Wong, H. A. Quigley, T. Aung, C.-Y. Cheng, *Ophthalmology* **2014**, *121*, 2081.
[19] R. N. Weinreb, T. Aung, F. A. Medeiros, *JAMA* **2014**, *311*, 1901.
[20] D. A. Lee, E. J. Higginbotham, *Am. J. Health. Syst. Pharm.* **2005**, *62*, 691.
[21] S. Dorairaj, M. P. Vianello, **n.d.**
[22] A. Robin, D. S. Grover, *Indian J. Ophthalmol.* **2011**, *59*, S93.
[23] A. G. P. Konstas, G. Maskaleris, S. Gratsonidis, C. Sardelli, *Eye* **2000**, *14*, 752.
[24] "Vision impairment and blindness," can be found under https://www.who.int/news-room/fact-sheets/detail/blindness-and-visual-impairment, **n.d.**
[25] A. J. Buller, B. Connell, A. F. Spencer, *Br. J. Ophthalmol.* **2005**, *89*, 1370.
[26] G. Reardon, G. F. Schwartz, E. Mozaffari, *Am. J. Ophthalmol.* **2004**, *137*, S3.
[27] "Ophthalmic Drugs Market Size & Share | Industry Report, 2019-2026," can be found under https://www.grandviewresearch.com/industry-analysis/ophthalmic-therapeutics-drug-market, **n.d.**

[28] A. R. and Consulting, “Ophthalmic Drugs Market Size to Hit US$ 40 Billion by 2026,” can be found under http://www.globenewswire.com/news-release/2019/04/29/1811371/0/en/Ophthalmic-Drugs-Market-Size-to-Hit-US-40-Billion-by-2026.html, **2019**.
[29] A. M. Research, “Global Ophthalmic Drugs Market Expected to Reach $42,663 Million by 2023 - Allied Market Research,” can be found under https://www.prnewswire.com/news-releases/global-ophthalmic-drugs-market-expected-to-reach-42663-million-by-2023---allied-market-research-657703433.html, **n.d.**
[30] “Eye Surgeons of Indiana,” can be found under https://www.eyesurgeonsofindiana.com/dry-eye-mgd-treatment, **n.d.**
[31] B. M. Boddupalli, Z. N. K. Mohammed, R. A. Nath, D. Banji, *J. Adv. Pharm. Technol. Res.* **2010**, *1*, 381.
[32] A. Makhlof, M. Werle, H. Takeuchi, *J. Drug Deliv. Sci. Technol.* **2008**, *18*, 375.
[33] K. Netsomboon, A. Bernkop-Schnürch, *Eur. J. Pharm. Biopharm. Off. J. Arbeitsgemeinschaft Pharm. Verfahrenstechnik EV* **2016**, *98*, 76.
[34] G. S. Asane, S. A. Nirmal, K. B. Rasal, A. A. Naik, M. S. Mahadik, Y. M. Rao, *Drug Dev. Ind. Pharm.* **2008**, *34*, 1246.
[35] A. R. Mackie, F. M. Goycoolea, B. Menchicchi, C. M. Caramella, F. Saporito, S. Lee, K. Stephansen, I. S. Chronakis, M. Hiorth, M. Adamczak, M. Waldner, H. M. Nielsen, L. Marcelloni, *Macromol. Biosci.* **2017**, *17*, 1600534.
[36] R. Shaikh, T. R. Raj Singh, M. J. Garland, A. D. Woolfson, R. F. Donnelly, *J. Pharm. Bioallied Sci.* **2011**, *3*, 89.
[37] P. Mahajan, A. Kaur, G. Aggarwal, S. L. Harikumar, *Int. J. Drug Dev. Res.* **2013**, *5*.
[38] S. K. Lai, Y.-Y. Wang, J. Hanes, *Adv. Drug Deliv. Rev.* **2009**, *61*, 158.
[39] S. K. Lai, J. S. Suk, A. Pace, Y.-Y. Wang, M. Yang, O. Mert, J. Chen, J. Kim, J. Hanes, *Biomaterials* **2011**, *32*, 6285.
[40] S. Shak, D. J. Capon, R. Hellmiss, S. A. Marsters, C. L. Baker, *Proc. Natl. Acad. Sci. U. S. A.* **1990**, *87*, 9188.
[41] P. L. Shah, S. F. Scott, R. A. Knight, C. Marriott, C. Ranasinha, M. E. Hodson, *Thorax* **1996**, *51*, 119.
[42] H. Boyapally, R. K. Nukala, P. Bhujbal, D. Douroumis, *Colloids Surf. B Biointerfaces* **2010**, *77*, 227.
[43] M. Petelin, Z. Pavlica, S. Bizimoska, M. Šentjurc, *Int. J. Pharm.* **2004**, *270*, 83.
[44] N. A. Nafee, F. A. Ismail, N. A. Boraie, L. M. Mortada, *Int. J. Pharm.* **2003**, *264*, 1.
[45] A. K. Jain, R. K. Khar, F. J. Ahmed, P. V. Diwan, *Eur. J. Pharm. Biopharm.* **2008**, *69*, 426.
[46] B. Luppi, F. Bigucci, A. Abruzzo, G. Corace, T. Cerchiara, V. Zecchi, *Eur. J. Pharm. Biopharm.* **2010**, *75*, 381.
[47] M. Melo, R. Nunes, B. Sarmento, J. das Neves, *Mater. Today Chem.* **2018**, *10*, 128.
[48] M. Jyotsana, B. Sagar, D. Mahesh, *Int. J. Res. Ayurveda Pharm.* **2010**, *1*, 8.

[49] M. Hornof, W. Weyenberg, A. Ludwig, A. Bernkop-Schnürch, *J. Controlled Release* **2003**, *89*, 419.
[50] E. Grześkowiak, *Eur. J. Pharm. Sci.* **1998**, *6*, 247.
[51] H. Qi, W. Chen, C. Huang, L. Li, C. Chen, W. Li, C. Wu, *Int. J. Pharm.* **2007**, *337*, 178.
[52] A. Lux, S. Maier, S. Dinslage, R. Süverkrüp, M. Diestelhorst, *Br. J. Ophthalmol.* **2003**, *87*, 436.
[53] E. Larrañeta, S. Stewart, M. Ervine, R. Al-Kasasbeh, R. F. Donnelly, *J. Funct. Biomater.* **2018**, *9*, DOI 10.3390/jfb9010013.
[54] V. H. K. Li, R. W. Wood, J. Kreuter, T. Harmia, J. R. Robinson, *J. Microencapsul.* **1986**, *3*, 213.
[55] A. Zimmer, E. Mutschler, G. Lambrecht, D. Mayer, J. Kreuter, *Pharm. Res.* **1994**, *11*, 1435.
[56] A. Zimmer, J. Kreuter, J. R. Robinson, *J. Microencapsul.* **1991**, *8*.
[57] A. de Campos, Y. Diebold, E. S. Carvalho, A. Sánchez, M. José Alonso, *Pharm. Res.* **2004**, *21*, 803.
[58] A. E. de Salamanca, Y. Diebold, M. Calonge, C. García-Vazquez, S. Callejo, A. Vila, M. J. Alonso, *Invest. Ophthalmol. Vis. Sci.* **2006**, *47*, 1416.
[59] L. Contreras-Ruiz, M. de la Fuente, C. García-Vázquez, V. Sáez, B. Seijo, M. J. Alonso, M. Calonge, Y. Diebold, *Cornea* **2010**, *29*, 550.
[60] Y. Diebold, M. Jarrín, V. Sáez, E. L. S. Carvalho, M. Orea, M. Calonge, B. Seijo, M. J. Alonso, *Biomaterials* **3**, *28*, 1553.
[61] X. Zhu, M. Su, S. Tang, L. Wang, X. Liang, F. Meng, Y. Hong, Z. Xu, *Mol. Vis.* **2012**, *18*, 1973.
[62] A. M. De Campos, A. Sánchez, M. J. Alonso, *Int. J. Pharm.* **8**, *224*, 159.
[63] İ. Yenice, M. C. Mocan, E. Palaska, A. Bochot, E. Bilensoy, İ. Vural, M. İrkeç, A. Atilla Hıncal, *Exp. Eye Res.* **9**, *87*, 162.
[64] E. H. Gökçe, G. Sandri, S. Eğrilmez, M. C. Bonferoni, T. Güneri, C. Caramella, *Curr. Eye Res.* **2009**, *34*, 996.
[65] E. Başaran, M. Demirel, B. Sırmagül, Y. Yazan, *J. Microencapsul.* **2010**, *27*, 37.
[66] E. Başaran, E. Yenilmez, M. S. Berkman, G. Büyükköroğlu, Y. Yazan, *J. Microencapsul.* **2014**, *31*, 49.
[67] C. Bucolo, A. Maltese, F. Maugeri, B. Busà, G. Puglisi, R. Pignatello, *J. Pharm. Pharmacol.* **2004**, *56*, 841.
[68] R. Katara, D. K. Majumdar, *Colloids Surf. B Biointerfaces* **January 3**, *103*, 455.
[69] K. Adibkia, M. R. S. Shadbad, A. Nokhodchi, A. Javadzedeh, M. Barzegar-Jalali, J. Barar, G. Mohammadi, Y. Omidi, *J. Drug Target.* **2007**, *15*, 407.
[70] E. Vega, M. A. Egea, O. Valls, M. Espina, M. L. García, *JPS J. Pharm. Sci.* **2006**, *95*, 2393.
[71] A. Badawi, H. El-Laithy, R. El Qidra, H. El Mofty, M. El dally, *Arch. Pharm. Res.* **2008**, *31*, 1040.
[72] N. Nagai, Y. Ito, N. Okamoto, Y. Shimomura, *Toxicology* **July 5**, *319*, 53.

[73] A. Sabzevari, K. Adibkia, H. Hashemi, B. G. De Geest, N. Mohsenzadeh, F. Atyabi, M. H. Ghahremani, M.-R. Khoshayand, R. Dinarvand, *Invest. Ophthalmol. Vis. Sci.* **2013**, *54*, 5520.
[74] A. Vasconcelos, E. Vega, Y. Pérez, M. J. Gómara, M. L. García, I. Haro, *Int. J. Nanomedicine* **1**, *10*, 609.
[75] H. L. Alvarado, G. Abrego, M. L. Garduño-Ramirez, B. Clares, A. C. Calpena, M. L. García, *Nanomedicine Nanotechnol. Biol. Med.* **4**, *11*, 521.
[76] R. Asasutjarit, T. Theerachayanan, P. Kewsuwan, S. Veeranodha, A. Fuongfuchat, G. Ritthidej, *AAPS PharmSciTech* **2015**, 1.
[77] T.-C. Chu, Q. He, D. E. Potter, *J. Ocul. Pharmacol. Ther.* **2002**, *18*, 507.
[78] G.-H. Hsiue, S. Hsu, C.-C. Yang, S.-H. Lee, I. K. Yang, *Biomaterials* **1**, *23*, 457.
[79] S. Wadhwa, R. Paliwal, S. R. Paliwal, S. P. Vyas, *J. Drug Target.* **2010**, *18*, 292.
[80] U. Shinde, M. H. Ahmed, K. Singh, *J. Drug Deliv.* **2013**, *2013*, 562727.
[81] M. H. Warsi, M. Anwar, V. Garg, G. K. Jain, S. Talegaonkar, F. J. Ahmad, R. K. Khar, *Colloids Surf. B Biointerfaces* **January 10**, *122*, 423.
[82] B. S. Gudmundsdottir, D. Petursdottir, G. M. Asgrimsdottir, M. S. Gottfredsdottir, S. H. Hardarson, G. Jóhannesson, S. V. Kurkov, P. Jansook, T. Loftsson, E. Stefánsson, *J. Ocul. Pharmacol. Ther.* **2014**, *30*, 35.
[83] G. Jóhannesson, M. D. Moya-Ortega, G. M. Ásgrímsdóttir, S. H. Lund, M. Thorsteinsdóttir, T. Loftsson, E. Stefánsson, *Acta Ophthalmol. (Copenh.)* **2014**, *92*, 550.
[84] H. Yang, C. T. Leffler, *J. Ocul. Pharmacol. Ther.* **2013**, *29*, 166.
[85] S. Katiyar, J. Pandit, R. S. Mondal, A. K. Mishra, K. Chuttani, M. Aqil, A. Ali, Y. Sultana, *Carbohydr. Polym.* **2**, *102*, 117.
[86] Ameeduzzafar, J. Ali, A. Bhatnagar, N. Kumar, A. Ali, *Int. J. Biol. Macromol.* **4**, *65*, 479.
[87] L. Gan, S. Han, J. Shen, J. Zhu, C. Zhu, X. Zhang, Y. Gan, *Int. J. Pharm.* **8**, *396*, 179.
[88] A. Fabiano, P. Chetoni, Y. Zambito, *Drug Dev. Ind. Pharm.* **2015**, *0*, 1.
[89] R. Chen, Y. Qian, R. Li, Q. Zhang, D. Liu, M. Wang, Q. Xu, *YAKUGAKU ZASSHI* **2010**, *130*, 419.
[90] R. Li, S. Jiang, D. Liu, X. Bi, F. Wang, Q. Zhang, Q. Xu, *J. Microencapsul.* **2011**, *28*, 134.
[91] J. Youshia, A. O. Kamel, A. El Shamy, S. Mansour, *Int. J. Nanomedicine* **5**, *7*, 2483.
[92] F. Wang, L. Chen, D. Zhang, S. Jiang, K. Shi, Y. Huang, R. Li, Q. Xu, *J. Drug Target.* **2014**, *22*, 849.
[93] P. Verma, R. N. Gupta, A. K. Jha, R. Pandey, *Drug Deliv.* **2013**, *20*, 269.
[94] J. Singh, G. Chhabra, K. Pathak, *Drug Dev. Ind. Pharm.* **2014**, *40*, 1223.
[95] P. Bhagav, H. Upadhyay, S. Chandran, *AAPS PharmSciTech* **2011**, *12*, 1087.
[96] K. Singh, U. Shinde, *Pharm.- Int. J. Pharm. Sci.* **2011**, *66*, 594.
[97] H. Yang, P. Tyagi, R. S. Kadam, C. A. Holden, U. B. Kompella, *ACS Nano* **2012**, *6*, 7595.

[98] W. Wu, J. Li, L. Wu, B. Wang, Z. Wang, Q. Xu, H. Xin, *AAPS PharmSciTech* **2013**, *14*, 1063.
[99] T. Musumeci, C. Bucolo, C. Carbone, R. Pignatello, F. Drago, G. Puglisi, *Int. J. Pharm.* **1**, *440*, 135.
[100] A. Leonardi, C. Bucolo, F. Drago, S. Salomone, R. Pignatello, *Int. J. Pharm.* **1**, *478*, 180.
[101] N. Nagai, C. Yoshioka, Y. Mano, W. Tnabe, Y. Ito, N. Okamoto, Y. Shimomura, *Exp. Eye Res.* **3**, *132*, 115.
[102] R. Cavalli, M. R. Gasco, P. Chetoni, S. Burgalassi, M. F. Saettone, *Int. J. Pharm.* **5**, *238*, 241.
[103] H. Gupta, M. Aqil, R. K. Khar, A. Ali, A. Bhatnagar, G. Mittal, *Nanomedicine Nanotechnol. Biol. Med.* **4**, *6*, 324.
[104] G. K. Jain, N. Jain, S. A. Pathan, S. Akhter, S. Talegaonkar, P. Chander, R. K. Khar, F. J. Ahmad, *J. Pharm. Biomed. Anal.* **January 5**, *52*, 110.
[105] H. Gupta, M. Aqil, R. K. Khar, A. Ali, A. Bhatnagar, G. Mittal, *J. Drug Target.* **2011**, *19*, 409.
[106] M. Abul Kalam, Y. Sultana, A. Ali, M. Aqil, A. K. Mishra, K. Chuttani, I. A. Aljuffali, A. Alshamsan, *J. Biomed. Mater. Res. A* **2013**, *101A*, 1828.
[107] H. Gupta, M. Aqil, R. K. Khar, A. Ali, A. Bhatnagar, G. Mittal, *J. Pharm. Bioallied Sci.* **2013**, *5*, 162.
[108] C. Giannavola, C. Bucolo, A. Maltese, D. Paolino, M. Vandelli, G. Puglisi, V. L. Lee, M. Fresta, *Pharm. Res.* **2003**, *20*, 584.
[109] K. Hu, J. Dou, F. Yu, X. He, X. Yuan, Y. Wang, C. Liu, N. Gu, *Vaccine* **April 2**, *29*, 1455.
[110] A. A. Mahmoud, G. S. El-Feky, R. Kamel, G. E. A. Awad, *Int. J. Pharm.* **7**, *413*, 229.
[111] R. S. Bhatta, H. Chandasana, Y. S. Chhonker, C. Rathi, D. Kumar, K. Mitra, P. K. Shukla, *Int. J. Pharm.* **January 8**, *432*, 105.
[112] W. Zhou, Y. Wang, J. Jian, S. Song, *Int. J. Nanomedicine* **9**, *8*, 3715.
[113] Y. S. Chhonker, Y. D. Prasad, H. Chandasana, A. Vishvkarma, K. Mitra, P. K. Shukla, R. S. Bhatta, *Int. J. Biol. Macromol.* **1**, *72*, 1451.
[114] M. de la Fuente, B. Seijo, M. J. Alonso, *Gene Ther* **2008**, *15*, 668.
[115] G. Konat Zorzi, L. Contreras-Ruiz, J. E. Párraga, A. López-García, R. Romero Bello, Y. Diebold, B. Seijo, A. Sánchez, *Mol. Pharm.* **2011**, *8*, 1783.
[116] L. Contreras-ruiz, G. K. Zorzi, D. Hileeto, A. López-garcía, M. Calonge, B. Seijo, A. Sánchez, Y. Diebold, *Gene Ther.* **2013**, *20*, 467.
[117] M. Jiang, L. Gan, C. Zhu, Y. Dong, J. Liu, Y. Gan, *Biomaterials* **10**, *33*, 7621.
[118] S. Alqawlaq, J. M. Sivak, J. T. Huzil, M. V. Ivanova, J. G. Flanagan, M. A. Beazely, M. Foldvari, *Nanomedicine Nanotechnol. Biol. Med.* **11**, *10*, 1637.
[119] D. Delgado, A. del Pozo-Rodríguez, M. Á. Solinís, M. Avilés-Triqueros, B. H. F. Weber, E. Fernández, A. R. Gascón, *Hum. Gene Ther.* **2012**, *23*, 345.
[120] A. Tandon, A. Sharma, J. T. Rodier, A. M. Klibanov, F. G. Rieger, R. R. Mohan, *PLoS ONE* **2013**, *8*, e66434.

[121] J. E. Parraga, G. K. Zorzi, Y. Diebold, B. Seijo, A. Sanchez, *Int. J. Pharm.* **12**, *477*, 12.
[122] R. C. Nagarwal, P. Nath Singh, S. Kant, P. Maiti, J. K. Pandit, *Chem. Pharm. Bull. (Tokyo)* **2011**, *59*, 272.
[123] R. C. Nagarwal, R. Kumar, M. Dhanawat, J. K. Pandit, *Colloids Surf. B Biointerfaces* **January 8**, *86*, 28.
[124] R. C. Nagarwal, R. Kumar, J. K. Pandit, *Eur. J. Pharm. Sci.* **11**, *47*, 678.
[125] Z. Liu, X. Zhang, H. Wu, J. Li, L. Shu, R. Liu, L. Li, N. Li, *Drug Dev. Ind. Pharm.* **2011**, *37*, 475.
[126] S. Chowdhury, R. Guha, R. Trivedi, U. B. Kompella, A. Konar, S. Hazra, *PLoS One* **2013**, *8*, DOI 10.1371/journal.pone.0070528.
[127] W. Wang, J. Despanie, P. Shi, M. C. Edman, Y.-A. Lin, H. Cui, M. Heur, M. E. Fini, S. F. Hamm-Alvarez, J. A. MacKay, *J. Mater. Chem. B* **2014**, *2*, 8131.
[128] S. M. Ahsan, C. M. Rao, *Nanoscale* **2017**, *9*, 9946.
[129] H. Chi, Y. Gu, T. Xu, F. Cao, *Int. J. Nanomedicine* **2017**, *12*, 1607.
[130] J. Ban, Y. Zhang, X. Huang, G. Deng, D. Hou, Y. Chen, Z. Lu, *Int. J. Nanomedicine* **2017**, *12*, 1329.
[131] S. Liu, M. D. Dozois, C. N. Chang, A. Ahmad, D. L. T. Ng, D. Hileeto, H. Liang, M.-M. Reyad, S. Boyd, L. W. Jones, F. X. Gu, *Mol. Pharm.* **2016**, *13*, 2897.
[132] R. E. Stratford Jr., D. C. Yang, M. A. Redell, V. H. Lee, *Curr. Eye Res.* **1982**, *2*, 1982.
[133] P. N. Shek, R. F. Barber, *Biochim. Biophys. Acta BBA - Biomembr.* **8**, *902*, 229.
[134] N. M. Davies, S. J. Farr, J. Hadgraft, I. W. Kellaway, *Pharm Res Pharm. Res. Off. J. Am. Assoc. Pharm. Sci.* **1992**, *9*, 1137.
[135] M. S. Nagarsenker, V. Y. Londhe, G. D. Nadkarni, *Int. J. Pharm.* **October 11**, *190*, 63.
[136] A. M. Durrani, N. M. Davies, M. Thomas, I. W. Kellaway, *Int. J. Pharm.* **August 12**, *88*, 409.
[137] U. Pleyer, S. Lutz, W. J. Jusko, K. D. Nguyen, M. Narawane, D. Rückert, B. J. Mondino, V. H. Lee, K. Nguyen, *Invest. Ophthalmol. Vis. Sci.* **1993**, *34*, 2737.
[138] I. Masuda, T. Matsuo, T. Yasuda, N. Matsuo, *Invest. Ophthalmol. Vis. Sci.* **1996**, *37*, 1914.
[139] K. Hironaka, Y. Inokuchi, Y. Tozuka, M. Shimazawa, H. Hara, H. Takeuchi, *J. Controlled Release* **6**, *136*, 247.
[140] A. Bochota, B. Mashhour, F. Puisieux, P. Couvreur, E. Fattal, *J. Drug Target.* **1998**, *6*, 309.
[141] T. Lajunen, K. Hisazumi, T. Kanazawa, H. Okada, Y. Seta, M. Yliperttula, A. Urtti, Y. Takashima, *Eur. J. Pharm. Sci.* **January 10**, *62*, 23.
[142] R. Srinivasan, S. K. Jain, *Drug Deliv.* **1998**, *5*, 53.
[143] A. K. Jain, K. B. Chalasani, R. K. Khar, F. J. Ahmed, P. V. Diwan, *J. Drug Target.* **2007**, *15*, 417.
[144] J. Zhang, S. Wang, *Int. J. Pharm.* **August 5**, *372*, 66.
[145] M. M. Mehanna, H. A. Elmaradny, M. W. Samaha, *Drug Dev. Ind. Pharm.* **2010**, *36*, 108.
[146] G. Abdelbary, *Pharm. Dev. Technol.* **2011**, *16*, 44.

[147] W. He, X. Guo, M. Feng, N. Mao, *Int. J. Pharm.* **12**, *458*, 305.
[148] D. Quinteros, M. Vicario-de-la-Torre, V. Andrés-Guerrero, S. Palma, D. Allemandi, R. Herrero-Vanrell, I. T. Molina-Martínez, *PloS One* **2014**, *9*, e110344.
[149] M. Fresta, A. PANICO, C. BUCOLO, C. GIANNAVOLA, G. PUGLISI, *J. Pharm. Pharmacol.* **1999**, *51*, 565.
[150] S. L. Law, K. J. Huang, C. H. Chiang, *J. Controlled Release* **March 1**, *63*, 135.
[151] P. Chetoni, S. Rossi, S. Burgalassi, D. Monti, S. Mariotti, M. F. Saettone, *J. Ocul. Pharmacol. Ther.* **2004**, *20*, 169.
[152] R. Cortesi, R. Argnani, E. Esposito, A. Dalpiaz, A. Scatturin, F. Bortolotti, M. Lufino, R. Guerrini, G. Cavicchioni, C. Incorvaia, E. Menegatti, R. Manservigi, *Int. J. Pharm.* **June 7**, *317*, 90.
[153] P. Chetoni, D. Monti, S. Tampucci, B. Matteoli, L. Ceccherini-Nelli, A. Subissi, S. Burgalassi, *Int. J. Pharm.* **8**, *492*, 120.
[154] R. Hathout, S. Mansour, N. Mortada, A. Guinedi, *AAPS PharmSciTech* **2007**, *8*, E1.
[155] M. M. Ibrahim, A.-E. H. Abd-Elgawad, O. A.-E. Soliman, M. M. Jablonski, *Transl. Vis. Sci. Technol.* **2015**, *4*, 12.
[156] Y. Shen, J. Tu, *AAPS J.* **2007**, *9*, E371.
[157] J. P. Craig, C. Purslow, P. J. Murphy, J. S. W. Wolffsohn, *Contact Lens Anterior Eye* **4**, *33*, 83.
[158] F. S. Habib, E. A. Fouad, M. S. Abdel-Rhaman, D. Fathalla, *Acta Ophthalmol. (Copenh.)* **2010**, *88*, 901.
[159] F. A. P. de Sá, S. F. Taveira, G. M. Gelfuso, E. M. Lima, T. Gratieri, *Colloids Surf. B Biointerfaces* **January 9**, *133*, 331.
[160] H. Shimazaki, K. Hironaka, T. Fujisawa, K. Tsuruma, Y. Tozuka, M. Shimazawa, H. Takeuchi, H. Hara, *Invest. Ophthalmol. Vis. Sci.* **2011**, *52*, 7289.
[161] M. W. Shafaa, N. M. Sabra, R. A. Fouad, *Biopharm. Drug Dispos.* **2011**, *32*, 507.
[162] J. Lin, H. Wu, Y. Wang, J. Lin, Q. Chen, X. Zhu, *Drug Deliv.* **2014**, *0*, 1.
[163] S. Yu, Q.-M. Wang, X. Wang, D. Liu, W. Zhang, T. Ye, X. Yang, W. Pan, *Int. J. Pharm.* **2015**, *480*, 128.
[164] Y. Huang, Q. Tao, D. Hou, S. Hu, S. Tian, Y. Chen, R. Gui, L. Yang, Y. Wang, *Int. J. Nanomedicine* **2017**, *12*, 1731.
[165] N. A. A. Nasir, P. Agarwal, R. Agarwal, I. Iezhitsa, R. Alyautdin, N. N. Nukolova, V. P. Chekhonin, N. M. Ismail, *Drug Deliv.* **2016**, *23*, 2765.
[166] N. Morsi, M. Ibrahim, H. Refai, H. El Sorogy, *Eur. J. Pharm. Sci.* **2017**, *104*, 302.
[167] M. Fischer, F. Vögtle, *Angew. Chem. Int. Ed.* **1999**, *38*, 884.
[168] T. F. Vandamme, L. Brobeck, *J. Controlled Release* **1**, *102*, 23.
[169] C. Durairaj, R. S. Kadam, J. W. Chandler, S. L. Hutcherson, U. B. Kompella, *Invest. Ophthalmol. Vis. Sci.* **2010**, *51*, 5804.
[170] W. Yao, K. Sun, H. Mu, N. Liang, Y. Liu, C. Yao, R. Liang, A. Wang, *Drug Dev. Ind. Pharm.* **2010**, *36*, 1027.
[171] V. Mishra, N. K. Jain, *Int. J. Pharm.* **1**, *461*, 380.

[172] E. G. Romanowski, K. A. Yates, R. M. Q. Shanks, O. K. Bernhard, J. R. A. Paull, R. P. Kowalski, *Invest. Ophthalmol. Vis. Sci.* **2015**, *56*.
[173] I. Bravo-Osuna, M. Vicario-de-la-Torre, V. Andres-Guerrero, J. Sanchez-Nieves, M. Guzman-Navarro, F. J. de la Mata, R. Gomez, B. de las Heras, P. Argueso, G. Ponchel, R. Herrero-Vanrell, I. T. Molina-Martinez, *Mol. Pharm.* **2016**, *13*, 2966.
[174] I. Bravo-Osuna, M. Noiray, E. Briand, A. M. Woodward, P. Argüeso, I. T. M. Martínez, R. Herrero-Vanrell, G. Ponchel, *Pharm. Res.* **2012**, *29*, 2329.
[175] C. Liu, K. Jiang, L. Tai, Y. Liu, G. Wei, W. Lu, W. Pan, *Acs Appl. Mater. Interfaces* **2016**, *8*, 19256.
[176] A. K. Gupta, S. Madan, D. K. Majumdar, A. Maitra, *Int. J. Pharm.* **11**, *209*, 1.
[177] J. Liaw, S. Chang, F. Hsiao, *Gene Ther.* **2001**, *8*, 999.
[178] Y.-C. Tong, S.-F. Chang, C.-Y. Liu, W. W. Y. Kao, C. H. Huang, J. Liaw, *J. Gene Med.* **2007**, *9*, 956.
[179] Y.-C. Tong, S.-F. Chang, W. W. Y. Kao, C.-Y. Liu, J. Liaw, *J. Controlled Release* **January 10**, *147*, 76.
[180] I. Pepić, A. Hafner, J. Lovrić, B. Pirkić, J. Filipović-Grčić, *J. Pharm. Sci.* **2010**, *99*, 4317.
[181] F. Rafie, Y. Javadzadeh, A. R. Javadzadeh, L. A. Ghavidel, B. Jafari, M. Moogooee, S. Davaran, *Curr. Eye Res.* **2010**, *35*, 1081.
[182] X. Li, Z. Zhang, J. Li, S. Sun, Y. Weng, H. Chen, *Nanoscale* **2012**, *4*, 4667.
[183] H.-R. Lin, P.-C. Chang, *JBM J. Biomed. Mater. Res. Part B Appl. Biomater.* **2013**, *101B*, 689.
[184] A. H. Salama, R. N. Shamma, *Int. J. Pharm.* **8**, *492*, 28.
[185] S. Beack, J.-S. Choi, J. H. Lee, H. Kim, K. H. Kim, C.-K. Joo, S. K. Hahn, *Nanomed.* **2015**, *10*, 2315.
[186] J. Li, Z. Li, T. Zhou, J. Zhang, H. Xia, H. Li, J. He, S. He, L. Wang, *Int. J. Nanomedicine* **2015**, *10*, 6027.
[187] S. Shi, Z. Zhang, Z. Luo, J. Yu, R. Liang, X. Li, H. Chen, *Sci. Rep.* **2015**, *5*, 11337.
[188] S. Liu, C. N. Chang, M. S. Verma, D. Hileeto, A. Muntz, U. Stahl, J. Woods, L. W. Jones, F. X. Gu, *Nano Res.* **2015**, *8*, 621.
[189] S. Vyas, N. Mysore, V. Jaitely, N. Venkatesan, *Pharm.* **1998**, *53*, 466.
[190] M. M. El-Sayed, A. K. Hussein, H. A. Sarhan, H. F. Mansour, *Drug Dev. Ind. Pharm.* **2017**, *43*, 902.
[191] G. Abdelbary, N. El-gendy, *AAPS PharmSciTech* **2008**, *9*, 740.
[192] D. Aggarwal, I. P. Kaur, *Int. J. Pharm.* **2**, *290*, 155.
[193] A. S. Guinedi, N. D. Mortada, S. Mansour, R. M. Hathout, *Int. J. Pharm.* **August 12**, *306*, 71.
[194] D. Aggarwal, D. Pal, A. K. Mitra, I. P. Kaur, *Int. J. Pharm.* **6**, *338*, 21.
[195] I. I. Abu Hashim, M. S. El-Dahan, R. M. Yusif, A.-E. H. Abd-Elgawad, H. Arima, *Biol. Pharm. Bull.* **2014**, *37*, 541.
[196] Y. Zubairu, L. M. Negi, Z. Iqbal, S. Talegaonkar, *Asian J. Pharm. Sci.* **2015**, *10*, 322.

[197] R. M. Khalil, G. A. Abdelbary, M. Basha, G. E. A. Awad, H. A. el-Hashemy, *J. Liposome Res.* **2016**, *0*, 1.
[198] C. Losa, M. J. Alonso, J. L. Vila, F. Orallo, J. Martinez, J. A. Saavedra, J. C. Pastor, *J. Ocul. Pharmacol. Ther.* **1992**, *8*, 191.
[199] C. Losa, L. Marchal-Heussler, F. Orallo, J. V. Jato, M. Alonso, *Pharm. Res.* **1993**, *10*, 80.
[200] L. Marchal-Heussler, D. Sirbat, M. Hoffman, P. Maincent, *Pharm. Res.* **1993**, *10*, 386.
[201] P. Calvo, M. J. Alonso, J. L. Vila-Jato, J. R. Robinson, *J. Pharm. Pharmacol.* **1996**, *48*, 1147.
[202] P. Calvo, J. L. Vila-Jato, M. J. Alonso, *Int. J. Pharm.* **7**, *153*, 41.
[203] P. Calvo, A. Sánchez, J. Martínez, M. López, M. Calonge, J. Pastor, M. Alonso, *Pharm. Res.* **1996**, *13*, 311.
[204] S. Reimondez-Troitino, I. Alcalde, N. Csaba, A. Inigo-Portugues, M. de la Fuente, F. Bech, A. C. Riestra, J. Merayo-Lloves, M. J. Alonso, *Drug Deliv. Transl. Res.* **2016**, *6*, 708.
[205] J. B. Suketu D. Desai, *Drug Deliv.* **2000**, *7*, 201.
[206] A. M. De Campos, A. Sánchez, R. Gref, P. Calvo, M. Alonso, amp, x, J. a, *Eur. J. Pharm. Sci.* **9**, *20*, 73.
[207] C. Carbone, T. Musumeci, M. R. Lauro, G. Puglisi, *Colloids Surf. B-Biointerfaces* **2015**, *125*, 190.
[208] G. Gaucher, M.-H. Dufresne, V. P. Sant, N. Kang, D. Maysinger, J.-C. Leroux, *J. Controlled Release* **2005**, *109*, 169.
[209] W. Abdelwahed, G. Degobert, S. Stainmesse, H. Fessi, *Adv. Drug Deliv. Rev.* **2006**, *58*, 1688.
[210] "General Chapters: <785> OSMOLALITY AND OSMOLARITY," can be found under http://www.pharmacopeia.cn/v29240/usp29nf24s0_c785.html, **n.d.**
[211] F. K. Bedu-Addo, **2004**.
[212] J. Barley, "Freeze Drying / Lyophilization Information: Basic Principles," can be found under https://www.spscientific.com/freeze-drying-lyophilization-basics/, **n.d.**
[213] M. J. Pikal, S. Shah, *Int. J. Pharm.* **1990**, *62*, 165.
[214] K. Greco, M. Mujat, K. L. Galbally-Kinney, D. X. Hammer, R. D. Ferguson, N. Iftimia, P. Mulhall, P. Sharma, W. J. Kessler, M. J. Pikal, *J. Pharm. Sci.* **2013**, *102*, 1773.
[215] J. H. Thrall, *Radiology* **2004**, *230*, 315.
[216] P. Boisseau, B. Loubaton, *Comptes Rendus Phys.* **2011**, *12*, 620.
[217] J. K. Patra, G. Das, L. F. Fraceto, E. V. R. Campos, M. del P. Rodriguez-Torres, L. S. Acosta-Torres, L. A. Diaz-Torres, R. Grillo, M. K. Swamy, S. Sharma, S. Habtemariam, H.-S. Shin, *J. Nanobiotechnology* **2018**, *16*, 71.
[218] F. Farjadian, A. Ghasemi, O. Gohari, A. Roointan, M. Karimi, M. R. Hamblin, *Nanomed.* **2018**, *14*, 93.
[219] A.-A. D. Jones, G. Mi, T. J. Webster, *Trends Biotechnol.* **2019**, *37*, 117.
[220] P. Preziosi, *Nat. Rev. Drug Discov.* **2004**, *3*, 521.

[221] S. S. Mehta, *Commercializing Successful Biomedical Technologies: Basic Principles for the Development of Drugs, Diagnostics and Devices*, Cambridge University Press, Cambridge ; New York, **2008**.
[222] N. Gregson, K. Sparrowhawk, J. Mauskopf, J. Paul, *Nat. Rev. Drug Discov.* **2005**, *4*, 121.
[223] K. L. Rascati, *Essentials of Pharmacoeconomics*, Wolters Kluwer Health/Lippincott Williams & Wilkins, Philadelphia, **2014**.
[224] *GEN - Genet. Eng. Biotechnol. News* **2014**.
[225] S. Liu, C. N. Chang, M. S. Verma, D. Hileeto, A. Muntz, U. Stahl, J. Woods, L. W. Jones, F. X. Gu, *Nano Res.* **2015**, *8*, 621.
[226] C. Di Tommaso, J.-L. Bourges, F. Valamanesh, G. Trubitsyn, A. Torriglia, J.-C. Jeanny, F. Behar-Cohen, R. Gurny, M. Möller, *Eur. J. Pharm. Biopharm.* **2012**, *81*, 257.
[227] J. El Annan, S. K. Chauhan, T. Ecoiffier, Q. Zhang, D. R. Saban, R. Dana, *Invest. Ophthalmol. Vis. Sci.* **2009**, *50*, 3802.
[228] F. Issa, A. Schiopu, K. J. Wood, *Expert Rev. Clin. Immunol.* **2010**, *6*, 155.
[229] J.-M. Zhang, J. An, *Int. Anesthesiol. Clin.* **2007**, *45*, 27.
[230] D. F. Emerich, C. G. Thanos, *Expert Opin Biol Ther* **2003**, 9.
[231] R. Ma, L. Shi, *Polym. Chem.* **2014**, *5*, 1503.
[232] W. L. A. Brooks, B. S. Sumerlin, *Chem. Rev.* **2016**, *116*, 1375.
[233] A. Matsumoto, A. J. Stephenson-Brown, T. Khan, T. Miyazawa, H. Cabral, K. Kataoka, Y. Miyahara, *Chem. Sci.* **2017**, *8*, 6165.
[234] M. J. Gidley, J. K. Sanders, *Biochem. J.* **1982**, *203*, 331.
[235] Z. Liu, Y. Jiao, Y. Wang, C. Zhou, Z. Zhang, *Adv. Drug Deliv. Rev.* **2008**, *60*, 1650.
[236] S. Shu, L. Sun, X. Zhang, Z. Wu, Z. Wang, C. Li, *J. Nanoparticle Res.* **2011**, *13*, 3657.
[237] C. Lemarchand, R. Gref, P. Couvreur, *Eur. J. Pharm. Biopharm.* **2004**, *58*, 327.
[238] F. Toda, *Acc. Chem. Res.* **1995**, *28*, 480.
[239] A. L. Korich, P. M. Iovine, *Dalton Trans.* **2010**, *39*, 1423.
[240] A. Khawam, D. R. Flanagan, *J. Phys. Chem. B* **2006**, *110*, 17315.
[241] A. Khawam, D. R. Flanagan, *J. Pharm. Sci.* **2006**, *95*, 472.
[242] E. J. Lehr, S. Hermary, R. T. McKay, D. N. H. Webb, A. Abazari, L. E. McGann, J. Y. Coe, G. S. Korbutt, D. B. Ross, *J. Surg. Res.* **2007**, *141*, 60.
[243] M.-H. Dufresne, E. Fournier, M.-C. Jones, M. Ranger, J.-C. Leroux, *Bull Tech Gattefosse* **2003**, *96*, 87.